J R C   T E C H N I C A L   R E P O R T S

JRC – Ispra Atmosphere – Biosphere – Climate Integrated monitoring Station

2011 report

J.P. Putaud, M. Adam, C. Belis, P. Bergamaschi, J. Cancellinha, F. Cavalli, A. Cescatti, D. Daou, A. Dell'Acqua, K. Douglas, M. Duerr, I. Goded, F. Grassi, C. Gruening, J. Hjorth, N. R. Jensen, F. Lagler, G. Manca, S. Martins Dos Santos, R. Passarella, V. Pedroni,, P. Rocha e Abreu, D. Roux, B. Scheeren, C. Schembari

2013

This publication is a Reference Report by the Joint Research Centre of the European Commission.

Europe Direct is a service to help you find answers to your questions about the European Union
Freephone number (*): 00 800 6 7 8 9 10 11
(*) Certain mobile telephone operators do not allow access to 00 800 numbers or these calls may be billed.

A great deal of additional information on the European Union is available on the Internet. It can be accessed through the Europa server http://europa.eu/.

Printed in Italy

Contents

ABC-IS mission

The aim of the Atmosphere-Biosphere-Climate Integrated monitoring Station (ABC-IS) is to measure changes in atmospheric variables to obtain data that are useful for the conception, development, implementation, and monitoring of the impact of European policies and International conventions on air pollution and climate change. Measurements include greenhouse gas concentrations, forest ⇆ atmosphere fluxes, and concentrations of pollutants in the gas phase, the particulate phase and precipitations, as well as aerosol physical and optical characteristics. The goal of ABC-IS is to establish real world interactions between air pollution, climate change and the biosphere, for highlighting possible trade-offs and synergies between air pollution and climate change related policies. Interactions include the role of pollutants in climate forcing and CO_2 uptake by vegetation, the impact of climate change and air pollution on CO_2 uptake by vegetation, the effect of biogenic emission on air pollution and climate forcing, etc.
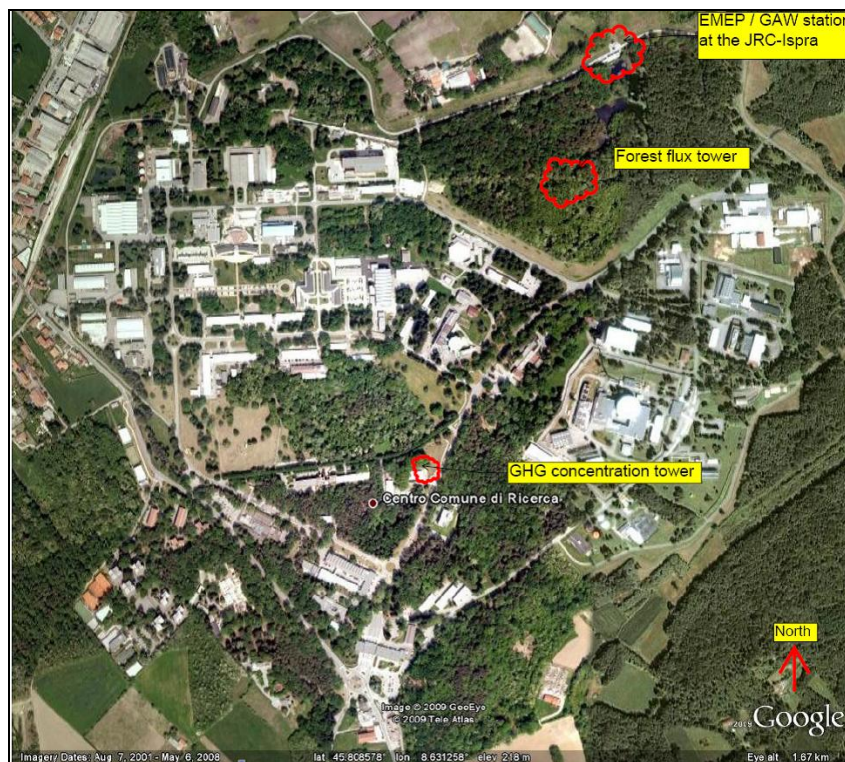
Fig. 1. *JRC-Ispra site and the location of the laboratory for greenhouse gas monitoring and the EMEP-GAW station within the site. The forest flux tower was not operational in 2011*

Measurements are performed in the framework of international monitoring programs like the future ESFRI (European Strategy Forum on Research Infrastructures) project ICOS (Integrated Carbon Observation System), EMEP (Co-operative program for monitoring and evaluation of the long range transmission of air pollutants in Europe of the UN-ECE *Convention on Long-Range Transboundary Air Pollution* CLRTAP) and GAW (the Global Atmosphere Watch program of the World Meteorological Organization). The ABC-IS infrastructure is also used in competitive projects (e.g ACTRIS, ECLAIRE). The participation of ABC-IS in international networks leads its staff to conduct inter-laboratory comparisons

and developments of standard methods in collaboration with the the European Reference Laboratory for Air Pollution.

Quality management system

ABC-IS is research infrastructure of JRC's Institute for Environment and Sustainability. JRC-IES achieved the ISO 9001 certificate in May 2010 and it is also valid for the year 2011 (ISO 9001 is mainly about "project management"), so the year 2011 was also used to set-up/run a quality management system at the JRC-Ispra ABC-IS regional station.

In addition, in Nov. 2010 the JRC-Ispra also achieved the ISO 14001 certificate (ISO 14001 is mainly about "environmental issues"), which is also valid for the year 2011.

Every year there are internal/external audits for the certificates (ISO 9001 / ISO 14001), which were also performed during the year 2011.

The "quality management system (QMS) for the ABC-IS regional station" includes server space at the following links:

\\ccunas3.jrc.it\H02QMS_year_2011_
\\ccunas3.jrc.it\H02QMS_year_2012_
\\Ccunas3\largefacilities\ABC-IS
\\Ccunas3\laboratories

where the following information can be found: List of instruments; information about calibrations; standards used and maintenance; standard operational procedures (SOP's); lifecycle sheets (e.g. log-books); manuals for the instruments; *etc*. For additional specific details about QMS, for the year 2011 and the ABC-IS station, see e.g. the file 2011_Instruments'_calibration_&_standards_&_maintenance.xls, that can be found under \\Ccunas3\largefacilities\ABC-IS\Quality_management

It should be mentioned, that more QMS information/details can also be found in the section "The measurement techniques" in this report.

Finally, it should also be mentioned, that more general QMS information/documentations about how the IES-AC Unit (H02) is run, the management of all of the projects within the Unit and the running of the JRC-Ispra EMEP-GAW station can be found at

\\ccunas3.jrc.it\H02QMS_year_2011_
\\ccunas3.jrc.it\H02QMS_year_2012_

especially in the six H02 Unit QMS documents listed here:

QMS_H02_SUMM_Scientific_Unit_Management_Manual_v7_0.pdf

QMS_H02_MANPROJ_PROJ_Laboratory_Management_v6_0.pdf

QMS_H02_MANPROJ_PROJ_Model_Management_v6_0.pdf

QMS_H02_MANPROJ_PROJ_Informatics_Management_v6_0.pdf

QMS_H02_MANPROJ_PROJ_Knowledge_Management_v6_0.pdf

QMS_H02_MANPROJ_PROJ_Review_Verification_Validation_Approval_v2_0.pdf

The latest versions of the documents are available in

\\ccunas3.jrc.it\H02QMS_year_2012_\1_UNIT\QMS_info\QMS_documents_H02

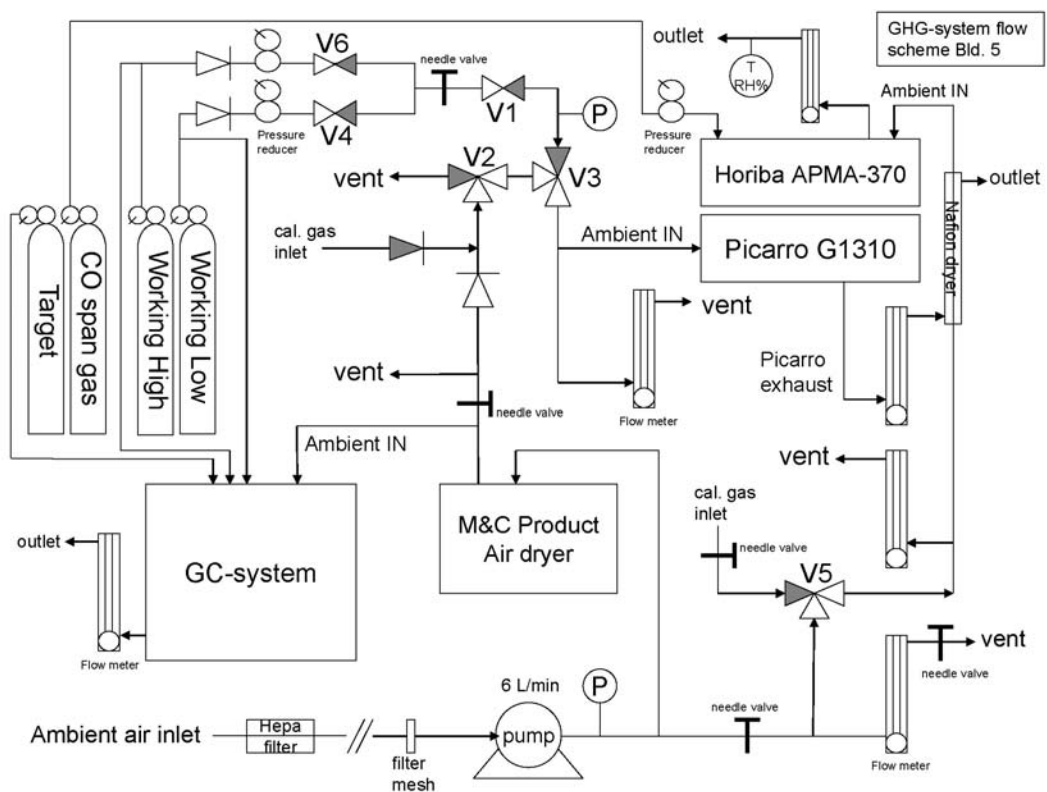Fig. 2: the laboratory for greenhouse gas concentration monitoring (Bd 5)

Fig. 3: Building 5 GHG-system flow scheme.

Greenhouse gas concentration monitoring at the JRC-Ispra site

Introduction

Location

The GHG monitoring station (Fig 1) is located at Building 5 (Fig. 2) of the JRC site Ispra (45.807°N, 8.631°E, 223 m asl). The station is currently the only low altitude measurement site for greenhouse gases near the Po Valley. The unique location of the station at the Eastern border of Lake Maggiore in a semi-rural area at the North-Western edge of the Po Valley allows sampling of highly polluted air masses from the Po Valley during meteorological conditions with southerly flow, contrasted by situations with northerly winds bringing relatively clean air to the site. The main cities around are Varese, 20 km to the East, Novara, 40 km South, Gallarate - Busto Arsizio, about 20 km southeast and Milan, 60 km to the south-east. Four industrial large point sources (CO_2 emissions > 1500 tons d^{-1}) are located between 5 and 45 km NE to SE from Ispra: two two cement factories at 5 and 8 km E and NE, and two power plants at 32 and 43 km SE. The two closest (HOLCIM Comabbio, COLACEM Caravate) also emit 2 and 3 tons of CO per day, respectively (<u>PRTR emissions</u>, 2010). However, they are outside the main wind sectors of the station..

Measurement program

The GHG monitoring station is in operation since October 2007 and is complementary to the JRC-Ispra EMEP-GAW (European Monitoring and Evaluation Programme - Global Atmospheric Watch) air quality station which started in 1985 (Jensen et al., 2010). Both activities together are referred to as ABC-IS (Atmosphere, Biosphere, Climate Integrated Monitoring Station), and will be merged in 2013 into a single monitoring and research platform with a new station building and tall tower for atmospheric sampling.

Instrumentation

Here we summarize the most important aspects of the GHG, ^{222}Radon and CO measurement systems. A more detailed description is given by Scheeren et al. (2010) and Scheeren et al. (2013, manuscript in preparation).

Sampling

Air is sampled from a 15 m high mast (Fig. 2) using a 50 m ½" Teflon tube at a flow rate of ~6 L /min using a KNF membrane pump (KNF N811KT.18).The sampled air is filtered from aerosols by a Pall Hepa filter (model PN12144) positioned 10 m downstream of the inlet and dried cryogenically by a commercial system from M&C products (model EC30 FD) down to a water vapor content of <0.015%v before being directed to the different instruments. The remaining water vapor is equivalent to a maximum 'volumetric error' of <0.06 ppmv of CO_2 or <0.3 ppbv of CH_4 or <0.05 ppbv N_2O. A schematic overview of the sample flow set-up is shown in Figure 1.
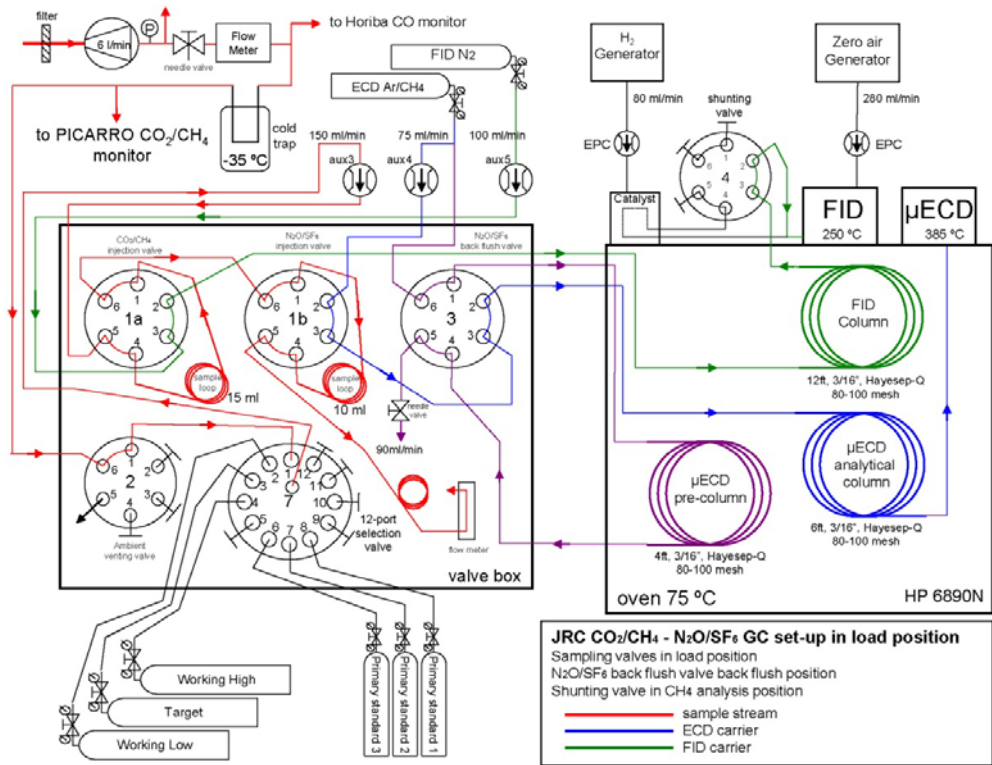
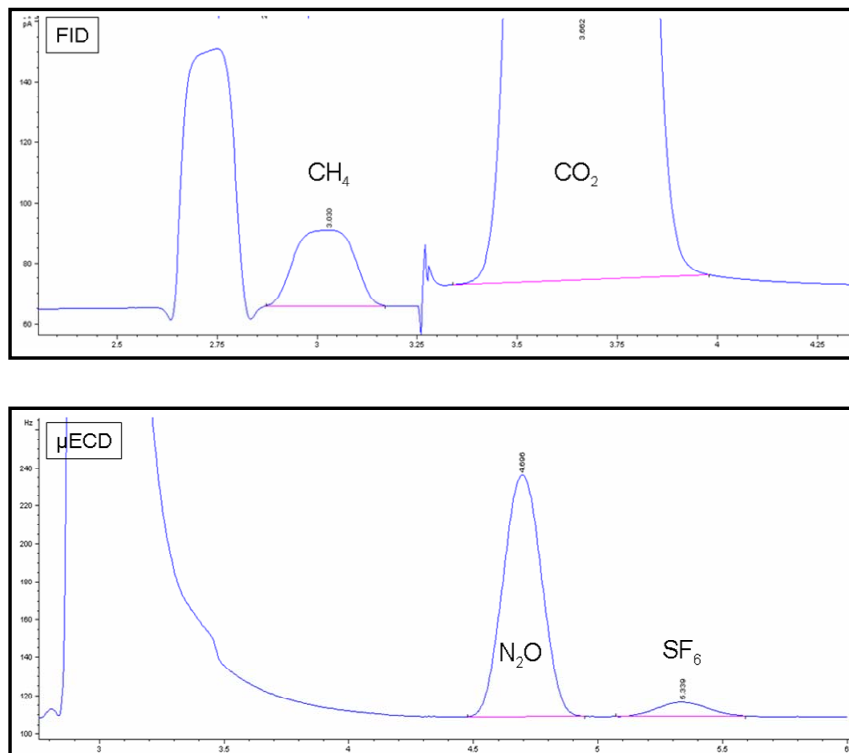Fig.4: Schematic of the GC-system set-up for greenhouse gas concentration measurements

Fig. 5: Typical chromatograms from the two detectors (FID and ECD).

Gas Chromatograph Agilent 6890N (S/N US10701038)

For continuous monitoring at a 6 minute time resolution of CO_2, CH_4, N_2O, and SF_6 we apply an Agilent 6890N gas chromatograph equipped with a Flame Ionization Detector and micro-Electron Capture Detector based on the set-up described by Worthy el al. (1998). The calibration strategy has been adopted from Pepin et al. (2001) and is based on applying a Working High (WH) and Working Low (WL) standards, which are calibrated regularly using NOAA primary standards. The WH and WL are both measured 2 times per hour for calculating ambient mixing ratios and a Target (TG) sample is measured every 6 hours for quality control (purchased from Deuste Steininger GmbH, Germany).

The GHG measurements are reported as dry air mole fractions (mixing ratios) using the WMO NOAA2004 scale for CO_2 and CH_4, the NOAA2006 scale for N_2O and SF_6 (and the NOAA2000 scale for CO). We apply a suite of five NOAA tanks ranging from 369-523 ppm for CO_2, 1782-2397 ppb for CH_4, 318-341 ppb for N_2O, 6.1-14.3 ppt for SF_6, and 53-750 ppb for CO as primary standards. The GC control and peak integration runs on *ChemStation* commercial software. Further processing of the raw data is based on custom built routines in Visual Basic 6.0 and Excel Vba. A schematic of the GC-system set-up and typical chromatograms are shown in Figure 2.

Cavity Ring-Down Spectrometer (Picarro G1301) (S/N CFDAS-42)

In addition to the low time resolution GC-system we have been operating a fast Picarro G1301 Cavity Ring-Down Spectrometer (Picarro CRDS) for CO_2 and CH_4 from February 2009 onwards sampling from the same inlet at a 12 second time resolution. From March 24, 2009 onwards we applied a commercial M&C Products Compressor gas Peltier cooler type EC30/FD for drying of the sampling air to below 0.02%v. This corresponds to a maximum 'volumetric error' of about 0.08 ppm CO_2 and 0.4 ppb CH_4. To compensate for the remaining water vapor fraction we apply an empirically determined instrument specific water vapor correction factor. From May 27, 2009 onwards, the monitor received a WL and WH standard for 10 minutes each once every two days which was reduced to once every 4 days from September 2011 onwards, to serve as a Target control sample and to allow for correction of potential instrumental drift. A full scale calibration with 5 NOAA standards is performed 2 to 3 times per year. The monitor response has shown to be highly linear and the calibration factors obtained with the 5-point calibration have shown negligible changes within the precision of the monitor over the course of a year. The monitor calibration factors to calculate raw concentration values have been set to provide near real-time raw data with an accuracy of <0.5 ppm for CO_2 and <2 ppb for CH_4.

Measurement uncertainties

For the GC-system the short-time repeatability (precision) has been evaluated as the 1σ standard deviation of a number of repetitive measurements of the Target during one day. The long-term reproducibility is defined as the deviation of the Target measurements from the assigned value, evaluated over 6-12 months. The overall accuracy depends on the reproducibility, the uncertainty of the calibration, and the uncertainty of the response function of the instrument. Better estimates of the overall accuracy are currently elaborated in the InGOS ("Integrated non-CO2 Greenhouse gas Observing System") project (http://www.ingos-infrastructure.eu/).

For the PICARRO G1301 we define the precision by the 1σ standard deviation of the average of a 10 minutes dry standard measurement. To determine the long-term reproducibility we evaluated the deviations of the Target from the assigned value over a period of about 7 months. We found that the reproducibility over this period was <0.04 ppm for CO_2 and <0.3 ppb for CH_4. The precision and reproducibility for the different gases and techniques are presented in Table 1.
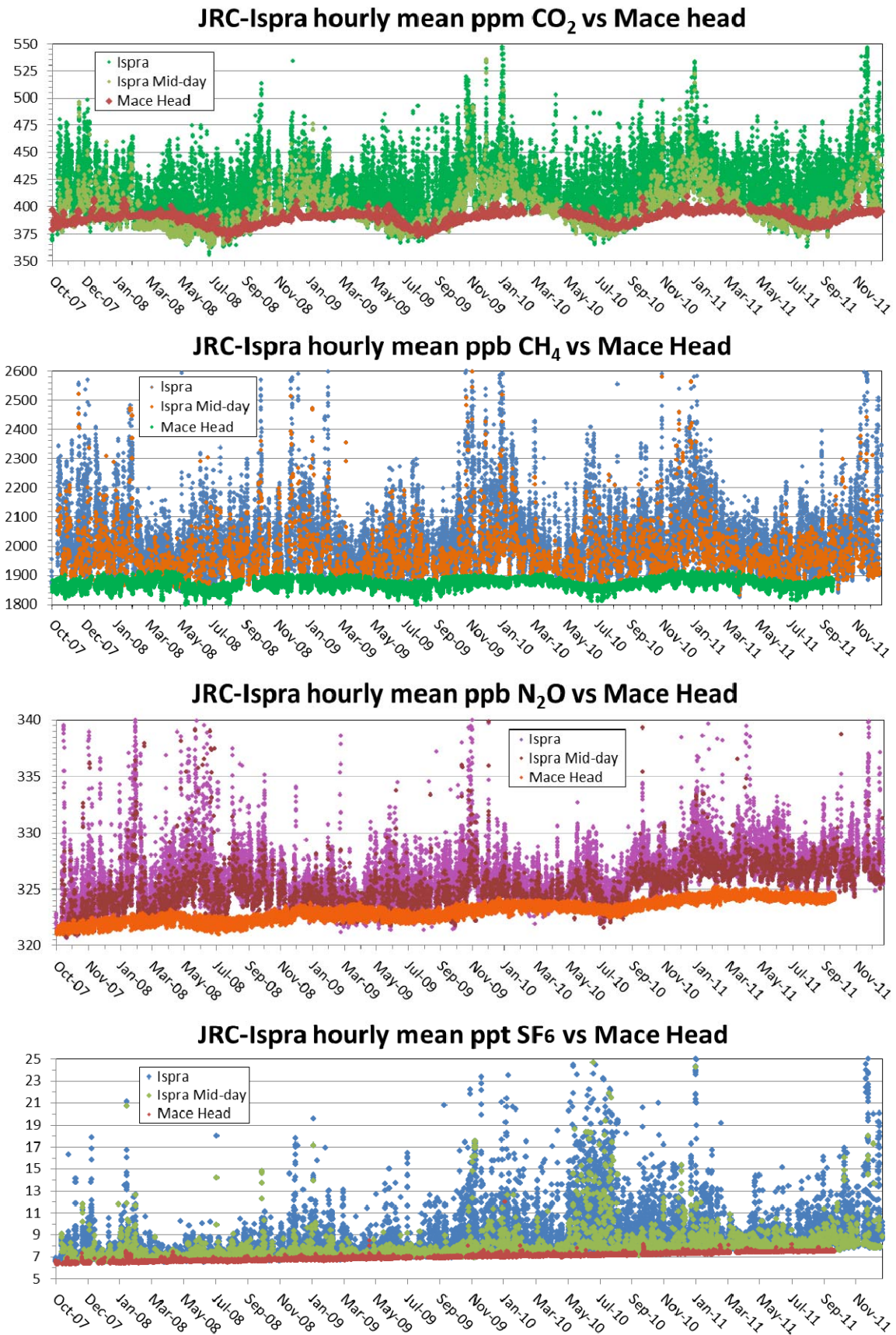
Fig. 6 *Time series of continuous CO_2, CH_4, N_2O, SF_6, measurements at Ispra between October 2007 and December 2011. The figure shows dry air mole fractions measured during mid-day (12:00-15:00 h LT). Measurements from the background station Mace Head on the West coast of Ireland are also included.*

Table 1: Precision and reproducibility for the different gas species and applied techniques.

Species-method	Precision	Reproducibility Long-term	WMO [1] compatibility goal
CO_2-GC	0.05 ppm	0.15 ppm	0.1 ppm
CO_2-CRDS	0.03 ppm	0.04 ppm	
CH_4-GC	0.4 ppb	0.8 ppb	2 ppb
CH_4-CRDS	0.2 ppb	0.3 ppb	
N_2O-GC	0.2 ppb	0.4 ppb	0.1 ppb
SF_6-GC	0.05 ppt	0.1 ppt	0.1 ppt

(1) WMO-GAW Report No. 194, 2010.

Radon analyser ANSTO (custom built)

^{222}Radon activity concentrations in Bq m^{-3} have been semi-continuously monitored (30 minute time integration) applying an ANSTO dual-flow loop two-filter detector (Zahorowski et al., 2004) since October of 2008. The monitor is positioned close to the GHG-sampling mast and used a separate inlet positioned at 3.5 m above the ground. A 500 L decay tank was placed in the inlet line to allow for the decay of Thoron (^{220}Rn with a half-life of 55.6 s) before reaching the ^{222}Radon monitor. The ANSTO ^{222}Radon monitor is calibrated once a month using a commercial passive ^{226}Radium source from Pylon Electronic Inc. (Canada) inside the calibration unit with an activity of 21.99 kBq, which corresponds to a ^{222}Radon delivery rate of 2.77 Bq min^{-1}. The lower limit of detection is 0.02 Bq m^{-3} for a 30% precision (relative counting error). The total measurement uncertainty is estimated to be <5% for ambient ^{222}Radon activities at Ispra.

Carbon Monoxide analyser Horiba APMA-370 *(S/N WYHEOKSN)*

From May 2010 onwards carbon monoxide (CO) has been continuously monitored at the station using a commercial Horiba APMA-370 CO monitor based on the principle of non-dispersive infrared absorption (NDIR). The Horiba APMA-370 uses solenoid valve cross flow modulation applying the same air for both the sample and the reference, instead of the conventional technique to apply an optical chopper to obtain modulation signals. This results in a low zero-drift and stable signal over long periods of time. The instrument was calibrated every 2-3 months against two primary NOAA standards based on the NOAA2000 scale of 500 and 750 ppb CO in dry air with an uncertainty of 0.7% (29 L Luxfer aluminum cylinders). In addition we applied a working standard at regular time intervals (Span gas) calibrated against the WMO/NOAA tanks with an initial CO concentration of 1035 ±10 ppb in dry air in (30 L Luxfer aluminum cylinder). Automatic instrument zero checks were performed every 72 h providing dry zero air to the monitor. The detection limit is ~30 ppb, and the overall measurement uncertainty is estimated to be ±4%, which includes the uncertainty of the calibration standard (1%), the H_2O interference (~1%), and the instrument precision (2%).

Overview of measurement results

Figure 6 gives an overview of the GC greenhouse gas measurements since the start of the measurements in October of 2007 until December of 2011. The figure shows mid-day (12:00-15:00 h L.T.) measurements (to illustrate mixing ratios during daytime, which are representative for larger scales, while measurements during night typically show large enrichments within the nocturnal boundary layer, mostly due to local and regional sources). Furthermore, continuous measurements from the Mace Head (Ireland) station are included in the Figure to illustrate the Atlantic background mixing ratios (Mace Head data from the WMO World Data Centre for
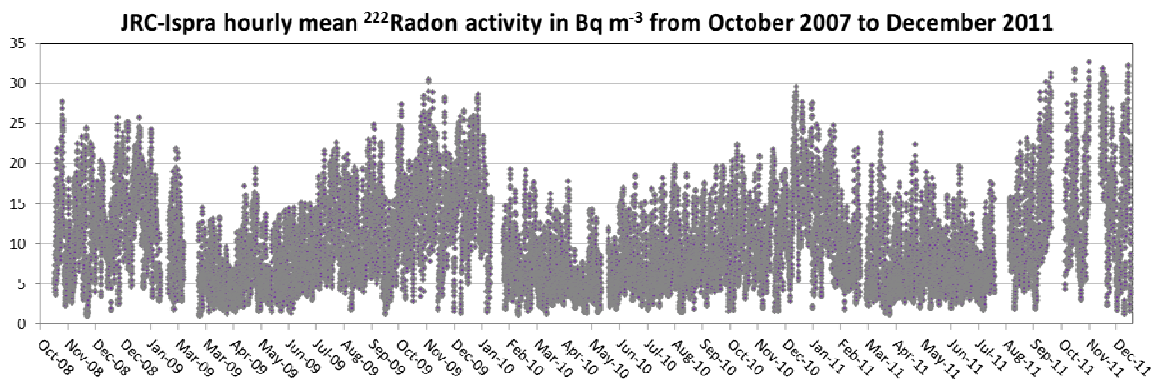
Fig. 7a:: *Time series of hourly mean* $^{222}Radon$ *activity from Oct. 2008 to Dec. 2011.*

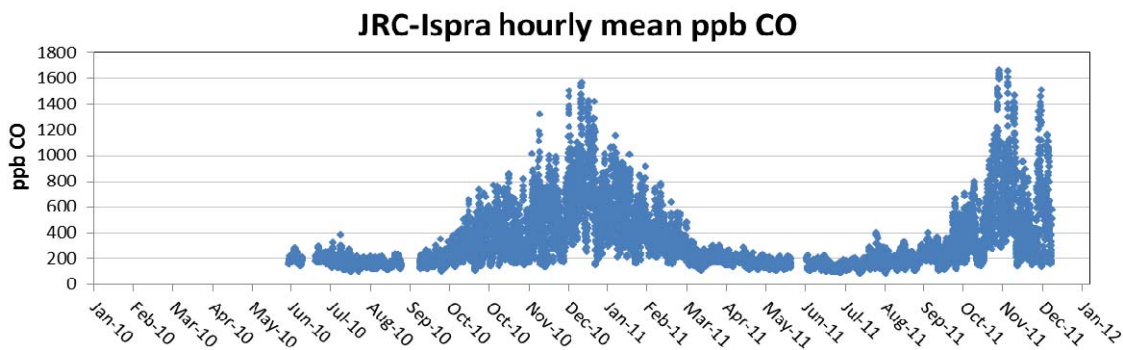
Fig. 7b: *Time series of hourly mean CO mixing ratios between June 2010 and Dec. 2011.*
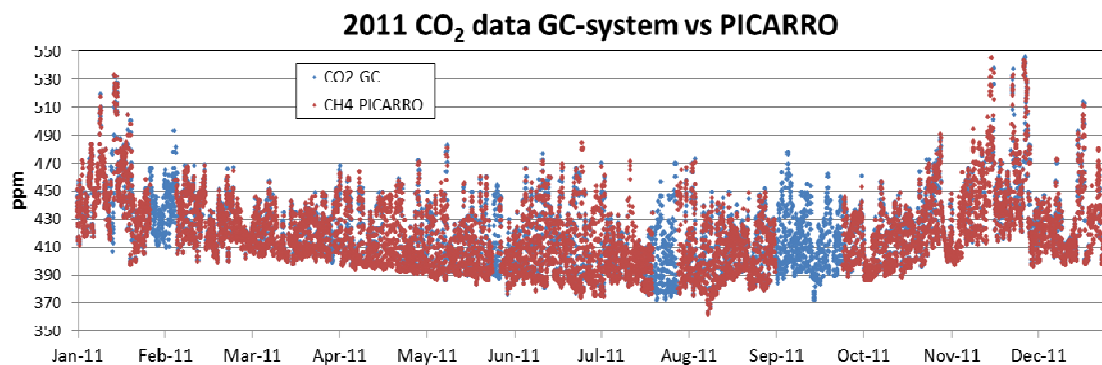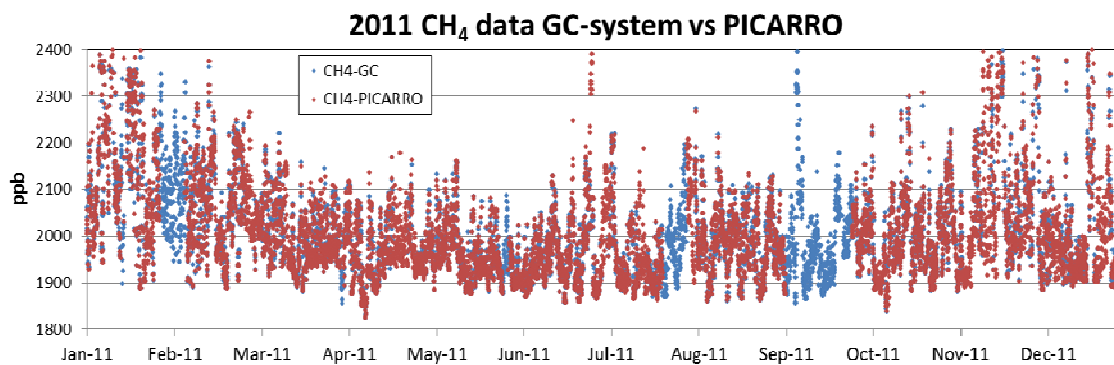
Fig. 8: *Time series of hourly mean CH$_4$ and CO$_2$ dry air mole fractions at Ispra during 2011 from the GC-system and the Picarro CRDS.*

Greenhouse gases: CO_2 from Michel Ramonet, LSCE, Paris; CH_4 and N_2O from Ed Dlugokencky, NOAA/ESRL, and SF_6 from Ray Wang, Georgia Institute of Technology).

Figure 7a shows hourly mean [222]Radon activities since October 2008, and Figure 7b CO hourly mean mixing ratios from June 2010 to December 2011.

Focus on 2011 data

In Figure 8 we show the CO_2 and CH_4 hourly mean time series from both the GC-system and the Picarro CRDS for 2011. In Figure 9 the excellent agreement between both measurements system is illustrated by the fact that the absolute difference between the hourly mean values of the Picarro and the GC-system is usually well within the variability (depicted as the 1-σ standard deviation) of the hourly mean data from the Picarro instrument.
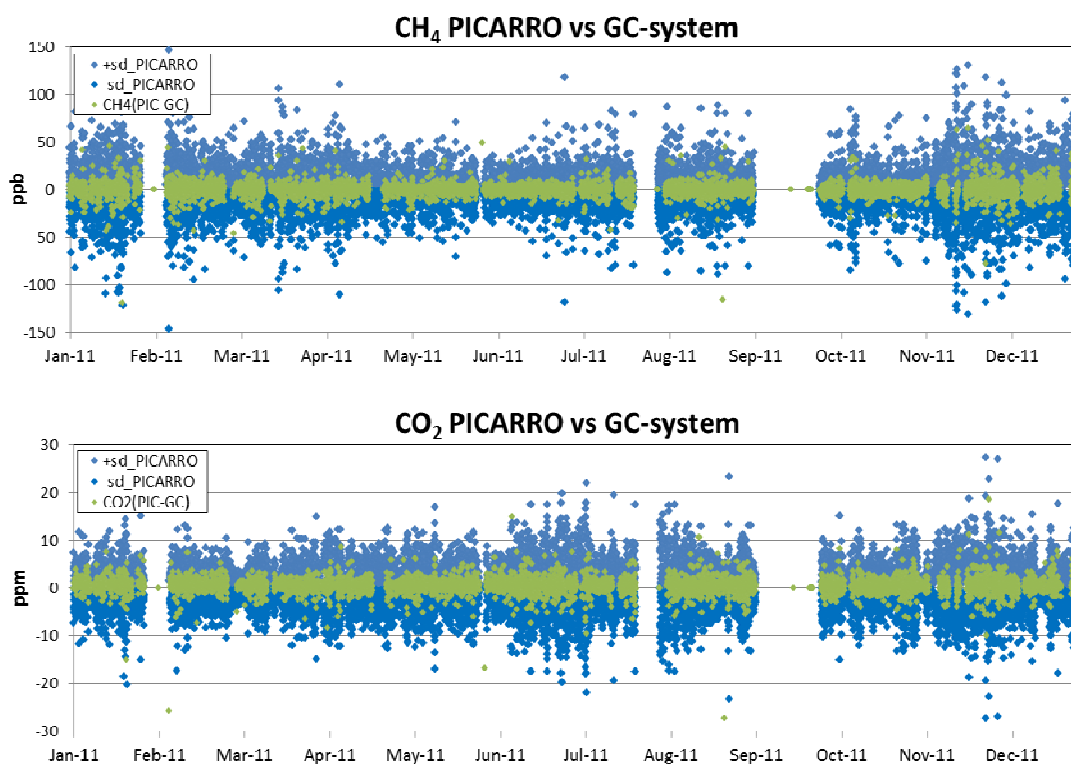
Fig.9 : *Comparison between the absolute difference of the hourly mean values of the Picarro and the GC-system and the variability (depicted as the 1-σ standard deviation) of the hourly mean data from the Picarro instrument.*

13

Fig 10: *most recent available map of the EMEP stations across Europe.*

Atmosphere watch at the JRC-Ispra site

Introduction

Location

Air pollution has been monitored since 1985 at the EMEP and regional GAW station for atmospheric research (45°48.881'N, 8°38.165'E, 209 m a.s.l.) located by the Northern fence of the JRC-Ispra site (see Fig. 1), situated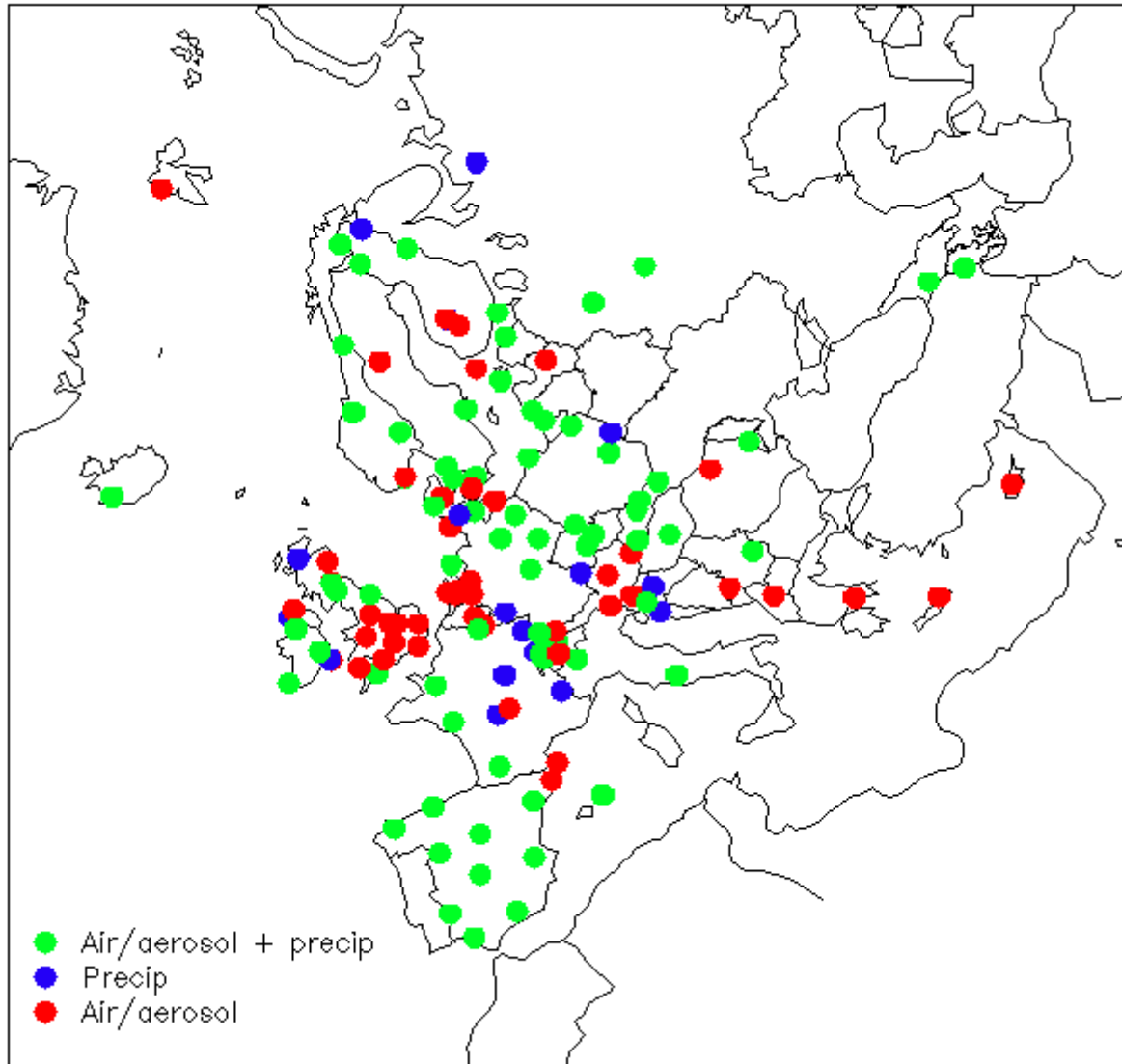 in a semi-rural area at the NW edge of the Po valley in Italy. The main cities around are Varese (20 km east), Novara (40 km south), Gallarate - Busto Arsizio (about 20 km south-east) and the Milan conurbation (60 km to the south-east). Busy roads and highways link these urban centers. Emissions of pollutants reported for the four industrial large point sources (CO_2 emissions > 1500 tons d^{-1}) located between 5 and 45 km NE to SE from Ispra also include 2 and 3 tons of CO per day, plus 3 and 5 tons of NOx (as NO_2) per day for the 2 closest ones (PRTR emissions, 2010).

Underpinning programs

The EMEP program (*http://www.emep.int/*)

Currently, about 50 countries and the European Community have ratified the CLRTAP. Lists of participating institutions and monitoring stations (Fig. 10) can be found at: *http://www.nilu.no/projects/ccc/network/index.html*

The set-up and running of the JRC-Ispra EMEP station resulted from a proposal of the Directorate General for Environment of the European Commission in Brussels, in agreement with the Joint Research Centre, following the Council Resolution N° 81/462/EEC, article 9, to support the implementation of the EMEP programme.

The JRC-Ispra station operates on a regular basis in the extended EMEP measurement program since November 1985. Data are transmitted yearly to the EMEP Chemical Coordinating Centre (CCC) for data control and statistical evaluation, and available from the EBAS data bank (Emep dataBASe, *http://ebas.nilu.no/*).

The GAW program (*http://www.wmo.int/web/arep/gaw/gaw_home.html*)

WMO's Global Atmosphere Watch (GAW) system was established in 1989 with the scope of providing information on the physico-chemical composition of the atmosphere. These data provide a basis to improve our understanding of both atmospheric changes and atmosphere-biosphere interactions. GAW is one of WMO's most important contributions to atmosphere-biosphere the study of environmental issues, with about 80 member countries participating in GAW's measurement program. Since December 1999, the JRC-Ispra station is also part of the GAW coordinated network of regional stations. Aerosol data submitted to EMEP and GAW are available from the World Data Centre for Aerosol (WDCA).
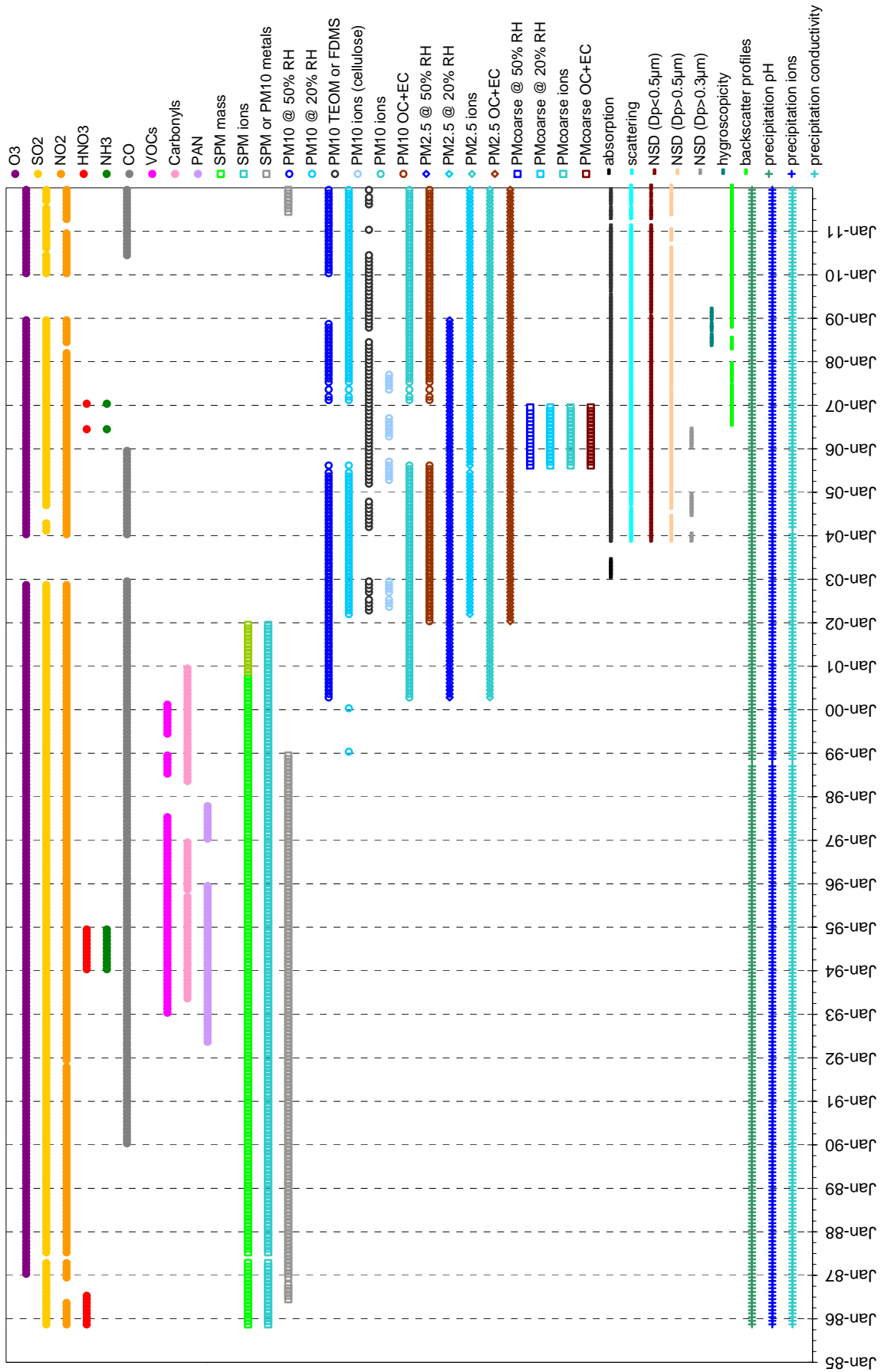
Fig. 11. *Measurements performed at the JRC-Ispra station for atmospheric research since 1985.*

The institutional program (***http://ccaqu.jrc.ec.europa.eu***)

Since 2002, the measurement program of the air pollution monitoring station of JRC-Ispra has gradually been focused on short-lived climate forcers such as tropospheric ozone and aerosols, and their precursors (Fig. 11). Concretely, more sensitive gas monitors were introduced, as well as a set of new measurements providing aerosol characteristics that are linked to radiative forcing. In 2012, the station's duty as listed in the Airclim action work plan was to deliver "data on regulated and non-regulated pollutants delivered to EMEP and the World Data Centre for Aerosols international databases"

The site is also being used for research and development purposes. Regarding particulate organic and elemental carbon, techniques developed in Ispra are implemented and validated by international research station networks (EUSAAR, ACTRIS), recommended in the EMEP sampling and analytical procedure manual, and considered by the European Committee for Standardisation (CEN) as possible future standard methods.

Additional information about the JRC-Ispra air monitoring station and other stations from the EMEP network can also be found in the following papers: Van Dingenen et al., 2004; Putaud et al., 2004; Mira-Salama et al., 2008; Putaud et al., 2010). Nowadays, all validated monitoring data obtained at the JRC-Ispra station within the EMEP and the GAW program and other international projects (EUSAAR, ACTRIS) can be retrieved from the EBAS database (*http://ebas.nilu.no/*), selecting Ispra as the station of interest.

Table 1. Parameters measured during 2011

| METEOROLOGICAL PARAMETERS	Pressure, temperature, humidity, wind, solar radiation
GAS PHASE	SO_2, NO, NO_X, O_3, CO
PARTICULATE PHASE	For $PM_{2.5}$: PM mass and Cl^-, NO_3^-, SO_4^{2-}, $C_2O_4^{2-}$, Na^+, NH_4^+, K^+, Mg^{2+}, Ca^{2+}, OC, and EC
	For PM_{10}: PM mass and Cl^-, NO_3^-, SO_4^{2-}, $C_2O_4^{2-}$, Na^+, NH_4^+, K^+, Mg^{2+}, Ca^{2+}, OC, and EC + 31 trace elements (from June)
	Number size distribution (10 nm - 10 µm)
	Aerosol absorption, scattering and back-scattering coefficient
	Altitude-resolved aerosol back-scattering
PRECIPITATION	Cl^-, NO_3^-, SO_4^{2-}, $C_2O_4^{2-}$, Na^+, NH_4^+, K^+, Mg^{2+}, Ca^{2+} pH, conductivity
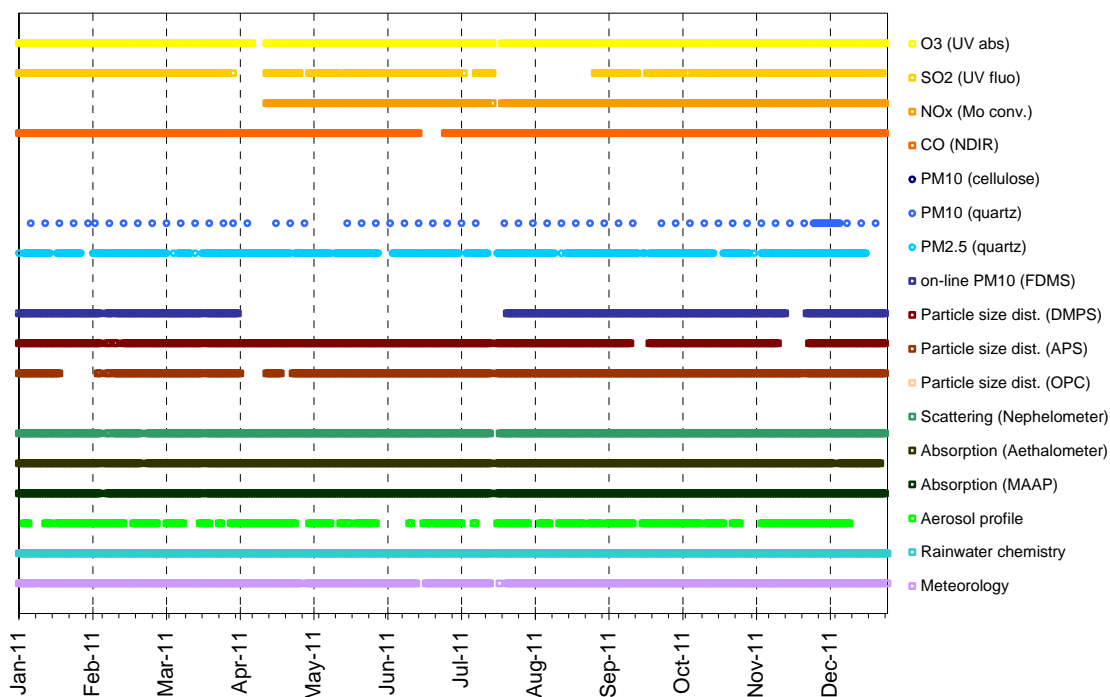
Fig. 12. *The year 2011 data coverage at the JRC EMEP-GAW station.*

Measurements and data processing

The air pollution monitoring program at the JRC- Ispra station in 2011

Since 1985, the JRC-Ispra air monitoring station program evolved significantly (Fig. 11). The variables measured at the JRC-Ispra station in 2011 are listed in Table 1. Fig. 12 shows the data coverage for 2011.

Meteorological parameters were measured during the whole year 2011.

SO_2, O_3 and CO were measured almost continuously during the year 2011 (except for a 40 days gap for SO_2 data from July 20th to August 29th due to instrumental problems). In 2011, NOx was measured continuously from April and onwards. The continuous measurement of CO was performed in 2011 from the complementary nearby JRC greenhouse gas monitoring station located about 900 m away from the ABC-IS station.

Particulate matter (PM2.5) samples were collected daily and analyzed for PM2.5 mass (at 20% RH), main ions, OC (organic carbon) and EC (elemental carbon). PM10 24-hour filter samples were collected every 6th day on average and analyzed in the same way as the daily PM2.5 samples, and for 31 trace elements from June (till July 2012). On-line PM measurements (FDMS-TEOM, Filter Dynamics Measurement System - Tapered Element Oscillating Microbalance) were carried out from 01.01.2010 to 15.07.2010 for PM10 and PM1; thereafter it was PM10 only.

Particle number size distribution (10 nm < Dp < 10 μm), aerosol absorption coefficient and scattering coefficient were measured continuously over the whole year 2011.

The LiDAR (Light Detection and Ranging) provided altitude resolved aerosol backscattering profiles during favourable weather conditions for all months.

Precipitation was collected throughout the year and analyzed for pH, conductivity, and main ions (collected water volume permitting).

19

Measurement techniques

On-line Monitoring

<u>Meteorological Parameters</u>

Meteorological data and solar radiation were measured directly at the EMEP station with the instrumentation described below.

WXT510 (S/N: A1410009 & A1410011)

Two WXT510 weather transmitters from <u>Vaisala</u> recorded simultaneously the six weather parameters temperature, pressure, relative humidity, precipitation and wind speed and direction from the top of a 10 m high mast.

The wind data measurements utilise three equally spaced ultrasonic transducers that determine the wind speed and direction from the time it takes for ultrasound to travel from one transducer to the two others. The precipitation is measured with a piezoelectrical sensor that detects the impact of individual raindrops and thus infers the accumulated rainfall. For the pressure, temperature and humidity measurements, separate sensors employing high precision RC oscillators are used.

CM11 (S/N: 058911) & CMP 11 (S/N: 070289)

To determine the solar radiation, a <u>Kipp and Zonen</u> CM11 was used. From 23.06.2008 and onwards an additional CMP11 Pyranometer have been installed that measures the irradiance (in W/m^2) on a plane surface from direct solar radiation and diffuse radiation incident from the hemisphere above the device. Both devices are ca. 1.5 m above the ground. The measurement principle is based on a thermal detector. The radiant energy is absorbed by a black disc and the heat generated flows through a thermal resistance to a heat sink. The temperature difference across the thermal resistance is then converted into a voltage and precisely measured. Both the CM11 & CMP11 feature a fast response time of 12 s, a small non stability of +/-0.5 % and a small non linearity of +/-0.2 %.

<u>Gas Phase Air Pollutants</u>

Sampling

SO_2, NO, NO_x and O_3 are sampled from a common inlet situated at about 3.5 m above the ground on the roof of the gas phase monitors' container (Fig. 13). The sampling line consists in an inlet made of a PVC semi-spherical cap (to prevent rain and bugs to enter the line), a PTFE tube (inner diameter = 2.7 cm, height = 150 cm), and a "multi-channel distributor" glass tube, with nine 14 mm glass connectors. This inlet is flushed by an about 60 L min^{-1} flow with a fan-coil (*measured with RITTER 11456*). Each instrument samples from the glass tube with its own pump through a 0.25 inch Teflon line and a 5 μm pore size 47 mm diameter Teflon filter (to eliminate particles from the sampled air).

CO was sampled from an 15 meter high mast located about 900 meter from the EMEP-GAW station at the JRC-Ispra greenhouse gas monitoring station (45.807°N, 8.631°E, 223 m asl).

SO_2: UV Fluorescent SO_2 Analyser

Thermo 43C TL (S/N 0401904668)

At first, the air flow is scrubbed to eliminate aromatic hydrocarbons. The sample is then directed to a chamber where it is irradiated at 214 nm (UV), a wavelength where SO_2 molecules absorb. The fluorescence signal emitted by the excited SO_2 molecules going back to the ground state is filtered between 300 and 400 nm (specific of SO_2) and amplified by a photomultiplier tube. A microprocessor receives the electrical zero and fluorescence reaction intensity signals and calculates SO_2 based on a linear calibration curve.

Calibration was performed with a certified SO_2 standard at a known concentration in N_2. Zero check was done, using a zero air gas cylinder from Air Liquide, Alphagaz 1, CnHm < 0.5 ppm).

The specificity of the trace level instrument (TEI 43C-TL) is that it uses a pulsed lamp. The 43C-TL's detection limit is 0.2 ppb (about 0.5 μg m^{-3}) according to the technical specifications.

For more details about the instrument, the manual for the instrument is available on \\Ccunas3\largefacilities\ABC-IS\Quality_management\Manuals
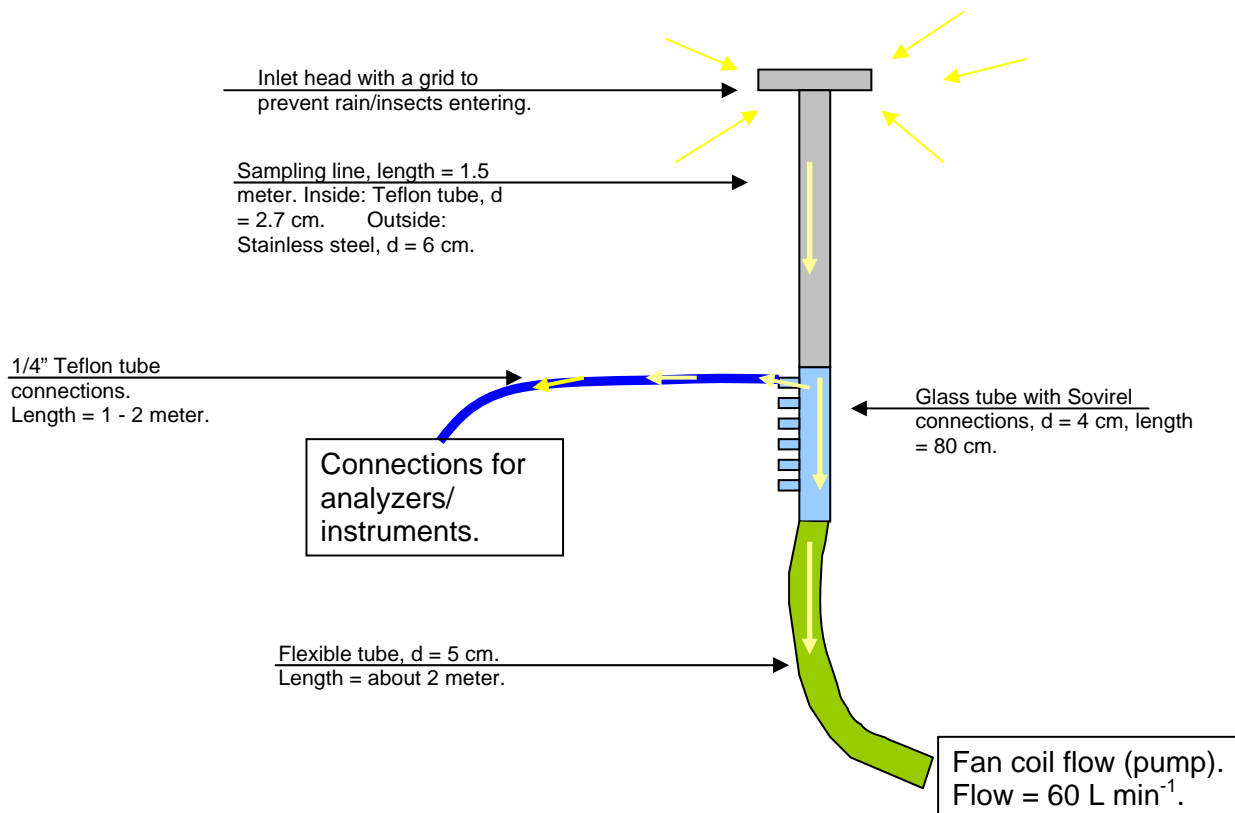
Inlet head with a grid to prevent rain/insects entering.

Sampling line, length = 1.5 meter. Inside: Teflon tube, d = 2.7 cm.   Outside: Stainless steel, d = 6 cm.

1/4" Teflon tube connections. Length = 1 - 2 meter.

Connections for analyzers/ instruments.

Glass tube with Sovirel connections, d = 4 cm, length = 80 cm.

Flexible tube, d = 5 cm. Length = about 2 meter.

Fan coil flow (pump). Flow = 60 L min^{-1}.

Fig. 13. *Sampling inlet system for the gases SO$_2$, NO,, NO$_x$ and O$_3$.*

In 2011, the gas phase monitors were calibrated about every month with suitable span gas cylinders and zero air (see below for more details). Sampling flow rates are as follow:

Compounds	Flow rates (L min^{-1})
SO$_2$	0.5
NO, NO$_x$	0.6
O$_3$	0.7
CO	1.5

NO + NO$_X$: Chemiluminescent Nitrogen Oxides Analyzer (NO$_2$=NO$_x$-NO)

Thermo 42C (S/N 62581-336 and S/N 0401304317)

This nitrogen oxide analyser is based on the principle that nitric oxide (NO) and ozone react to produce excited NO$_2$ molecules, which emit infrared photons when going back to lower energy states:

$$NO + O_3 \rightarrow [NO_2]^* + O_2 \rightarrow NO_2 + O_2 + h\nu$$
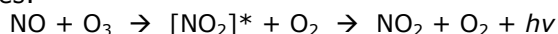
A stream of purified air (dried with a Nafion Dryer) passing through a silent discharge ozonator generates the ozone concentration needed for the chemiluminescent reaction. The specific luminescence signal intensity is therefore proportional to the NO concentration. A photomultiplier tube amplifies this signal.
NO$_2$ is detected as NO after reduction in a Mo converter heated at about 325 °C.
The ambient air sample is drawn into the analyzer, flows through a capillary, and then to a valve, which routes the sample either straight to the reaction chamber (NO detection), or through the converter and then to the reaction chamber (NO$_X$ detection). The calculated NO and NO$_X$ concentrations are stored and used to calculate

21

NO$_2$ concentrations (NO$_2$ = NO$_x$ - NO), assuming that only NO$_2$ is reduced in the Mo converter.

Calibration was performed using a zero air gas cylinder (Air Liquide, Alphagaz 1, CnHm<0.5 ppm) and a NO span gas. Calibration with a span gas was performed with a certified NO standard at a known concentration in N$_2$.

For more details about the instrument, the manual for the instrument is available on \\Ccunas3\largefacilities\ABC-IS\Quality_management\Manuals

O$_3$:   *UV Photometric Ambient Analyzer*

Thermo 49C (S/N 55912-305 and S/N 0503110499)

The UV photometer determines ozone concentrations by measuring the absorption of O$_3$ molecules at a wavelength of 254 nm (UV light) in the absorption cell, followed by the use of Bert-Lambert law. The concentration of ozone is related to the magnitude of the absorption. The reference gas, generated by scrubbing ambient air, passes into one of the two absorption cells to establish a zero light intensity reading, I$_0$. Then the sample passes through the other absorption cell to establish a sample light intensity reading, I. This cycle is reproduced with inverted cells. The average ratio R=I/I$_0$ between 4 consecutive readings is directly related to the ozone concentration in the air sample through the Beer-Lambert law. Calibration is performed using externally generated zero air and external span gas. Zero air is taken from a gas cylinder (Air Liquide, Alphagaz 1, CnHm < 0.5 ppm). Span gas normally in the range 50 - 100 ppb is generated by a TEI 49C-PS transportable primary standard ozone generator (S/N 0503110396) calibrated/check by ERLAP (European Reference Laboratory of Air Pollution) and/or TESCOM annually.

For more details about the instrument, the manual for the instrument is available on \\Ccunas3\largefacilities\ABC-IS\Quality_management\Manuals
A Nafion Dryer system is connected to the O$_3$ instruments.

CO: *Non-Dispersive Infrared Absorption CO Analyzer*

Horiba AMPA-370 (S/N WYHEOKSN)

In 2011, carbon monoxide (CO) has been continuously monitored using a commercial Horiba AMPA-370 CO monitor based on the principle of non-dispersive infrared absorption (NDIR). The Horiba APMA-370 uses solenoid valve cross flow modulation applying the same air for both the sample and the reference, instead of the conventional technique to apply an optical chopper to obtain modulation signals. With this method the reference air is generated by passing the sample air over a heated oxidation catalyst to selectively remove CO which is then directly compared to the signal of the untreated sample air at a 1 Hz frequency. The result is a very low zero-drift and stable signal over long periods of time.

To reduce the interference from water vapor to about 1% the sample air was dried to a constant low relative humidity level of around 30% applying a Nafion dryer (Permapure MD-070-24P) tube in the inlet stream. The instrument was calibrated every 2-3 months against two primary NOAA standards based on the NOAA/WMO-2004 scale of 500 and 750 ppbv CO in dry air with an uncertainty of 0.7% (29 L Luxfer aluminum cylinders). In addition we applied a working standard at regular time intervals calibrated against the WMO/NOAA tanks with an initial CO concentration of 1030 ±10 ppbv in dry air in (30 L Luxfur aluminum cylinder). Automatic instrument zero checks were performed every 72 h feeding dry zero air (lab. air treated with Silica Gel, Molecular Sieve 4 A°, Sofnocat 514 (platinum, palladium and tin oxide coated spheres) at room temperature) to the zero air inlet of the monitor, which is further treated by an internal Horiba CO-scrubber containing Hopcalite (copper manganese oxide coated spheres) capable of removing CO from under dry conditions at room temperature. The detection limit of the Horiba AMPA-370 is ~20 ppbv for a one minute sampling interval, and the overall measurement uncertainty is estimated to be ±5%, which includes the uncertainty of the calibration standards, the H$_2$O interference, and the instrument precision (~2%).

Additional information (e.g. "manuals", calibrations and standards, etc.) can be found at \\Pb2\NEWLabData\LabData\Quality_Management\GHG-Station_equipment_manuals, and \\Pb2\NEWLabData\LabData\Quality_Management\GHG-Station_calibration_maintenance

Atmospheric Particles

Sampling conditions

Since 2008, all instruments for the physical characterization of aerosols (Aethalometer, Nephelometer, Aerodynamic Particle Sizer, Differential Mobility Particle Sizer) sample isokinetically from nn inlet pipe (Aluminium), diameter = 15 cm, length of horizontal part ~280 cm and vertical part ~220 cm (seeJensen et al., 2010) The Tapered Element Oscillating Mass balance (FDMS-TEOMs) and the Multi-Angle Absorption Photometer (MAAP) use their own inlet systems.

The size dependent particle losses along the pipe radius were determined by measuring the ambient aerosol size distribution with two DMPS at the sampling points P0 and P2 for different radial positions relative to the tube centre (0, 40 and 52 mm) at P2 (Gruening et al., 2009). Data show a small loss of particles towards the rim of the tube can be observed, but it stays below 15 %. The bigger deviation for particles smaller than 20 nm is again a result of very small particle number concentrations in this diameter range and thus rather big counting errors.

PM10 mass concentration: Tapered Element Oscillating Mass balance (TEOM), Series 1400a

Thermo FDMS – TEOM (S/N 140AB233870012 & 140AB253620409)

The Series 1400a TEOM® monitor incorporates an inertial balance patented by Rupprecht & Patashnick, now Thermo. It measures the mass collected on an exchangeable filter cartridge by monitoring the frequency changes of a tapered element. The sample flow passes through the filter, where particulate matter is collected, and then continues through the hollow tapered element on its way to an electronic flow control system and vacuum pump. As more mass collects on the exchangeable filter, the tube's natural frequency of oscillation decreases. A *direct* relationship exists between the tube's change in frequency and mass on the filter. The TEOM mass transducer does not require recalibration because it is designed and constructed from non-fatiguing materials. However, calibration is yearly verified using a filter of known mass.

The instrument set-up includes a Sampling Equilibration System (SES) that allows a water strip-out without sample warm up by means of Nafion Dryers. In this way the air flow RH is reduced to < 30%, when TEOM® operates at 30 °C only. The Filter Dynamic Measurement System (FDMS) is based on measuring changes of the TEOM filter mass when sampling alternatively ambient and filtered air. The changes in the TEOM filter mass while sampling filtered air is attributed to sampling (positive or negative) artefacts, and is used to correct changes in the TEOM filter mass observed while sampling ambient air.

Particle number size distribution: Differential Mobility Particle Sizer (DMPS)

DMPS "B, DMA serial no. 158", CPC TSI 3010 (S/N 2051), CPC TSI 3772 (S/N 70847419), neutraliser ^{85}Kr 10 mCi (2007)

The Differential Mobility Particle Sizer consists in a home-made medium size (inner diameter 50 mm, outer diameter 67 mm and length 280 mm) Vienna-type Differential Mobility Analyser (DMA) and a Condensation Particle Counter (CPC), TSI 3010 (S/N 2051) or TSI 3772 (S/N 70847419). Its setup follows the EUSAAR specifications for DMPS systems.

DMA's use the fact that electrically charged particles move in an electric field according to their electrical mobility. Electrical mobility depends mainly on particle size and electrical charge. Atmospheric particles are brought in the bipolar charge equilibrium in the bipolar diffusion charger (Eckert & Ziegler neutralizer with 370 MBq): a radioactive source (^{85}Kr) ionizes the surrounding atmosphere into positive and negative ions. Particles carrying a high charge can discharge by capturing ions of opposite polarity. After a very short time, particles reach a charged equilibrium such that the aerosol carries the bipolar Fuchs-Boltzman charge distribution. A computer program sets stepwise the voltage between the 2 DMA's electrodes (from 10 to 11500 V). Negatively charged particles are so selected according to their mobility. After a certain waiting time, the CPC measures the number concentration for each mobility bin. The result is a particle mobility distribution. The number size distribution is calculated from the

mobility distribution by an inversion routine (from Stratmann and Wiedensohler, 1996) based on the bipolar charge distribution and the size dependent DMA transfer function. The DMPS measured aerosol particles in the range 10 – 600 nm during an 8 minute cycle until 12.06.2009 and afterwards in the range 10 to 800 nm with a 10 minute cycle. It records data using 45 size channels for high-resolution size information. This submicrometer particle sizer is capable of measuring concentrations in the range from 1 to 2.4 x 10^6 particles cm^{-3}. Instrumental parameters that are necessary for data evaluation such as flow rates, relative humidity, ambient pressure and temperature are measured and saved as well.

The CPC detection efficiency curve and the particle diffusion losses in the system are taken into account at the data processing stage.

Accessories include:
- FUG High voltage cassette power supplies Series HCN7E – 12500 Volts.
- Rotary vacuum pump vane-type (sampling aerosol at 1 LPM)
- Controlled blower (circulating dry sheath air)
- Sheath air dryer only using silica gel until 27.10.2009, thereafter sheath and sample air dryer using Nafion dryer; this mean that the DMPS started to sample in dry conditions from 27 October 2009 onwards.
- Mass flow meter and pressure transducer (to measure sheath air and sample flows).

Particle number size distribution: Aerodynamic Particle Sizer (APS)

APS TSI 3321 (S/N 70535014)

The APS 3321 is a time-of-flight spectrometer that measures the velocity of particles in an accelerating air flow through a nozzle.

Ambient air is sampled at 1 L min^{-1}, sheath air (from the room) at 4 L min^{-1}. In the instrument, particles are confined to the center-line of an accelerating flow by sheath air. They then pass through two broadly focused laser beams, scattering light as they do so. Side-scattered light is collected by an elliptical mirror that focuses the collected light onto a solid-state photodetector, which converts the light pulses to electrical pulses. By electronically timing between the peaks of the pulses, the velocity can be calculated for each individual particle.

Velocity information is stored in 1024 time-of-flight bins. Using a polystyrene latex (PSL) sphere calibration, which is stored in non-volatile memory, the APS Model 3321 converts each time-of-flight measurement to an aerodynamic particle diameter. For convenience, this particle size is binned into 52 channels (on a logarithmic scale).

The particle range spanned by the APS is from 0.5 to 20 µm in both aerodynamic size and light-scattering signal. Particles are also detected in the 0.3 to 0.5 µm range using light-scattering alone, and are binned together in one channel. The APS is also capable of storing correlated light-scattering-signal. *dN/dLogDp* data are averaged over 10 min.

Particle scattering and back-scattering coefficient

Nephelometer TSI 3563 (S/N 1081)

The integrating nephelometer is a high-sensitivity device capable of measuring the scattering properties of aerosol particles. The nephelometer measures the light scattered by the aerosol and then subtracting light scattered by the walls of the measurement chamber, light scattered by the gas, and electronic noise inherent in the detectors.

Dried ambient air is sampled at 5.3 L min^{-1} since 18.11.2009 from a PM10 inlet. .

The three-color detection version of TSI nephelometer detects scattered light intensity at three wavelengths (450, 550, and 700 nm). Normally the scattered light is integrated over an angular range of 7–170° from the forward direction, but with the addition of the backscatter shutter feature to the Nephelometer, this range can be adjusted to either 7–170° or 90–170° to give total scatter and backscatter signals. A 75 Watt quartz-halogen white lamp, with a built-in elliptical reflector, provides illumination for the aerosol. The reflector focuses the light onto one end of an optical pipe where the light is carried into the internal cavity of the instrument. The optical pipe is used to thermally isolate the lamp from the sensing volume. The output end of the optical light pipe is an opal glass diffuser that acts as a *quasi*-cosine (Lambertian) light source. Within the measuring volume, the first aperture on the detection side of the instrument limits the light integration to angles greater than 7°, measured from the horizontal at the opal glass. On the other side, a shadow plate limits the light to

angles less than 170°. The measurement volume is defined by the intersection of this light with a viewing volume cone defined by the second and fourth aperture plates on the detection side of the instrument. The fourth aperture plate incorporates a lens to collimate the light scattered by aerosol particles so that it can be split into separate wavelengths. The nephelometer uses a reference chopper to calibrate scattered signals. The chopper makes a full rotation 23 times per second. The chopper consists of three separate areas labelled: signal, dark, and calibrate.

The signal section simply allows all light to pass through unaltered. The dark section is a very black background that blocks all light. This section provides a measurement of the photomultiplier tube (PMT) background noise. The third section is directly illuminated this section to provide a measure of lamp stability over time. To reduce the lamp intensity to a level that will not saturate the photomultiplier tubes, the calibrate section incorporates a neutral density filter that blocks approximately 99.9 % of the incident light. To subtract the light scattered by the gas portion of the aerosol, a high-efficiency particulate air (HEPA) filter is switched in line with the inlet for 300 s every hour. This allows compensation for changes in the background scattering of the nephelometer, and in gas composition that will affect Rayleigh scattering of air molecules with time. When the HEPA filter is not in line with the inlet, a small amount of filtered air leaks through the light trap to keep the apertures and light trap free of particles. A smaller HEPA filter allows a small amount of clean air to leak into the sensor end of the chamber between the lens and second aperture. This keeps the lens clean and confines the aerosol light scatter to the measurement volume only.

Nephelometer data are corrected for angular non idealities and truncation errors according to Anderson and Ogren, 1998. From 18.11.2009 onwards, a Nafion dryer has been installed at the inlet to measure dry aerosols. Internal RH ranged from 0 to 50 % (average 18%, 99th percentile 41%), with values > 40% occurring between June 30th and July 22nd. At 40% RH, aerosol scattering is on average increased by 20% compared to 0% RH in Ispra (Adam et al., 2011, in preparation). However, aerosol particle scattering coefficients presented in this report are **not** corrected for RH effects, except when specified.

Particle absorption coefficient

Aethalometer Magee AE-31 ('A' S/N 408: 0303 & 'B' S/N 740:0609)

The principle of the Aethalometer is to measure the attenuation of a beam of light transmitted through a filter, while the filter is continuously collecting an aerosol sample. Suction is provided by an internally-mounted pump. Attenuation measurements are made at successive regular intervals of a time-base period. The objectives of the Aethalometer hardware and software systems are as follows:

(a) to collect the aerosol sample with as few losses as possible on a suitable filter material;

(b) to measure the optical attenuation of the collected aerosol deposit as accurately as possible;

(c) to calculate the rate of increase of the equivalent black carbon (EBC) component of the aerosol deposit and to interpret this as an EBC concentration in the air stream;

(d) to display and record the data, and to perform necessary instrument control and diagnostic functions.

The optical attenuation of the aerosol deposit on the filter is measured by detecting the intensity of light transmitted through the spot on the filter. In the AE-31, light sources emitting at different wavelengths (370, 470, 520, 590, 660, 880 and 950 nm) are also installed in the source assembly. The light shines through the lucite aerosol inlet onto the aerosol deposit spot on the filter. The filter rests on a stainless steel mesh grid, through which the pumping suction is applied. Light penetrating the diffuse mat of filter fibers can also pass through the spaces in the support mesh. This light is then detected by a photodiode placed directly underneath the filter support mesh. As the EBC content of the aerosol spot increases, the amount of light detected by the photodiode will diminish.

For better accuracy, further measurements are necessary: the amount of light penetrating the combination of filter and support mesh is relatively small, and a correction is needed for the 'dark response signal' of the overall system. This is the electronics' output when the lamps are off: typically, it may be a fraction of a percent of the response when the lamps are on. To eliminate the effect of the dark response, we take 'zero' readings of the system response with the lamps turned off, and subtract this 'zero' level from the response when the lamps are on.

The other measurement necessary is a 'reference beam' measurement to correct for any small changes in the light intensity output of the source. This is achieved by a second photodiode placed under a different portion of the filter that is not collecting the aerosol, on the left-hand side where the fresh tape enters. This area is illuminated by the same lamps. If the light intensity output of the lamps changes slightly, the response of this detector is used to mathematically correct the 'sensing' signal. The reference signal is also corrected for dark response 'zero' as described above.

The algorithm in the computer program (see below) can account for changes in the lamp intensity output by always using the ratio quantity [Sensing]/[Reference]. As the filter deposit accumulates EBC, this ratio will diminish.

In practice, the algorithm can account for lamp intensity fluctuations to first order, but we find a residual effect when operating at the highest sensitivities. To minimize this effect and to realize the full potential of the instrument, it is desirable for the lamps' light output intensity to remain as constant as possible from one cycle to the next, even though the lamps are turned on and off again. The computer program monitors the repeatability of the reference signal, and issues a warning message if the fluctuations are considered unacceptable. When operating properly, the system can achieve a reference beam repeatability of better than 1 part in 10000 from one cycle to the next. The electronics circuit board converts the optical signals directly from small photocurrents into digital data, and passes it to the computer for calculation. A mass flow meter monitors the sampled air flow rate. These data and the result of the EBC calculation are written to disk and displayed on the front panel of the instrument.

Aethalometer data are corrected for the shadowing effect and for multiple-scattering in the filter to derive the aerosol absorption coefficient (Arnott et al., 2005) with a correction factor C = 3.65 for green light.

Multi Angle Absorption Photometer (S/N 4254515)

A new Multi Angle Absorption Photometer (MAAP) model 5012 from Thermo Scientific has been installed at the EMEP station in September 2008 and provides equivalent black carbon concentrations (EBC) and aerosol absorption (α) data at a nominal wavelength of 670 nm. Note that during a EUSSAR workshop (www.eusaar.org) in 2007 it has been observed that the operating wavelength of all MAAP instruments present at that workshop was 637 nm with a line width of 18 nm fwhm. The operating wavelength of this MAAP instrument has not been measured yet, therefore it is assumed to work at 670 nm as stated by the manufacturer.

The MAAP is based on the principle of aerosol-related light absorption and the corresponding atmospheric equivalent black carbon (EBC) mass concentration. The Model 5012 uses a multi angle absorption photometer to analyze the modification of scattering and absorption in the forward and backward hemisphere of a glass-fibre filter caused by deposited particles. The internal data inversion algorithm of the instrument is based on a radiation transfer model and takes multiple scattering processes inside the deposited aerosol and between the aerosol layer and the filter matrix explicitly into account (see Petzold et al., 2004).

The sample air is drawn into the MAAP and aerosols are deposited onto the glass fibre filter tape. The filter tape accumulates the aerosol sample until a threshold value is reached, then the tape is automatically advanced. Inside the detection chamber (Fig. 14), a 670-nanometer light emitting diode is aimed towards the deposited aerosol and filter tape matrix. The light transmitted into the forward hemisphere and reflected into the back hemisphere is measured by a total of five photo-detectors. During sample accumulation, the light intensities at the different photo-detectors change compared to a clean filter spot. The reduction of light transmission, change in reflection intensities under different angles and the air sample volume are continuously measured during the sample period. With these data and using its proprietary radiation transfer scheme, the MAAP calculates the equivalent black carbon concentration (EBC) as the instruments measurement result.

Using the specific absorption cross section σ_{BC} = 6.6 m^2/g of equivalent black carbon at the operation wavelength of 670 nm, the aerosol absorption (α) at that wavelength can be readily calculated as:

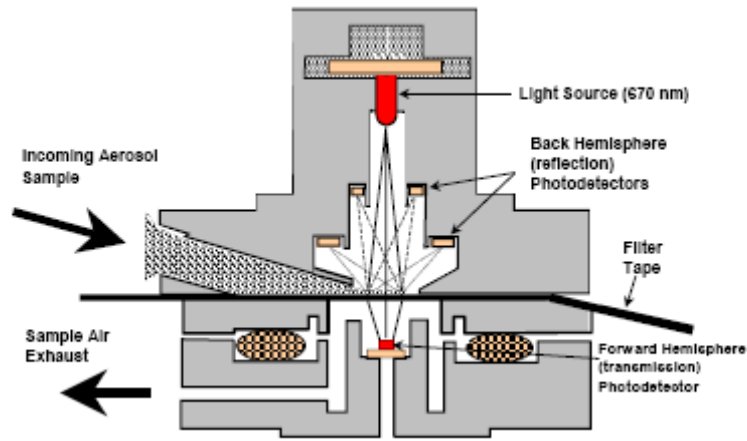$$\alpha = EBC \times \sigma_{BC} \qquad \textit{Eq. 1}$$

Fig. 14. MAAP detection chamber (sketch from the manual of the instrument).

Range-resolved aerosol backscattering, extinction and aerosol optical thickness

Cimel Aerosol Micro Lidar (CAML) CE 370-2 (laser & electronics: S/N 0507-846 and telescope: S/N 0507- 847)

In 2006, an aerosol backscatter LIDAR instrument (LIght Detection And Ranging) has been installed at the EMEP-GAW station for the range-resolved optical remote sensing of aerosols. It serves to bridge the gap between local, in-situ measurements of aerosols at the ground and satellite based characterizations of the aerosol column above ground. To reach this, altitude resolved aerosol backscattering, aerosol extinction and the aerosol optical thickness (AOT) are derived from LIDAR data with high time resolution.

LIDAR measurements are based on the time resolved detection of the backscattered signal of a short laser pulse that is sent into the atmosphere (for an introduction see Weitkamp, C., 2005). Using the speed of light, time is converted to the altitude where the backscattering takes place. Utilising some assumptions about the atmospheric composition, aerosol backscattering and extinction coefficients as well as aerosol optical thickness can be derived using the LIDAR equation. The received power P of the detector is therein given as a function of distance and wavelength by *Eq. 2*:

$$P(R,\lambda) = P_0 \, {}^{c\tau}\!/_{2} \, A\eta \, \frac{O(R)}{R^2} \, \beta(R,\lambda) \exp\left(-2\int_{0}^{R} \alpha(r,\lambda)dr\right)$$

Eq. 2: P_0: Power of the laser pulse, c: speed of light, τ: laser pulse length, A: area of the telescope, η: system efficiency, R: distance, O: overlap function (between laser beam and receiving optics field of view), λ: wavelength, β: backscatter coefficient, α: absorption coefficient

LIDAR measurements were performed with a Cimel Aerosol Micro Lidar (CAML) during the year 2011 (see Fig. 12). CAML is an eye-safe, single-wavelength, monostatic aerosol backscatter lidar. The lidar emitter is a diode pumped, frequency doubled Nd:YAG laser operating at a wavelength of 532 nm, with a repetition rate of 4.7 kHz, pulse energy of 8 μJ/pulse and a width of the laser pulse of less than 15 ns. The short integration time of the detector of 100 ns allows for a vertical resolution of 15 m. With 2048 time bins of the detector, the maximum altitude is ~30 km. However, depending on the actual atmospheric conditions and the quality of signal to noise ratio (SNR), the vertical limit for probing the atmosphere usually goes up to 15 km. Eye-safety of the system is reached by expanding the laser beam trough a 20 cm diameter, 1 m focal length refractive telescope. The emission and reception optical paths coincide through a single, 10 m long optical fibre that connects both the laser output and receiving detector with the telescope. The telescope field of view is approximately 50 µrad. The backscatter signal is sent to the receiver passing through a narrow band-pass interference filter (0.2 nm fwhm, centred at 532 nm) to reduce the background level. To avoid saturation of the detector immediately after the laser pulse is emitted and thus reduce the afterpulse signal, an acousto-optical modulator is placed before the

detector that blocks the light from the detector that is directly backscattered from optical components in the light path. The detector is an avalanche photodiode photon-counting module with a high quantum efficiency approaching 55 % with maximum count rates near 20 MHz.

Data evaluation is done with an inversion algorithm based on an iteration-convergence method for the LIDAR equation (see *Eq. 2*) that has been implemented in-house using the MATLAB programming environment. Starting with the CAML raw data, the 10 minutes time averages of the backscatter profiles are space–averaged over 60 m. Then the background signal (including afterpulse component) is subtracted. The afterpulse component originates from light that is scattered back to the detector from all surfaces on the optical path to the telescope. As its intensity is rather high compared to the atmospheric backscatter, it influences the raw detector signal. Furthermore, the overlap function O(R) (see *Eq. 2*) is applied to the data before it is range corrected, i.e. multiplied by R^2. The shape of this overlap function varied significantly and thus gives rise to a potentially large error in the evaluation of the lidar data. The range corrected signal constitutes the level 0 data.

Usually, the US standard atmosphere is used to calibrate the molecular backscattering in an aerosol free region and an assumed LIDAR ratio (i.e. extinction-to-backscatter ratio) that is constant with height is used to retrieve the aerosol backscatter, extinction and optical thickness (AOT) profiles (provided as level 1 data). During 2011, the molecular extinction and backscatter profiles are computed using radiosonde measurements (launched at Linate airport) for air number of molecules. The Lidar Ratio (LR) is determined using as a constraint the AOT measured by sun photometer. The mean (median) estimate of the LIDAR ratios (LR = Lidar Ratios) that have been used for the data inversion was LR = 29.73 sr (with median = 22).

In 2011, the Lidar measurement program was "running for 20 min, and off for 2 min". This cycle 22 min-cycle was repeated continuously during favourable weather conditions, i.e. no precipitation and no cloud coverage that would absorb the laser pulse and thus prevent meaningful aerosol LIDAR measurements.

Sampling and off-line analyses

Particulate Matter

PM2.5 from quartz fibre filters

PM2.5 was continuously sampled at 16.7 L min^{-1} on quartz fibre filters with a Partisol sampler equipped with carbon honeycomb denuder. The sampled area is 42 mm. Filters were from PALL Life Sciences (type TISSUEQUARTZ 2500QAT-UP). Filter changes occurred daily at 08:00 UTC.

Filters were weighed at 20 % RH before and after exposure with a microbalance Sartorius MC5 placed in a controlled (dried or moisture added and scrubbed) atmosphere glove box. They were stored at 4 °C until analysis.

Main ions (Cl^-, NO_3^-, SO_4^{2-}, $C_2O_4^{2-}$, Na^+, NH_4^+, K^+, Mg^{2+}, Ca^{2+}) were analysed by ion chromatography (Dionex DX 120 with electrochemical eluent suppression) after extraction of the soluble species in an aliquot of 16 mm Ø in 20 ml 18.2 MOhm cm resistivity water (Millipore mQ).

Organic and elemental carbon (OC+EC) were analysed using a Sunset Dual-optical Lab Thermal-Optical Carbon Aerosol Analyser (S/N 173-5). PM2.5 samples were analysed using the EUSAAR-2 thermal protocol that has been developed to minimize biases inherent to thermo-optical analysis of OC and EC (Cavalli et al., 2010):

Fraction Name Sunset Lab.	Plateau Temperature (°C)	Duration (s)	Carrier Gas
OC 1	200	120	He 100%
OC 2	300	150	He 100%
OC 3	450	180	He 100%
OC 4	650	180	He 100%
cool down		30	He 100%
EC1	500	120	He:O_2 98:2
EC2	550	120	He:O_2 98:2
EC3	700	70	He:O_2 98:2
EC4	850	80	He:O_2 98:2

PM10 from quartz fibre filters

PM10 was usually sampled every 6th day for a 24 h period at 16.7 L min^{-1} on quartz fibre filters (TISSUEQUARTZ 2500QAT-UP) with a Partisol Plus 2025 sampler using a PM10 sampling head (in total 48 filters in 2010) without denuder. Filter preparation and analysis has been performed exactly as described above for PM2.5 samples to check for differences in the chemical composition of coarse particles compare to PM2.5. In total, 49 filters have been sampled and analyzed for 2011.

Wet-only deposition

For the precipitation collection, two Eigenbrodt wet-only samplers (S/N 3311 and 3312) were used that automatically collect the rainfall in a 1 L polyethylene container. The collection surface is 550 cm^2. 24-hr integrated precipitation samples (if any) are collected every day starting at 8:00 UTC. All collected precipitation samples were stored at 4 °C until analyses (ca. every 3 months).
Analyses include the determinations of pH and conductivity at 25 °C with a Sartorius Professional Meter PP-50 and principal ion concentrations (Cl$^-$, NO$_3^-$, SO$_4^{2-}$, C$_2$O$_4^{2-}$, Na$^+$, NH$_4^+$, K$^+$, Mg^{2+}, Ca^{2+}) by ion chromatography (Dionex DX 120 with electrochemical eluent suppression).

On-line data acquisition system/data management

The JRC EMEP-GAW station Data Acquisition System (DAS) is a specifically tailored set of hardware and software (implemented by NOS s.r.l), designed to operate instruments, acquire both analog and digital output from instruments and store pre-processed measurement data into a database for further off-line evaluation. The DAS operated and controlled the instrumentation during 2011, and updates regarding manual and automatic calibration of gas monitors (except ozone) were implemented. A standalone program to run the wet samplers was developed and put in production, with the aim to simplify the use of the samplers and allow operator to read data from the last 5 days, without querying the database for samples retrieval.

During this year the development of the H-TDMA software reached the goal to allow the humidification system run. Together with the scanning part of the code, the instrument now is ready for last tunings (hardware and software) before tests.

The software environment of the DAS is Labview 7.1 from National Instruments and the database engine for data storage is Microsoft SQL Server 2008.

The DAS is designed to continuously run the following tasks:

- Start of the data acquisition at a defined time (must be full hour);
- Choose the instruments that have to be handled;
- Define the database path where data will be stored;
- Define the period (10 minutes currently used) for storing averaged data, this is the data acquisition cycle time;
- Obtain data (every 10 seconds currently set) for selected instruments within the data acquisition cycle:
  o For analog instruments (currently only the CM11 and CMP11 Pyranometers), apply the calibration constants to translate the readings (voltages or currents) into analytical values;
  o Send commands to query instruments for data or keep listening the ports for instruments that have self defined output timing;
  o Scan instruments outputs to pick out the necessary data;
- Calculate average values and standard deviations for the cycle period;
- Query instruments for diagnostic data (when available), once every 10 minutes;
- Store all data in a database
  o With a single timestamp for the gas analyzers, FDMS-TEOM and Nephelometer
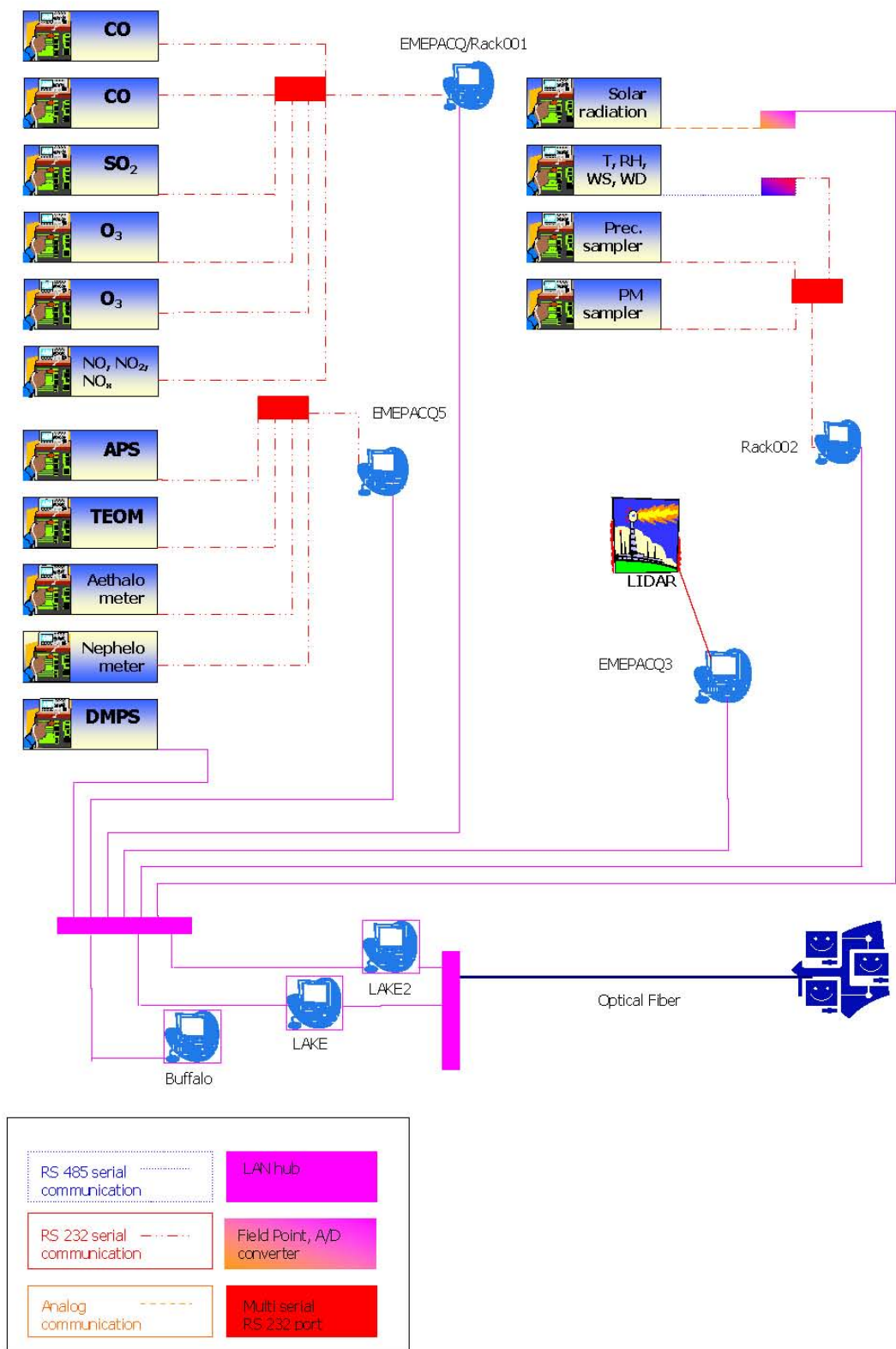 o With the timestamp of their respective measurement for all other instruments.

Fig. 14. *Set-up of the EMEP- GAW station Data Acquisition System.*

The following instruments are managed with the DAS, using two PCs (currently called emepacq2 and emepacq5):

Emepacq5:

- Number size distribution for particles diameter >0.500 µm, APS
- On-line FDMS-TEOMs
- Aerosol light absorption, Aethalometer
- Aerosol light absorption, MAAP
- Aerosol light scattering, Nephelometer

Rack001:

o Reactive gases: CO, SO2, NO, NO_2, NO_x, O_3

Rack002:

- Solar radiation
- Weather transmitter (temperature, pressure, relative humidity, wind speed and direction, precipitation)
- Precipitation data

An additional pc, **Buffalo**, was set-up to manage the near real time data submission to NILU, in the frame of the competitive project EUSAAR and ACTRIS, to submit hourly values of MAAP raw data. The data submission software has been developed and deployed by NOS in Matlab. The software, with an hourly timestamp, retrieves the data from the ABC-IS database, compile a file in ASCII text NASA-Ames 1001 format and save the file on **Lake2**. This pc through an ftp-upload routine uploads the file to NILU. The system is tailored to recover any interruption in the file upload (e.g. network problems, upload failure).

Due to a planned refurbishment of the electrical lines of the Station, performed on July 2011, between 18th and 22nd, the Station shut down. At the reboot, **Emepacq** failed and was replaced with **Rack001**.

A third PC (**emepacq3**) is dedicated to operate the LIDAR system, a fourth PC (**emepdma**) to operate the DMPS and to store its data directly to the database.

Data acquired are stored on the central database e***mep_db*** hosted on the PC **Lake**. The PC "**Lake**" also connects the laboratory to the JRC network (*Eidomain*, later *ccdom,* and then *ies* domain) via optical line. The schematic setup of the data acquisition system is shown in Fig. 14.

The four containers at building 77p that make up the EMEP-GAW station are connected to each others by user configurable point-to-point lines (see Fig. 15).

Through these point-to-point connections, data are exchanged via TCP-IP and RS232 protocols, depending on the instruments connected to the lines.

The acquisition time is locally synchronized for all PCs via a network time server running on lake and is kept at UTC, without adjustment for summer/winter time. Data are collected in a Microsoft SQL Server 2005 database, called ***emep_db*** that runs on "**Lake**".

On March, 2011, the database was moved to a new database server, called **Lake2**. Also with this computer, the back-up is automatically performed twice a day, at 8:00 and at 20:00.

Lake remained as user gateway for the Station user, to allow granted staff remotely access acquisitions pc's. This pc is also used to share information (life cycle sheets, lidar data) between IES domain and bd.77p network.

During this transition, the database had some maintenance: tables beginning with an underscore, used for debugging, and out-dated tables were removed. The database name was also changed, from ***emep_db.db*** it passed to ***abc-is.db***, with the aim of integrating flux towers and greenhouse gases data.

During 2011 the ABC-IS web site was deployed: http://abc-is.jrc.ec.europa.eu/. The aim of this product is to have of the Station presented as whole on the Internet: measurements distributed over different points within the JRC site, also covering different branches of environmental sciences, long-lived greenhouse gases, short-lived pollutants, and biosphere-atmosphere fluxes. The various sets of preliminary data reported on 24 hours window plots, updated every 10 minutes, are publically available.

In the web site the projects to which ABC-IS contributes and contact persons can also be retrieved.

The web site runs over two machines. The first is the web server, **ccuprod2**, in the DMZ (demilitarized zone), where the web page code runs and is managed by the Air and Climate Unit IT staff. The development environment was Python and Ajax. The second computer, **emeimag**, in the JRC network, queries the database for data, generate plots and store plots in a folder in ccuprod2, to make them available to the internet. This second machine is managed by ABC-IS data management team and the software has been developed in C-sharp.

Data evaluation

The structured data evaluation system (EMEP_Main.m) with a graphic user interface (see Fig. 16) has been used with Matlab Release R2007b (www.mathworks.com) as the programming environment. The underlying strategy of the program is:

1) Load the necessary measurement data from all selected instruments from the data acquisition database as stored by the DAS (source database).
2) Apply the necessary individual correction factors, data analysis procedures, etc. specific to each instrument at the time base of the instrument.
3) Perform the calculation of hourly averages for all parameters.
4) Calculate results that require data from more than one instrument.
5) Store hourly averages of all results into a single Microsoft Access database, organized into different tables for gas phase, aerosol phase and meteorological data (save database).

Only the evaluation of gas phase data has an automatic removal algorithm for outliers / spikes implemented: d_i = 10 minute average value at time i, std_i = standard deviation for the 10 minute average (both saved in the raw data)

$$\text{if } std_i > 100 \cdot \overline{std} \text{ and } |d_i - d_{i\pm1}| > 10 \cdot \overline{std}$$

$$\Rightarrow d_i = 1/2\left(d_{i-1} + d_{i+1}\right) \text{ for } d_{i-1} \text{ and } d_{i+1} \text{ no outliers,}$$

otherwise $d_i = missig\ data$.

This algorithm corrects for single point outliers and removes double point outliers. All other situations are considered correct data. To check these data and to exclude outliers for all other measurements, a visual inspection of the hourly data needs to be performed.

In addition, quick looks of evaluated data for selected time periods can be produced as well as printed timelines in the pdf-format for the evaluated data. All database connections are implemented via ODBC calls (Open DataBase Connectivity) to the corresponding Microsoft (MS) Access database files.

With a second program (EMEP_DailyAverages.m), daily averages (8:00 < t ≤ 8:00 +1 day) of all parameters stored in the hourly averages database can be calculated and are subsequently stored in a separate MS Access database.
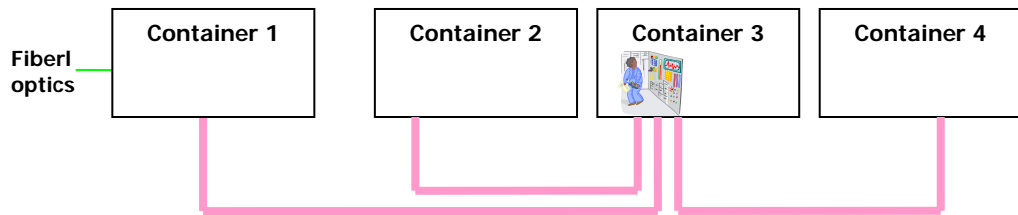
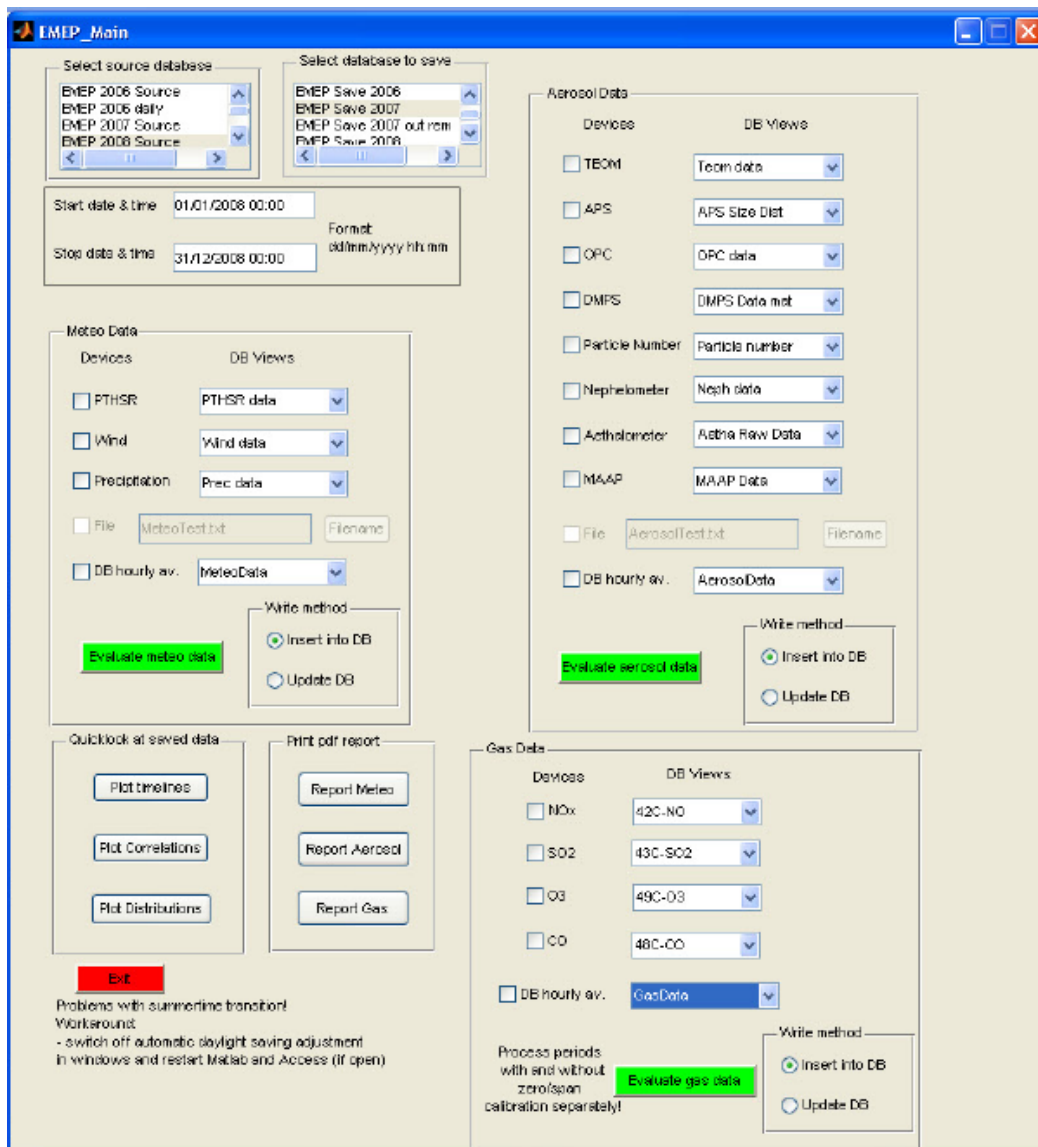Fig. 15. *Interconnections of the laboratory container at the EMEP station.*

Fig. 16. *Graphic user interface of the EMEP data evaluation program.*

Page left intentionally blank

Quality assurance

At JRC level the quality system is based on the Total Quality Management philosophy the implementation of which started at the Environment Institute in December 1999. It should be mentioned that we now work under ISO 9001 and ISO 14001 (from 2010 and onwards), and more informations about our QMS system can also be found on in the chapter "Quality management system". Lacking personnel to specifically follow this business, the JRC-Ispra station for atmospheric research did not renew the accreditation for the monitoring of SO_2, NO, NO_2 and O_3 under EN 45001 obtained in 1999. However, most measurements and standardized operating procedures are based on recommendations of the EMEP manual (1995, revised 1996; 2001; 2002), WMO/GAW 153, ISO and CEN standards. Moreover, the JRC-Ispra gas monitors and standards are checked by the European Reference Laboratory for Air Pollution (ERLAP) regularly (see specific measurement description for details). For on-line aerosol instrumentation, last intercomparisons took place in 2009 at the world calibration center for aerosol physics (WCCAP) in Leipzig (D) in the frame of EUSAAR (www.eusaar.org): one for DMPS in June 2009 in Leipzig where new DMPS system constructed according to EUSAAR specifications were tested, and a second one at the beginning of July 2009, during which absorption/scattering instruments were addressed. At the second intercomparison, also the two Aethalometers participated. In addition, in 2010 (22-24.03.2010), there was an audit performed within the frame of EUSAAR (www.eusaar.org) by Dr. T. Tuch, World Calibration Centre for Aerosol Physics (WCCAP), Leipzig, Germany. The audit went very well and a report is available within the frame of EUSAAR.
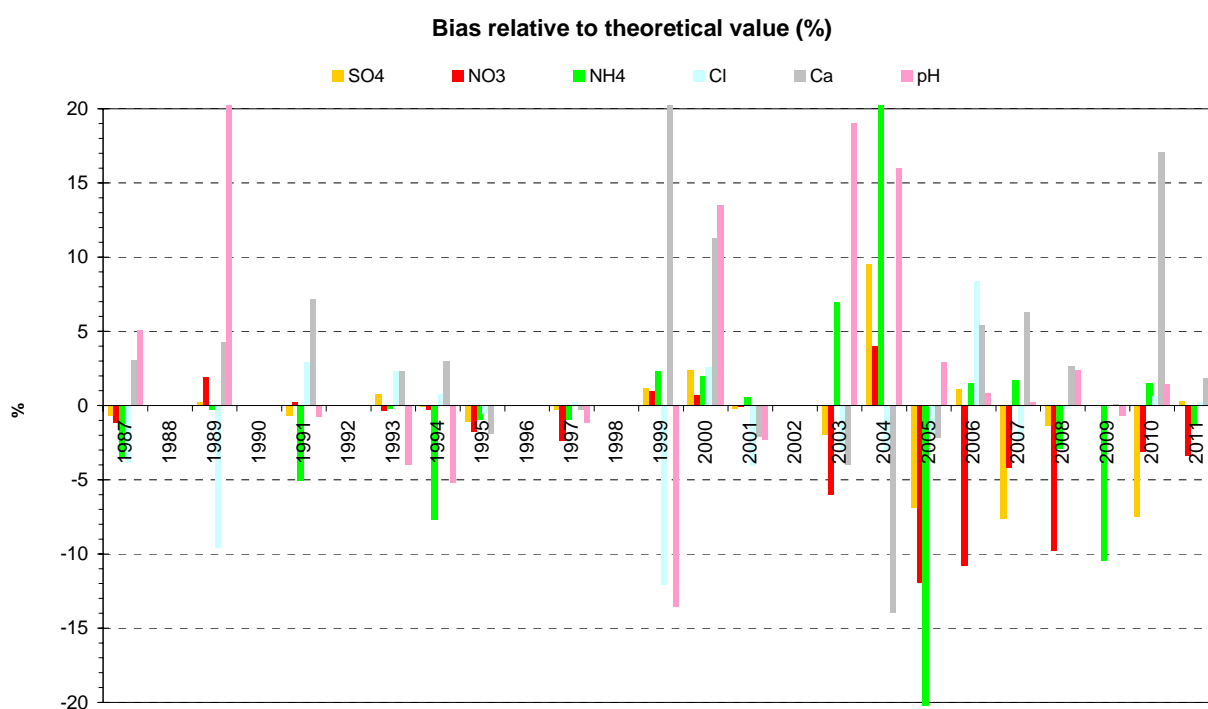
Fig. 17. *JRC-Ispra results of the EMEP intercomparison for rainwater analyses (1987-2011).*
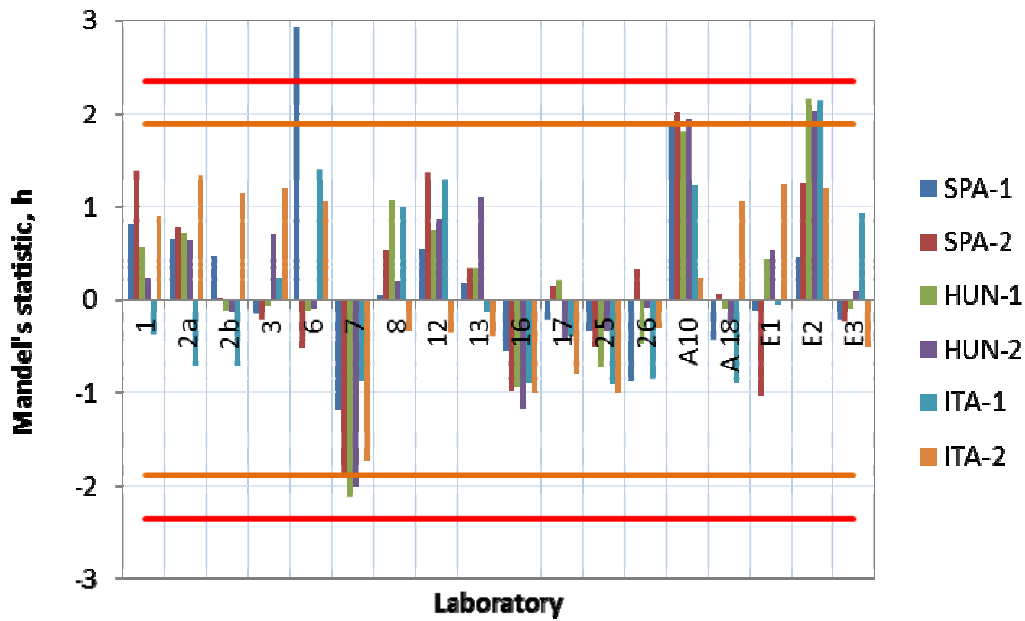
Fig. 18a. Mandel's h statistic values for between laboratory consistency on TC data from the 2011' inter-laboratory comparison. JRC is Lab. 17. For 18 laboratories, *h* values should be < 2.36 at 1% significance level (red line) and < 1.88 at 5% significance level (orange line).
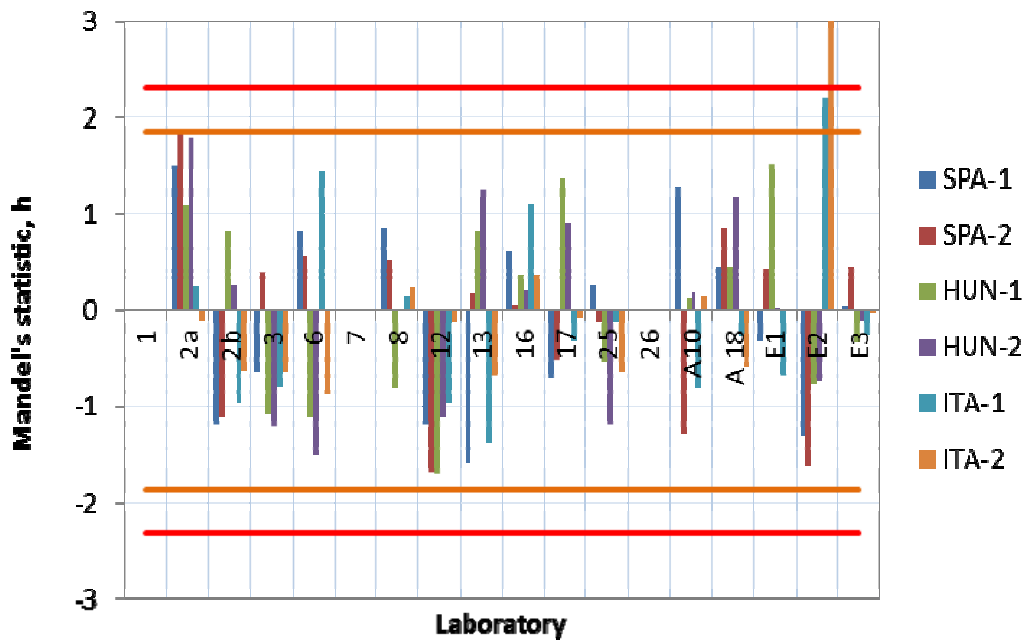

Fig. 18b. Mandel's h statistic values for between laboratory consistency on EC/TC ratios obtained from the 2011' inter-laboratory comparison. JRC is Lab. 17. For 15 laboratories, h values should be < 2.32 at 1% significance level (red line) and < 1.86 at 5% significance level (orange line).

The results of the JRC-Ispra station's participation in the yearly EMEP intercomparison exercise for rainwater analyses are shown in Fig. 17. In the 2011 exercise, Ca^{2+} concentration was overestimated by 17 %, on average. Ions concentrations for the inter-comparison samples were calculated neglecting the contribution of the reagent blank, i.e. 13 ml of mQH_2O. In case of Ca^{2+}, the contribution of the reagent blank was not negligible and, when subtracted, the Ca concentration overestimation decreased to 10 %, on average.

For the analysis of total, organic and elemental carbon (TC, OC and EC, respectively), a Round Robin test including ACTRIS partners and laboratories responsible for aerosol chemical speciation at the EMEP stations of their countries (i.e. CNRII-IT, UBA-DE, ISCIII-ES and EMPA-CH) was organized by the ABC-IS laboratory for aerosol chemistry. In 2011 the intercomparison was based on ambient PM10 aerosol collected at K-Puzsta (HUN), Ispra (ITA), and Montseny (SPA).

As shown in Figure 18a, the ABC-IS laboratory for aerosol chemistry (JRC) obtained TC values very close to the assigned value (determined as the grand average among all participants, outliers excluded) for all 6 filters.

The standard deviations in EC/TC ratios are somewhat larger for TC for all participants. However, for all test filters but one, the ABC-IS laboratory for aerosol chemistry (JRC) showed deviation from the assigned values within 1 z-score (Fig. 18b), i.e. within ± 1 σ*, the standard deviation for proficiency assessment calculated from data obtained in a round of a proficiency testing scheme.

Data quality for other measurements is also checked whenever possible through comparison among different instruments (for gases), mass closure (for PM) and ion balance (for precipitation) exercises.

In addition, most instruments were regularly calibrated through maintenance contracts.

Station representativeness

The representativeness of the JRC EMEP-GAW station has been evaluated to check:

- what area are the data currently acquired at the EMEP-GAW station representative for?
- would a move from the actual location to building 51 (or to "Roccolo hill, nido blu" 150 m from building 51 on Rocolo hill) lead to a break in the data series collected during the past 2 decades?

Summarizing the comparisons which are discussed in details in Dell'Acqua et al. (2010): No relevant difference in the daily maximum concentration of the compared parameters was observed. However, daily minimum are generally lower at the current site compared to Bd. 51 on Rocolo hill. The fact that O_3 daytime maximum concentrations are very similar at the EMEP-GAW station compared to the top of JRC Bd. 51 located 50 m higher also indicates that there are no significant local sources of O_3 precursors at the current site. However, O_3 minima and SO_2 concentrations in general are lower at the EMEP-GAW station, suggesting stronger sinks at the EMEP site.
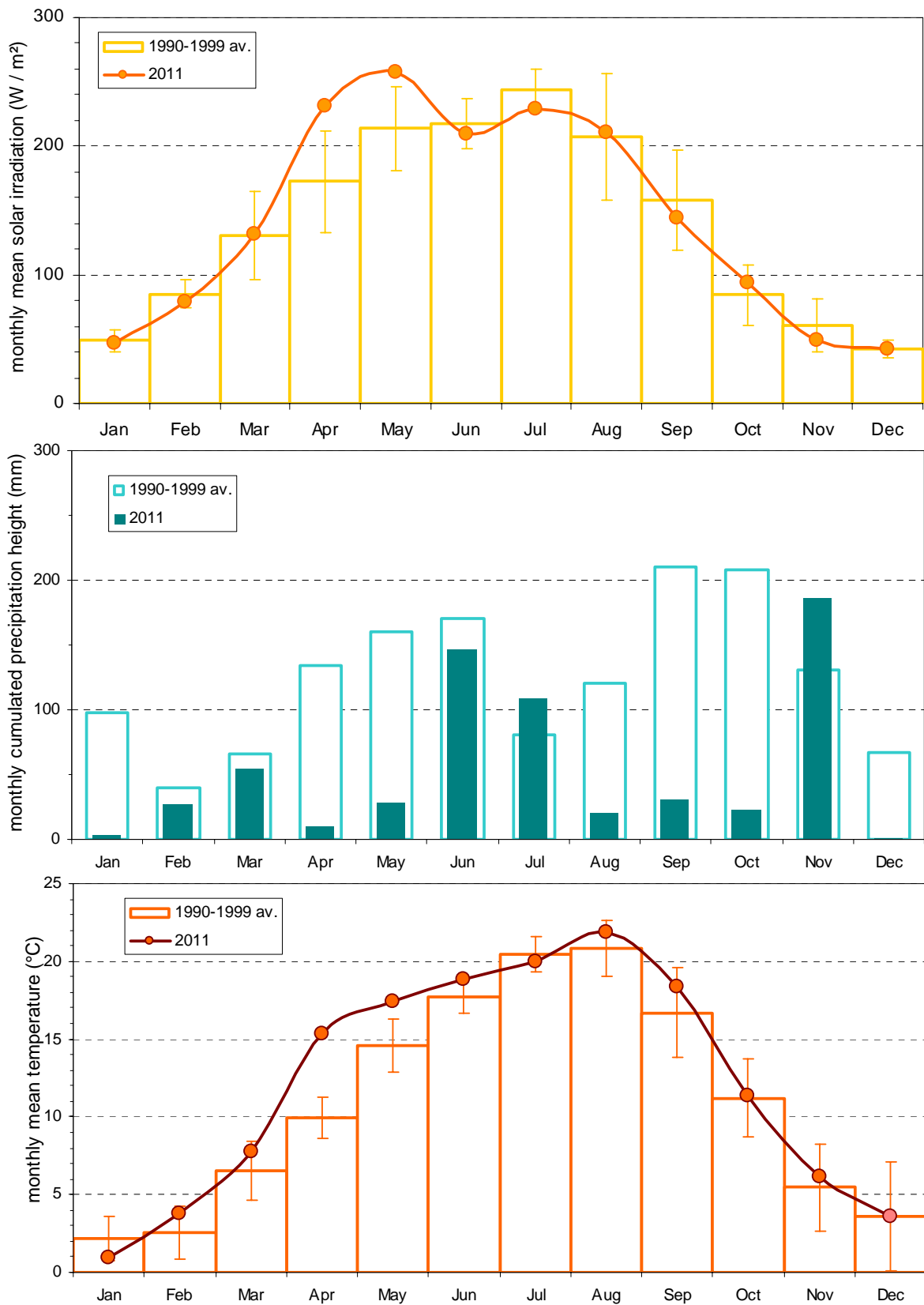
Fig. 14. *Solar global irradiation, precipitation amount, and temperature monthly means observed at the EMEP station in the JRC-Ispra in 2010, compared to the 1990-1999 period ± standard deviations.*

Results of the year 2011

Meteorology

Meteorological data were acquired directly at the EMEP site using the weather transmitter (T, P, RH, precipitation) and a pyranometer (solar radiation) at 10 m and 1.5 m above the ground, respectively. Fig. 14 shows monthly values of meteorological parameters for 2011 compared to the 1990-1999 average used as reference period.

The monthly averaged solar radiation for 2011 shows that April and May were particularly sunny in 2011 compared to the reference period "1990-1999 average".

The total yearly rainfall was accumulated to 1067 mm, about 28 % lower compared to the 1990-1999 average (1484 mm). All months but July and November were dryer than during the "1990-1999" reference period. January and December were particularly dry.

Regarding temperature, April and May were significantly warmer than during the reference period "1990-1999". The temperature average in 2011 was 12.2 °C compared to 11.0 °C over 1990-1999.

Gas phase air pollutants

SO_2 and O_3 were measured almost continuously during the year 2011 (except for a 40 day gap for SO_2 data from July 20th to August 29th due to instrumental problems). A leak occurred in the inlet tube from which O_3 and SO_2 during Jan., Feb. and March, which could probably disturb the data with up to 30 % (see discussions in Jensen et al., 2012). For the rest of the year an uncertainty of 15 % is applied in accordance with *European Directive 2008/50/EC.*

NOx was measured continuously from April and onwards and an uncertainty of 15 % is applied in accordance with *European Directive 2008/50/EC.*

The continuous measurement of CO was performed in 2011 from the complementary nearby JRC greenhouse gas monitoring station located about 900 m away from the ABC-IS station. An uncertainty of 5 % is applied (see discussions in the chapter "Measurement techniques").

In 2011, seasonal variations in SO_2, NO, NO_2, NO_x and O_3 were similar to those observed over the 1990-1999 period (Fig. 20). Concentrations are generally highest during wintertime for primary pollutants (SO_2, CO, NO_x), and in summertime for O_3. The higher concentrations of SO_2, CO, NO_x in winter result from a least dispersion of pollutant during cold months, whereas the high concentration of O_3 during summer is due to enhanced photochemical production.

SO_2 concentrations (average = 0.65 µg/m³) were generally about one tenth compared to the reference period (1990-1999) and on average also 10% lower than in 2010.
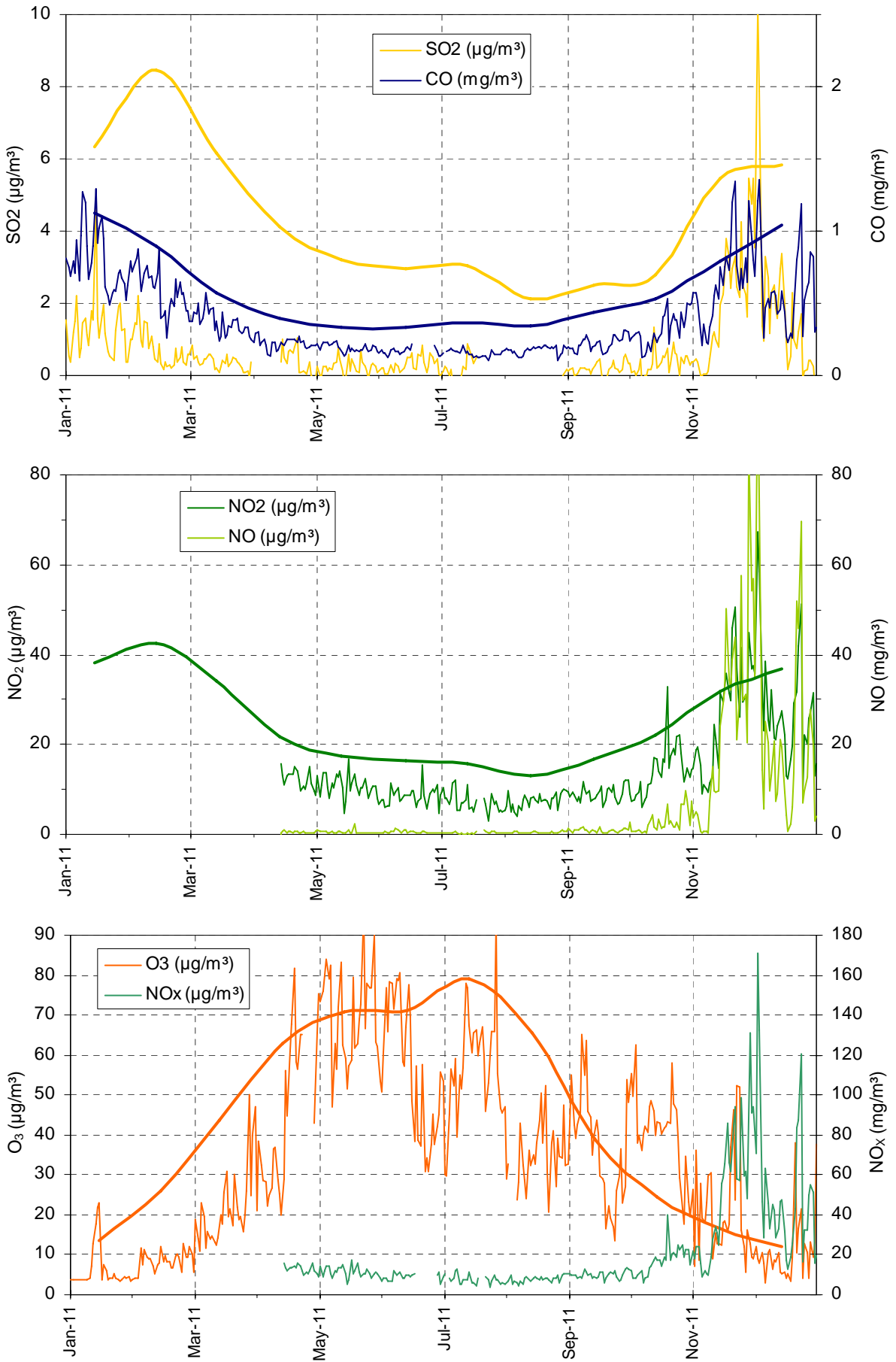
Fig. 20. *Seasonal variations of the 24 hr averaged concentrations of SO₂, CO, NO₂, NO, O₃ and NOₓ in 2011 (thin lines) and 1990-1999 monthly averages (thick lines: yellow=SO2, blue=CO, green=NO2, orange=O3).*

Daily mean CO concentrations ranged from 0.15 to 1.35 µg m^{-3} (~0.1 – 1.2 ppmv), which are typical values in a regional background station like the ABC-IS station in Ispra. The lowest values were observed in very clean air masses during Föhn events and also during summer, and the highest during winter night time conditions.

NO_2 concentrations were on average 40% lower than during 1990-1999 and also 25% lower than the 2010 levels. In contrast NO concentrations from 2011 were twice as large as in 2010 over the same period (April – December), mainly due to exceptionally large values observed in November 2011.

The mean O_3 concentration in 2011 (33.8 µg/m³, 16.9 ppb) was close to 25% smaller compared to the reference period 1990-1999, and about 10% lower than in 2010. However, several ozone indicators (Fig. 21) did not improve compared to previous years, probably partly due to the fact that 2011 was sunnier and warmer than previous years.

The vegetation exposure to above the ozone threshold of 40 ppb (AOT 40 = Accumulated dose of ozone Over a Threshold of 40 ppb, normally uses for "crops exposure to ozone") was 10548 ppb h in 2011 (with a data coverage for O_3 of 96 % for the whole year), i.e. low compared to 34000 ppb h yr^{-1} over the 1990-1999 decade (Fig. 21). However, AOT 40 was 4006 ppb h in 2010 (but a leak in sampling line for several months also during summer could have disturbed the data by 30%), and 10789 ppb h for 2008. There was therefore no detectable decrease in AOT over the 4 last years.

For quantification of the health impacts (population exposure), the World Health Organisation uses the SOMO35 indicator (Sum of Ozone Means Over 35 ppb, where means stands for maximum 8-hour mean over day), i.e. the accumulated ozone concentrations dose over a threshold of 35 ppb (WHO, 2008). In 2011, SOMO35 was 2313 ppb day (Fig. 16), i.e. greater than in 2007 (1590 ppb day), 2008 (1830 ppb day), and 2010 (1206 ppb day) but lower than in 2006 (2993 ppb day). In contrast, extreme O_3 concentrations (>180 µg m^{-3} over 1 hour) were never observed in 2011. This value corresponds to the threshold above which authorities have to alert the public (European Directive 2008/50/EC on ambient air quality and cleaner air for Europe). During the reference period 1990-1999, the information level of 180 µg m^{-3} has been exceeded 29 times per year on average. The other "protection of human health factor" mentioned by the European Directive 2008/50/EC (120 µg m^{-3} as maximum daily 8-hour average) was exceeded 21 times in 2011, i.e. slightly below the threshold of 25 exceedances per year (averaged over three years).
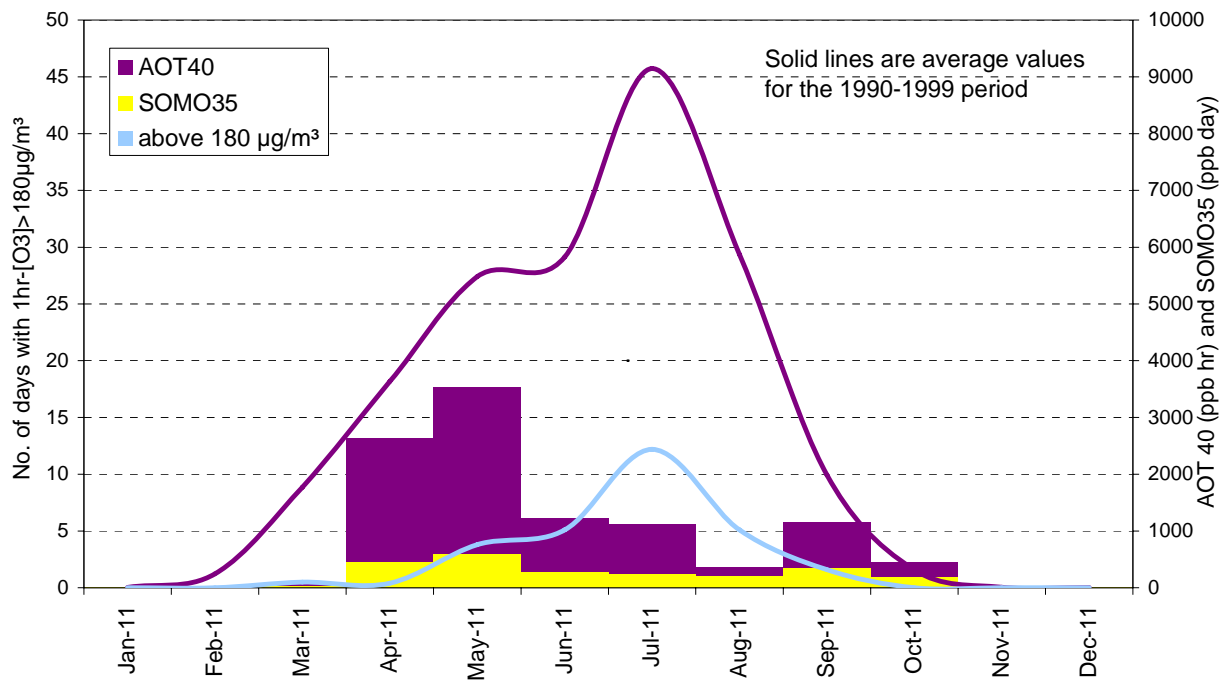
Fig.21.: *AOT 40, SOMO35 and number of exceedances of the 1-hour averaged 180 µg/m³ threshold values in 2011 (bars), and reference period values 1990-1999 (lines). No 1hr O₃ average value > 180 µg/m³ (90 ppb) was observed in 2011.*
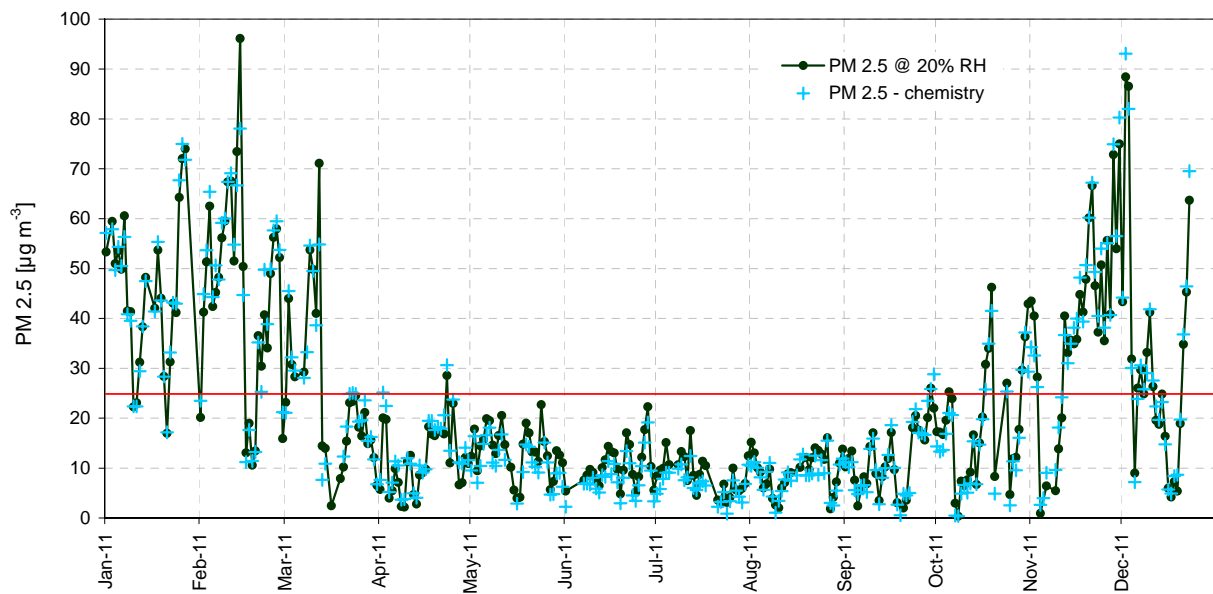

Fig. 22. *24hr-integrated PM2.5 mass concentrations from off-line gravimetric measurements at 20 % RH and chemical determination of main constituents in 2011.The red line indicates the annual limit value of 25 µg/m³ to be reached by 2015 (European directive 2008/50/EC)*

Particulate phase

<u>Particulate matter mass concentrations</u>

$PM_{2.5}$ concentrations (Fig. 22) measured gravimetrically at 20 % relative humidity (RH) averaged 22.0 µg /m³ over 2011. This value is higher than the ones measured in 2009 of (19.0 µg/m³) and 2010 (17.5 µg/m³), but still below the European annual limit value of 25 µg/m³ that has to be reached by 2015 (<u>European directive 2008/50/EC</u>). Over the PM10 samples collected every 6th day (n = 64) in 2011, PM_{10} averaged 37.0 µg/m³. It was however noticed that monthly averages calculated over 5 filter samples were sometimes not representative. The correlation between $PM_{2.5}$ and PM_{10} concentrations measured simultaneously (Fig. 23, left hand) is good (R²=0.96). $PM_{2.5}$ concentration was generally 10-15 % lower than PM_{10}. The intercept may be due to larger positive sampling artefacts in the PM_{10} filters (no denuder) and/or larger negative artefacts in the $PM_{2.5}$ filters (with denuder).

FDMS-TEOM_B (s/n 253620409) and FDMS-TEOM_A (s/n 233870012) were used to measure PM_{10} from 9 Feb. to 18 Jul., and 26 Jul. to 31 Dec. 2011, respectively. 54 exceedances of the 24-hr limit value for PM10 (50 µg/m³) were observed over the period 9 Feb. – 31 Dec. 2011 (94% annual data coverage). The annual PM10 average (30 µg/m³) was still below the 40 µg/m³ annual average limit value though.

The regression between PM_{10} concentrations measured gravimetrically at 20 % RH and PM10-TEOM data averaged over the corresponding sampling periods (Fig. 23, right hand) show a good agreement between these 2 methods (R²= 0.86, slope = 1.01, n = 58).
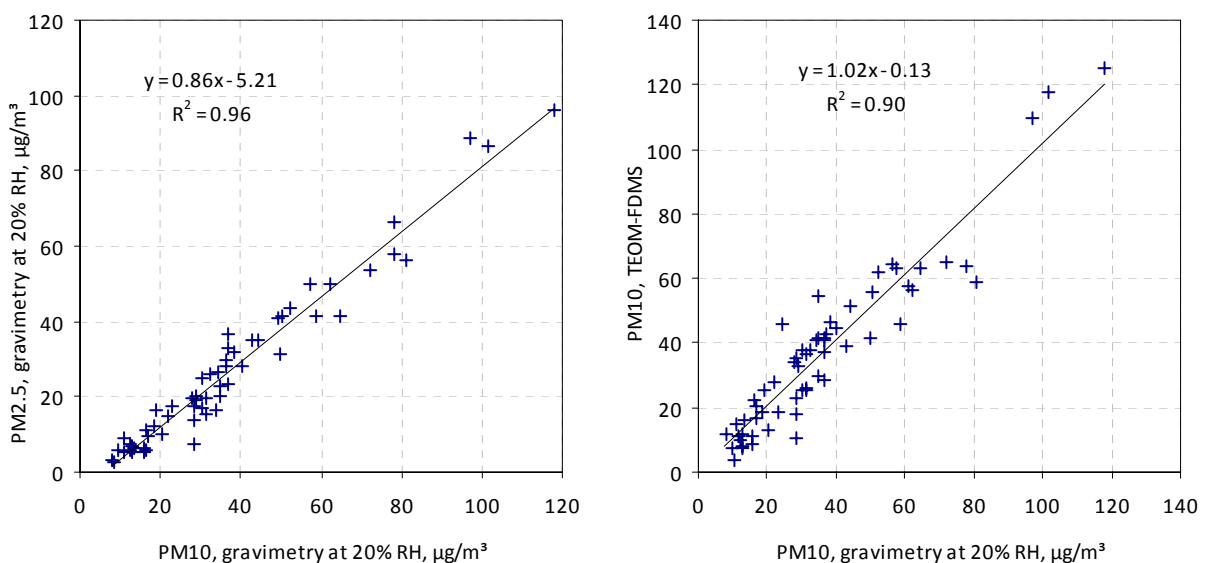
Fig. 23. *Regressions between gravimetric PM2.5 measurements at 20 % RH (right) and FDMS-TEOM PM10 (left) and vs. gravimetric PM10 measurements at 20 % RH in 2011.*
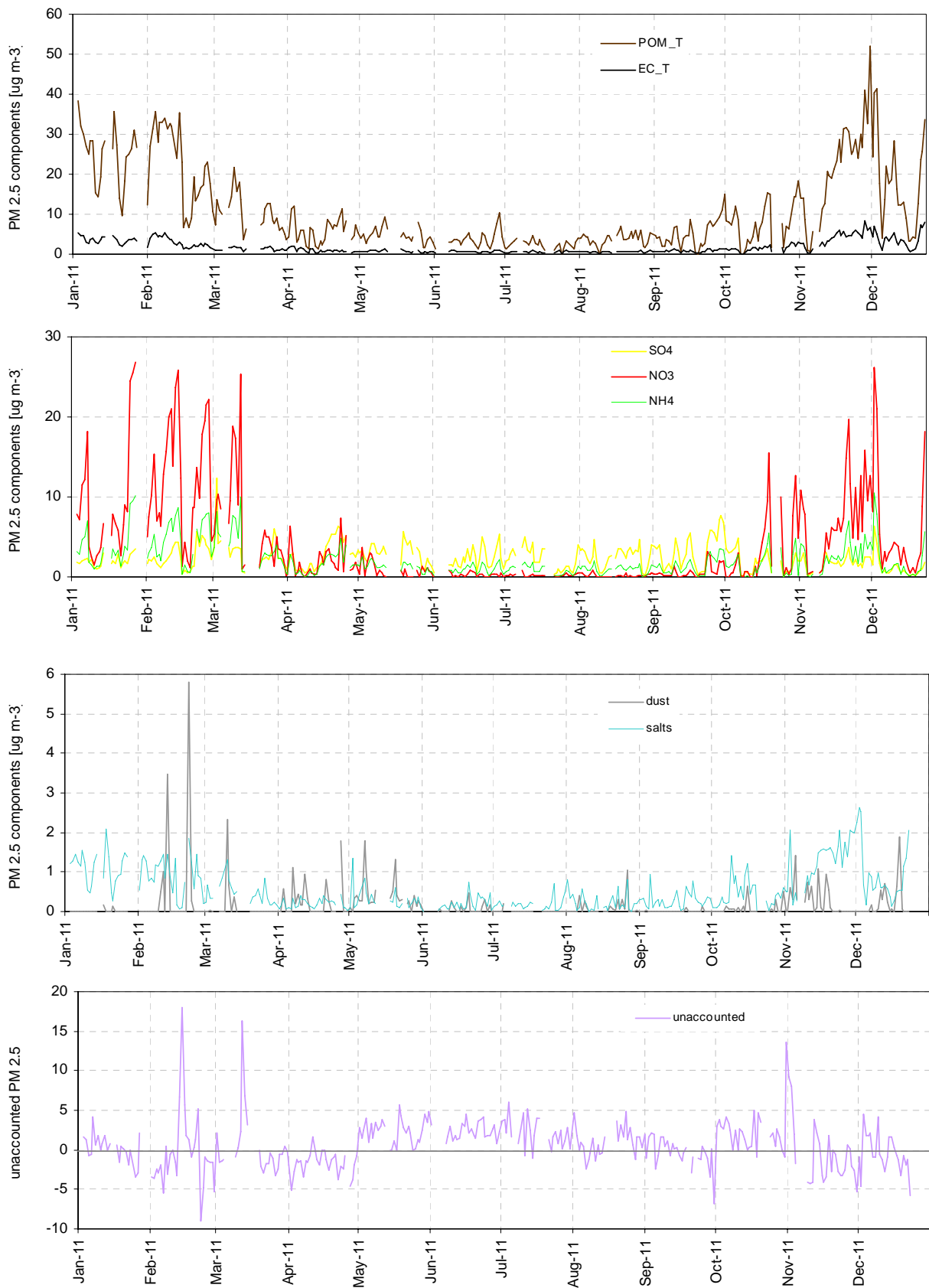
Fig. 24. *24-hr integrated concentrations of the main aerosol constituents of PM2.5 during 2011.*

PM2.5 chemistry:

Main ions (Cl^-, NO_3^-, SO_4^{2-}, $C_2O_4^{2-}$, Na^+, NH_4^+, K^+, Mg^{2+}, and Ca^{2+}), OC and EC were determined from the quartz fibre filters (for the whole year) collected for PM mass concentration measurements.

Fig. 24 shows the temporal variations in the PM2.5 main components derived from these measurements. Particulate organic matter (POM) is calculated by multiplying OC (organic carbon) values by the 1.4 conversion factor to account for non-C atoms contained in POM (Russell et al., 2003). "Salts" include Na^+, K^+, Mg^{2+}, and Ca^{2+}. Dust is calculated from Ca^{2+} concentrations and the regression (slope = 4.5) found between ash and Ca^{2+} in the analyses of ash-less cellulose filters (Whatman 40) in previous years. Most components show seasonal variations with higher concentrations in winter and fall, and lower concentrations in summer, like $PM_{2.5}$ mass concentrations. This is mainly due to changes in pollutant horizontal and vertical dispersion, related to seasonal variations in meteorology (e.g. lower inversion layer in the winter season). The amplitude of the POM, NH_4^+ and NO_3^- seasonal cycles may be enhanced due to equilibrium shifts towards the gas phase, and/or to enhanced losses (negative artefact) from quartz fibre filters during warmer months.

NH_4^+ follows $NO_3^- + SO_4^{2-}$ very well as indicated by the regression shown in Fig. 25. This correlation results from the atmospheric reaction between NH_3 and the secondary pollutants H_2SO_4 and HNO_3 produced from SO_2 and NO_x, respectively. The slope of this regression is smaller than 1, which means that NH_3 was sufficiently available in the atmosphere to neutralise both H_2SO_4 and HNO_3. This furthermore indicates that PM2.5 aerosol was generally not acidic in 2010.

$y = 0.95x$
$R^2 = 0.98$
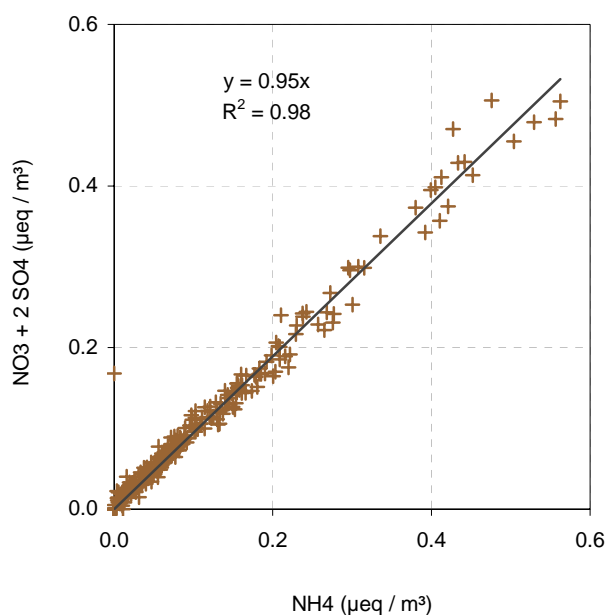
Fig. 25. $SO_4^{2-} + NO_3^-$ vs. NH_4^+ (µeq/m³) in $PM_{2.5}$ for 2011

Table 2: *annual mean concentrations and contributions of major PM$_{2.5}$ constituents in 2011*

constituent	salts Cl$^-$, Na$^+$, K$^+$, Mg^{2+}, and Ca^{2+}	NH$_4^+$	NO$_3^-$	SO$_4^{2-}$	POM	EC	dust	unaccounted
Mean conc. (µg m^{-3})	0.48	1.81	3.43	2.12	9.38	1.54	0.14	0.49
Mean cont. (%)	3.1	9.2	11.8	16.1	46.4	8.9	1.5	3.1
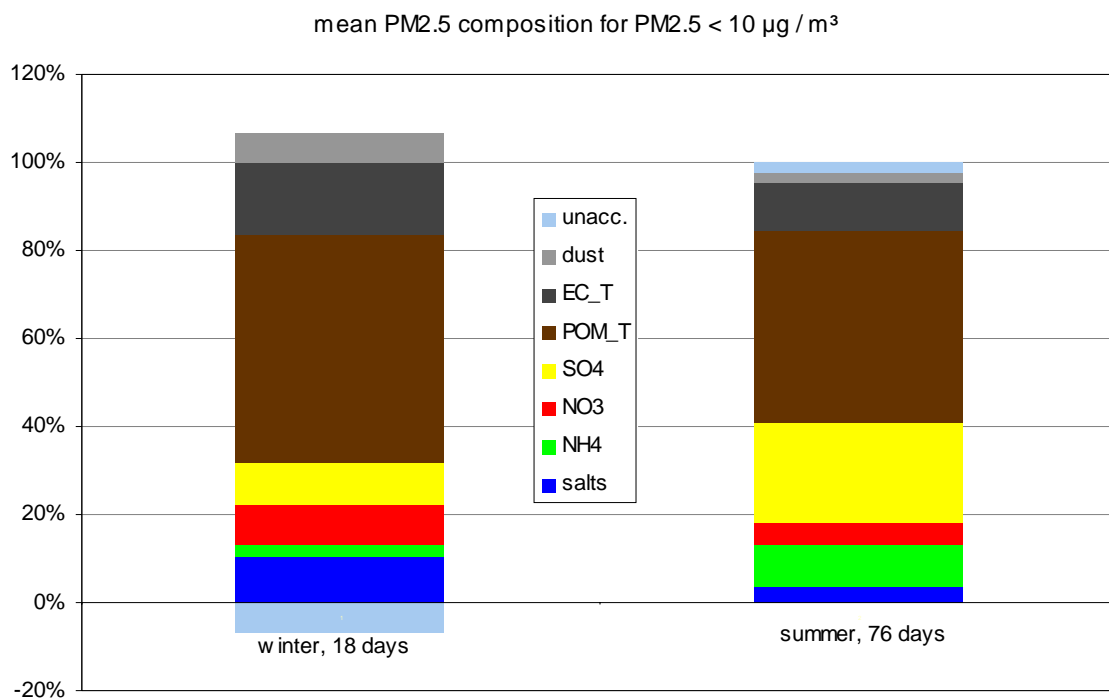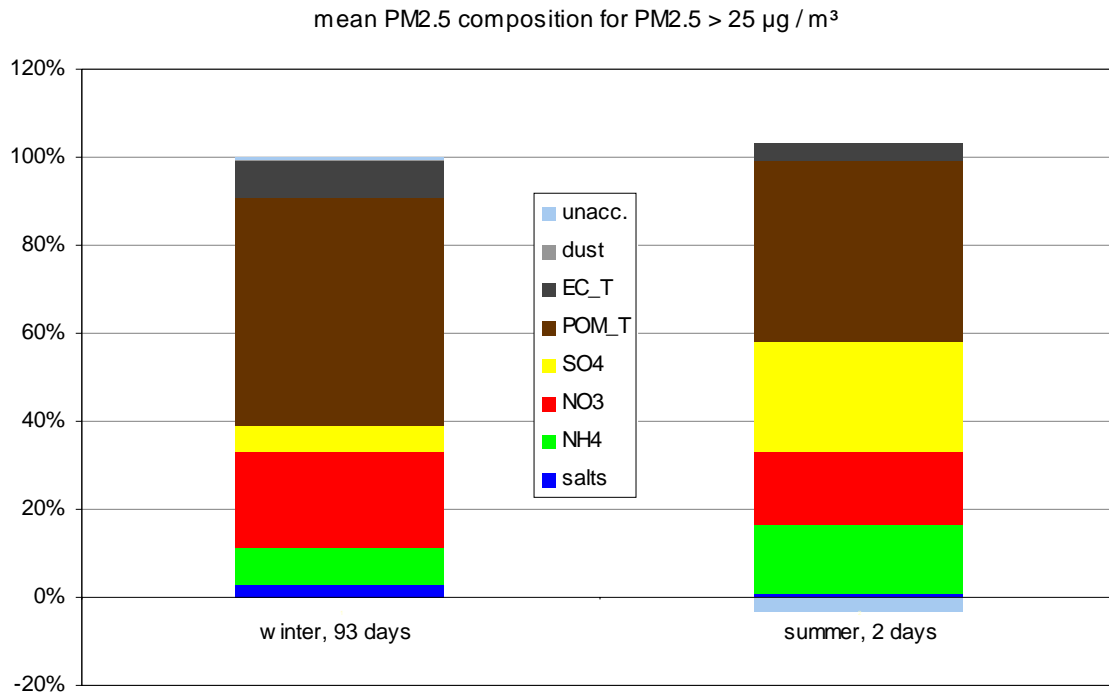
Fig. 26. *Average composition of PM2.5 for days during which PM2.5 > 25 µg/m³(top) and PM2.5 < 10 µg/m³(bottom), in winter (Jan., Feb., Dec.) and extended summer (Apr. – Oct.)*

46

Contribution of the main aerosol components in PM2.5

The contributions of the main aerosol components to PM2.5 are presented in Table x (annual averages) and in Fig. 26 (a) for days on which the "24-hr limit value for PM2.5 of >25 µg/m³ was exceeded" in winter (Jan., Feb., March, Nov. and Dec., 69 cases) and extended summer (Apr. to Oct, 16 cases) and (b) for days on which 24-hr integrated PM2.5 concentration was below 10 µg / m³ in winter (29 cases) and in extended summer (105 cases).

These $PM_{2.5}$ compositions may not always represent accurately the actual composition of particulate matter in the atmosphere (due to various sampling artefacts), but are suitable to assess which components contributed to the PM2.5 mass concentration when collected by a quartz fiber filter downstream of a 20 cm-long carbon monolith denuder.

Over the whole year 2011, carbonaceous species accounted for 55% of $PM_{2.5}$ (EC:9%, POM: 45%), and secondary inorganics for 37% (NH_4: 9 %, NO_3: 12%, and SO_4:16%). In both winter and (extended) summer, particulate air pollution days are characterised by a strong increase in NO_3 contribution. Considering low $PM_{2.5}$ concentration days, summertime is characterised by higher SO_4^{2-} concentrations (faster SO_2 photochemical conversion) and lower NO_3^- concentrations ($HNO_3 + NH_3 \leftrightarrows NH_4NO_3$ equilibrium moves towards the gas phase, on the left side, as temperature increases). Dust and salts do not contribute significantly to the $PM_{2.5}$ mass (2 to 3 % each.). Their contribution is slightly larger on cleanest days compared to most polluted days.
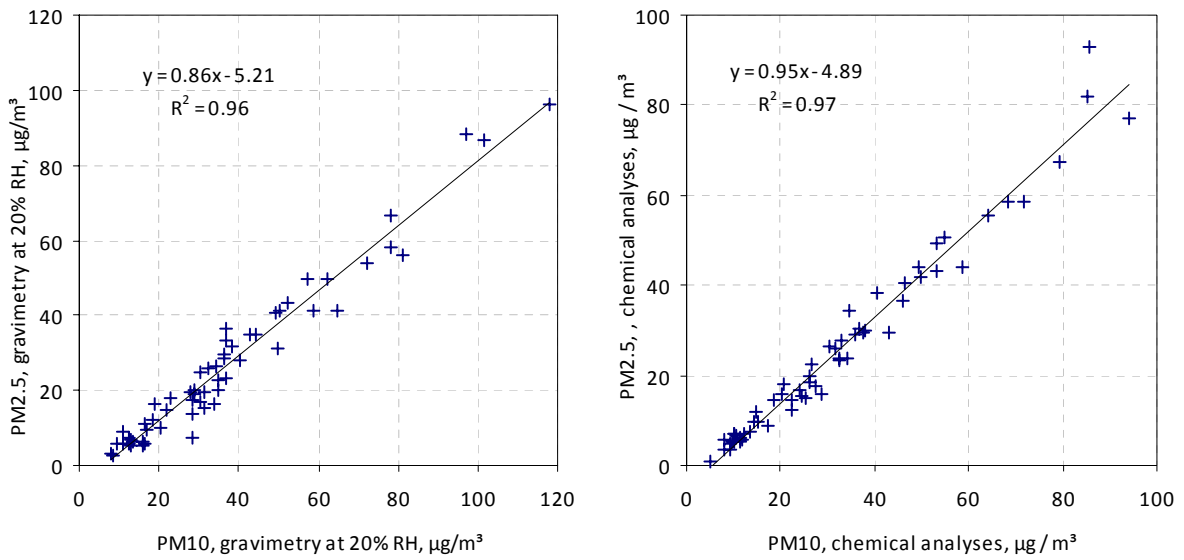
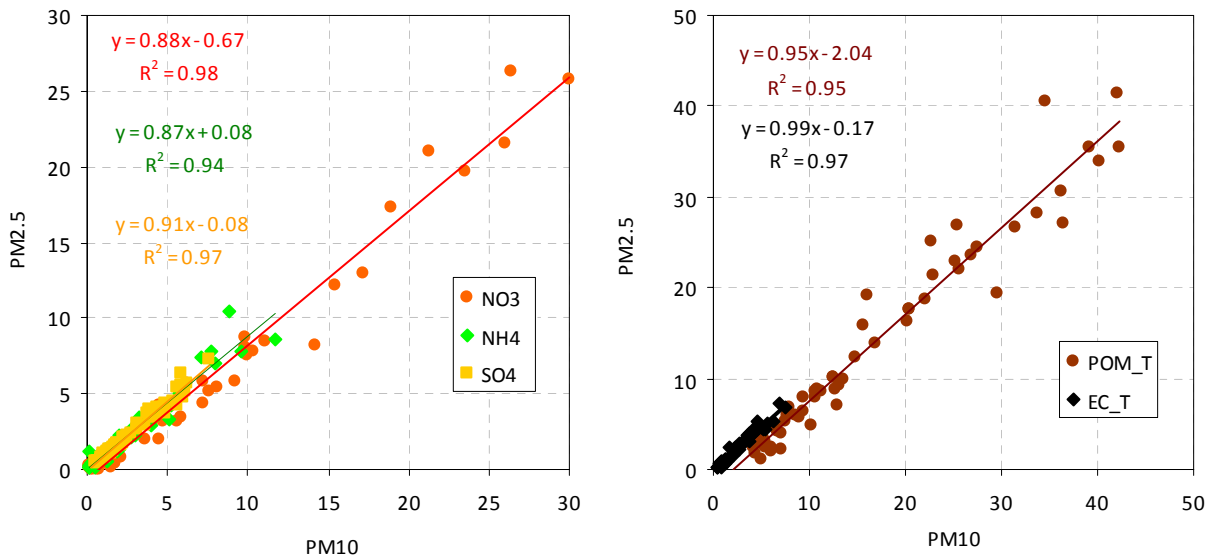Fig. 27. *Regressions between PM$_{10}$ and PM$_{2.5}$ determined gravimetrically at 20% RH and from chemical analyses.*

Fig. 28. *Correlation between chemical components (NH$_4$, SO$_4$ and NO$_3$ on the right hand and POM and EC on the left hand) in PM10 and PM2.5.*

Table 3*: annual mean concentrations and contributions of major PM$_{10}$ constituents in 2011*

constituent	salts Cl$^-$, Na$^+$, K$^+$, Mg^{2+}, and Ca^{2+}	NH$_4^+$	NO$_3^-$	SO$_4^{2-}$	POM	EC	dust	unaccounted
Mean conc. (µg m^{-3})	1.18	2.57	6.15	2.66	15.92	2.38	1.10	4.18
Mean cont. (%)	3.5	6.3	13.7	8.5	43.6	6.9	4.5	13.1

<u>PM10 chemistry</u>

PM10 has been collected and analyzed for a total of 64 filters in 2011. Concentrations and contributions of major PM_{10} constituents are listed in Table 3. Carbonaceous species account for more than 50% of PM10 mass, as for PM2.5. NH_4NO_3 is the main inorganic constituent of PM10. Comparing weighted masses of PM2.5 and PM10, it shows that PM2.5 makes up about 85 % of the total PM10 mass (Fig. 27, left hand). For the chemical masses, PM2.5 accounts for about 95 % PM10 (Fig. 27, right hand).

Looking at single constituents of PM10 and PM2.5, the regressions of Fig. 28 indicate that NO_3, NH_4, SO_4, POM and EC in PM2.5 account for 83 – 99% of these same species in PM10. There is significantly less NH_4NO_3 in PM2.5 compared to PM10 (ratio = 0.78). It is difficult to state if this difference is real or due to increased losses of semi-volatile inorganics (namely NH_4NO_3) due to the use of the OC denuder (PM2.5 filters were sampled with a denuder and PM10 filters were sampled without denuder).
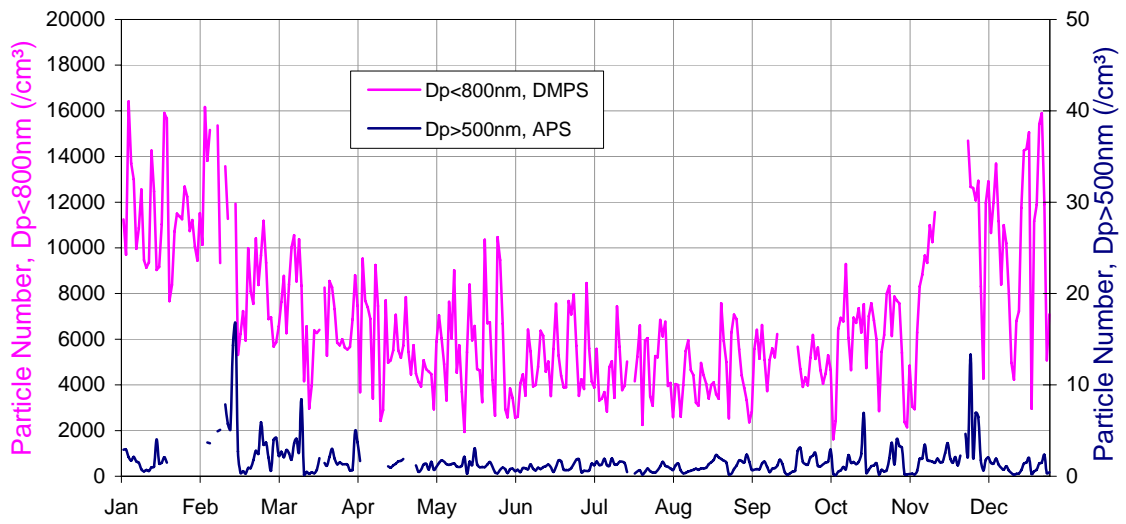
Fig. 29. *24 hr – mean particle number concentrations for Dp > 500 nm and Dp< 600 nm.*
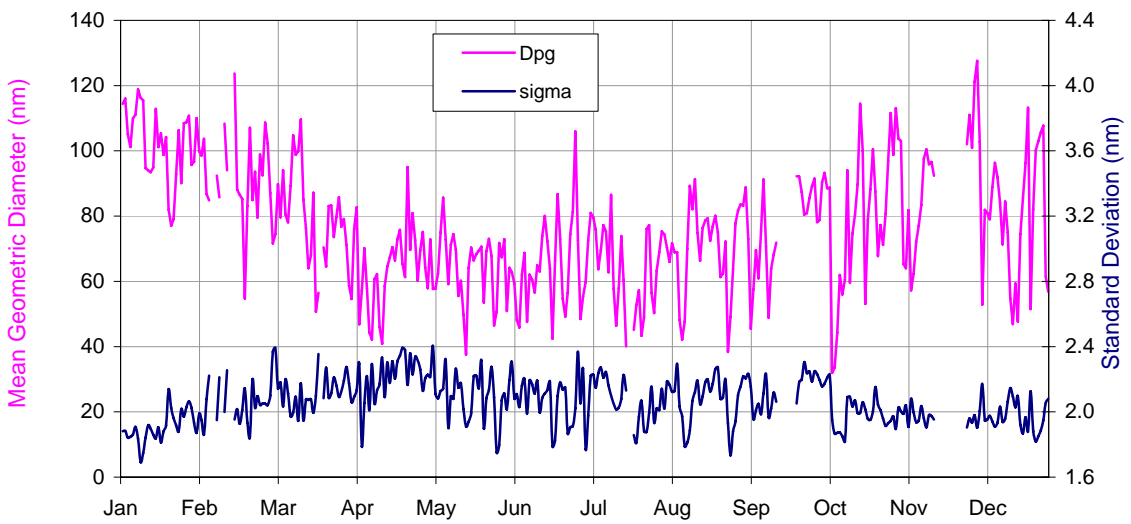
Fig. 30*. 24 hr - averaged particle geometric mean diameter (measured with DMPS) and standard deviation*
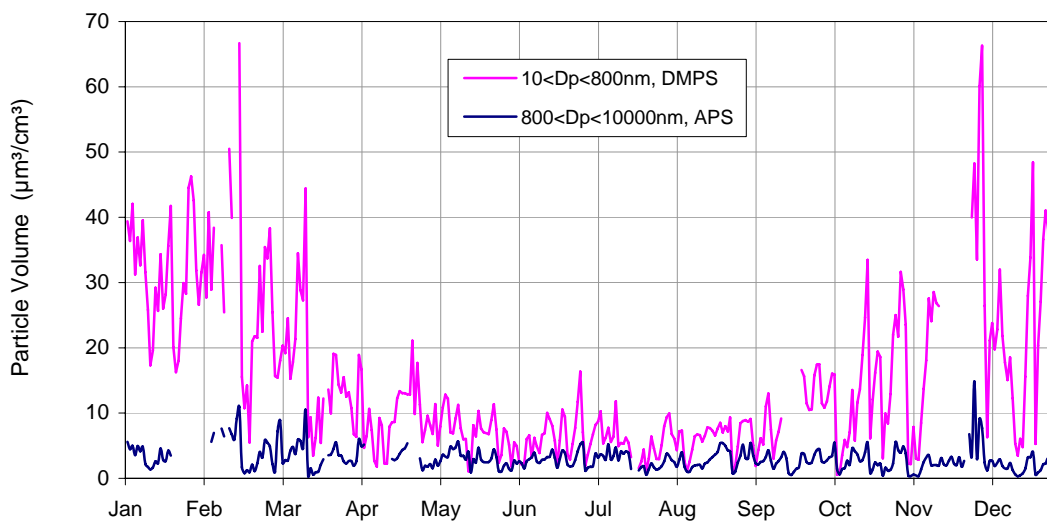
Fig. 31*. 24 hr - averaged particle volume concentrations for Dp< 800 nm and Dp > 800 nm.*

<u>Aerosol physical properties</u>

Measurements of the particle number size distributions smaller than 800 nm diameter were carried out using a Differential Mobility Particle Sizer almost continuously in 2011 (data coverage 93%). Major breaks occurred from 16 to 22 Sep. and from 17 – 28 Nov.

Particle number concentrations averaged over 24 hr (from 08:00 to 08:00 UTC) ranged from 1620 to 16400 cm^{-3} (average: 6870 cm^{-3}) and followed a seasonal cycle comparable to that of PM mass concentration, with maxima in winter and minima in summer (Fig. 29). It should be mentioned, that the DMPS data presented here have not been corrected for inlet diffusion losses and CPC efficiency, but this is normally only a few percent on the numbers and it has no impact on the other parameters.

The mean mode diameter at RH < 30 % ranged 32 – 128 nm (average = 77 nm) in 2011. The variations in particle size distributions parameters (Fig. 30) show seasonal patterns as well: the mean geometric diameter is generally larger in winter (around 100 nm) than in summer (around 40 nm), whereas the standard deviation of the distribution follows an opposite trend (larger in summer than in winter).

The size distribution of particles larger than 500 nm was measured using an Aerodynamic Particle Sizer almost continuously over 2011 too (data coverage: 90%). Aerodynamic diameters were converted to geometric diameter assuming a particle density of 1.50. As previously observed, particles larger that 500 nm generally (90th percentile) accounted for <0.5% of the total particle number only (Fig. 29), but for about 25 % of the total particle volume on average (Fig. 31). The seasonal variations in particle volume concentration reflect the changes in particle number and mean geometric diameter, with larger volumes in winter than in summer.
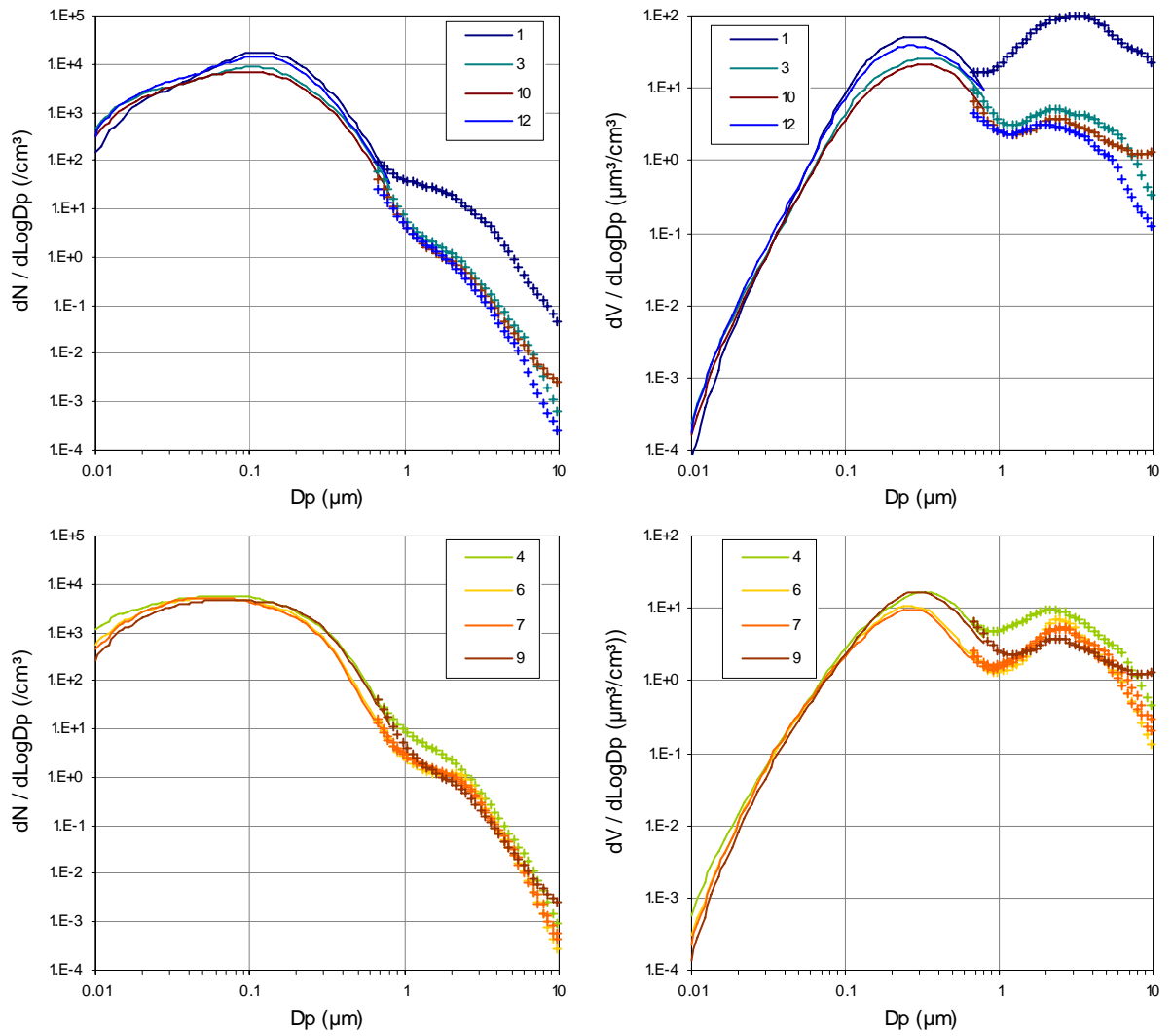
Fig. 32. *Monthly mean particle number (left) and volume (right) size distributions measured with a DMPS (10-800 nm, solid lines) and an APS (0.85-10 μm, crosses). Legends indicate months. A density of 1.5 g cm^{-3} was used to convert aerodynamic to geometric diameters.*
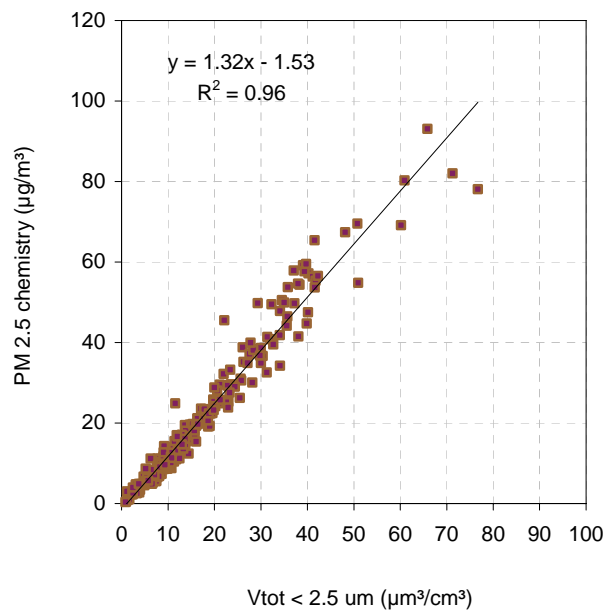

Fig. 33. *2011 regression between PM2.5 mass concentrations determined from gravimetric measurements at 20 % RH and particle volume (Dp < 2.5 μm) calculated from DMPS and APS measurements*

Looking at particle number size distributions (Fig. 32) reveals generally good agreements between the DMPS and the APS, but clear inconsistencies appear in particle volume size distributions from above all in December, perhaps due to the fact that the assumed particle density of 1.5 g cm^{-3} does not hold for this month. Actually, an aerosol density of 1.0 g cm^{-3} should be used to get a good match between DMPS and APS in December, while a density = 1.7 g cm^{-3} would lead to a perfect agreement over the overlapping size range for summer months.

The comparison between PM2.5 mass and aerosol volume concentration (for Dp < 2.5 µm) shows a good correlation (Fig. 33). The slope of the regression between PM2.5 at 20 % RH and particle volume suggests an aerosol density of 1.38 (to be compared to 1.32 and 1.37 in 2009 and 2010, respectively), but still lower than the value of 1.5 g cm^{-3} assumed to convert aerodynamic diameters. It should be mentioned that a density factor in the range of 1.6 ± 0.1 is normally considered for atmospheric aerosols (McMurry et al., 2002).
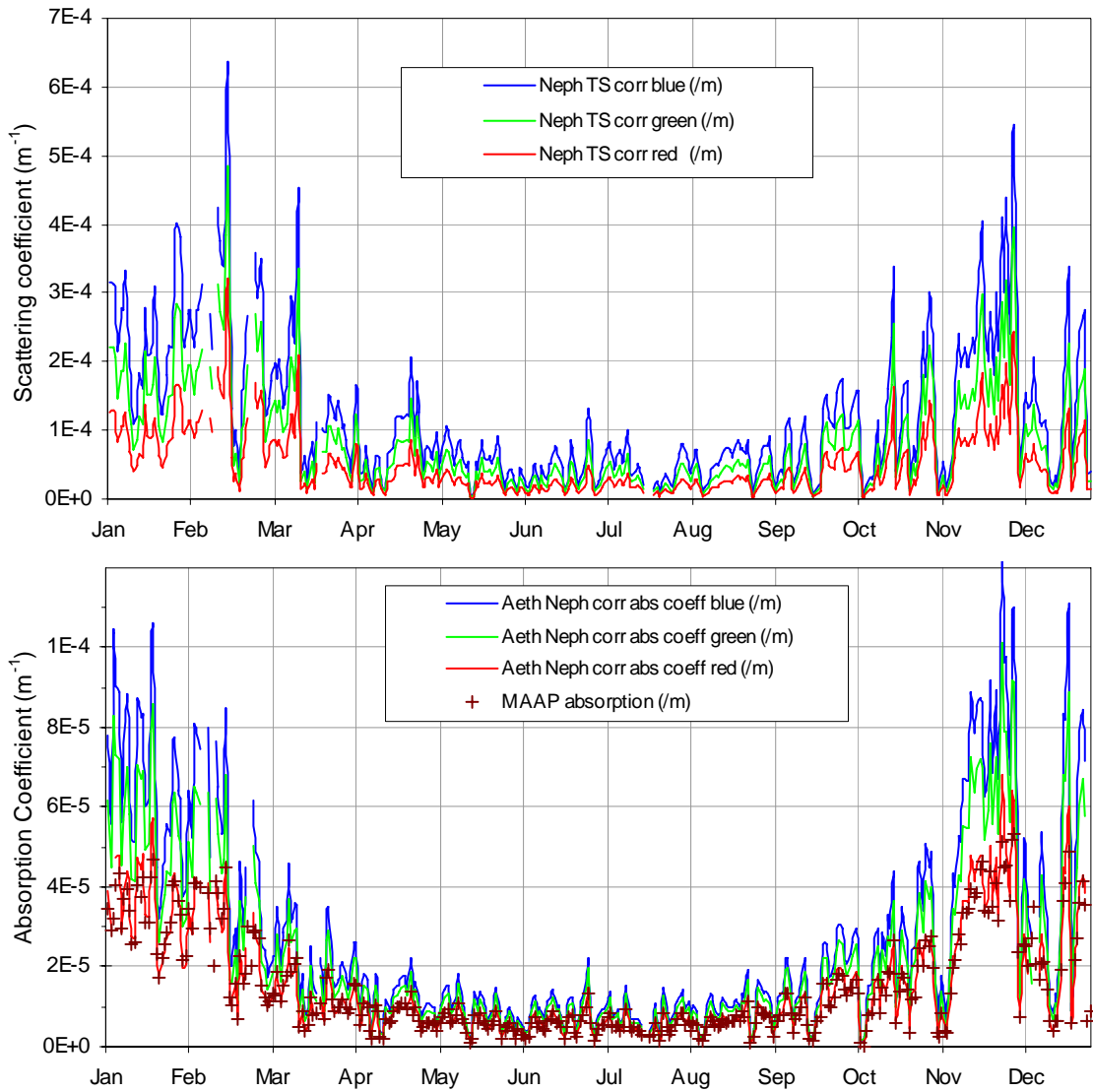
Fig. 34 *Daily mean atmospheric particle scattering (top) and absorption (bottom) coefficients at three wavelengths, derived from Nephelometer, Aethalometer and MAAP measurements (not corrected for RH, except if specified).*

Aerosol optical properties

Aerosol optical properties have been monitored continuously during 2011 (data coverage = 98%). Data from the Nephelometer (Fig. 34a) have been corrected for angular non idealities (truncation to 7 – 170°, slightly not cosine-weighted distribution of illumination) according to Anderson and Ogren (1998), but not for RH effects. Although a Nafion dryer is implemented to dry the air entering the nephelometer, RH > 40% commonly occurred between August 1st and Sep. 18th 2011. At 40% RH, aerosol scattering is on average increased by 20% compared to 0% RH in Ispra (Adam et al., 2012).

Atmospheric particle absorption coefficients at 7 wavelengths (Fig. 34b) were derived from the Aethalometer AE-31 data corrected for the shadowing and multiple scattering effects when Nephelometer data were available, according to Weingartner et al (2003), making use of coefficients derived from Schmid et al. (2006).

Both scattering and absorption coefficients follow seasonal variations (Fig. 34) in line with PM mass variations, mainly controlled by pollutant dispersion rates.

The uncertainty of the multiple scattering correction factor may introduce a much larger uncertainty in the aerosol absorption coefficient values, since correction factors ranging from 2 to 4 have been proposed (Weingartner et al., 2003; Arnott et al., 2005). The correction factors we used were 3.6, 3.65 and 3.95 for blue, green and red light, respectively. However, it should be noted that the use of the correction factors proposed by Schmid et al. (2006) leads to an aerosol absorption coefficient at 660 nm in good agreement with the absorption coefficient obtained from the Multi Angle Absorption Photometer (MAAP) for 670 nm (Fig. 35, R² = 0.98, slope = 1.07). Deviations from the 1:1 line are mainly observed for absorption coefficient values > 0.04 km^{-1}. This behavior strictly depends on the aerosol absorption and not on instrumental parameters such as the filter loading.
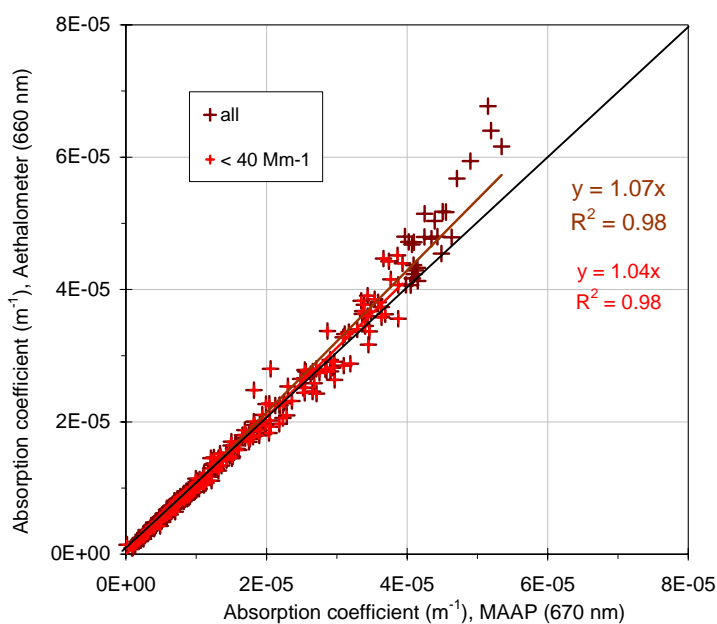

Fig. 35. *Comparison of Aethalometer and MAAP derived absorption coefficients at 660 and 670 nm, respectively. Data points are daily averages.*
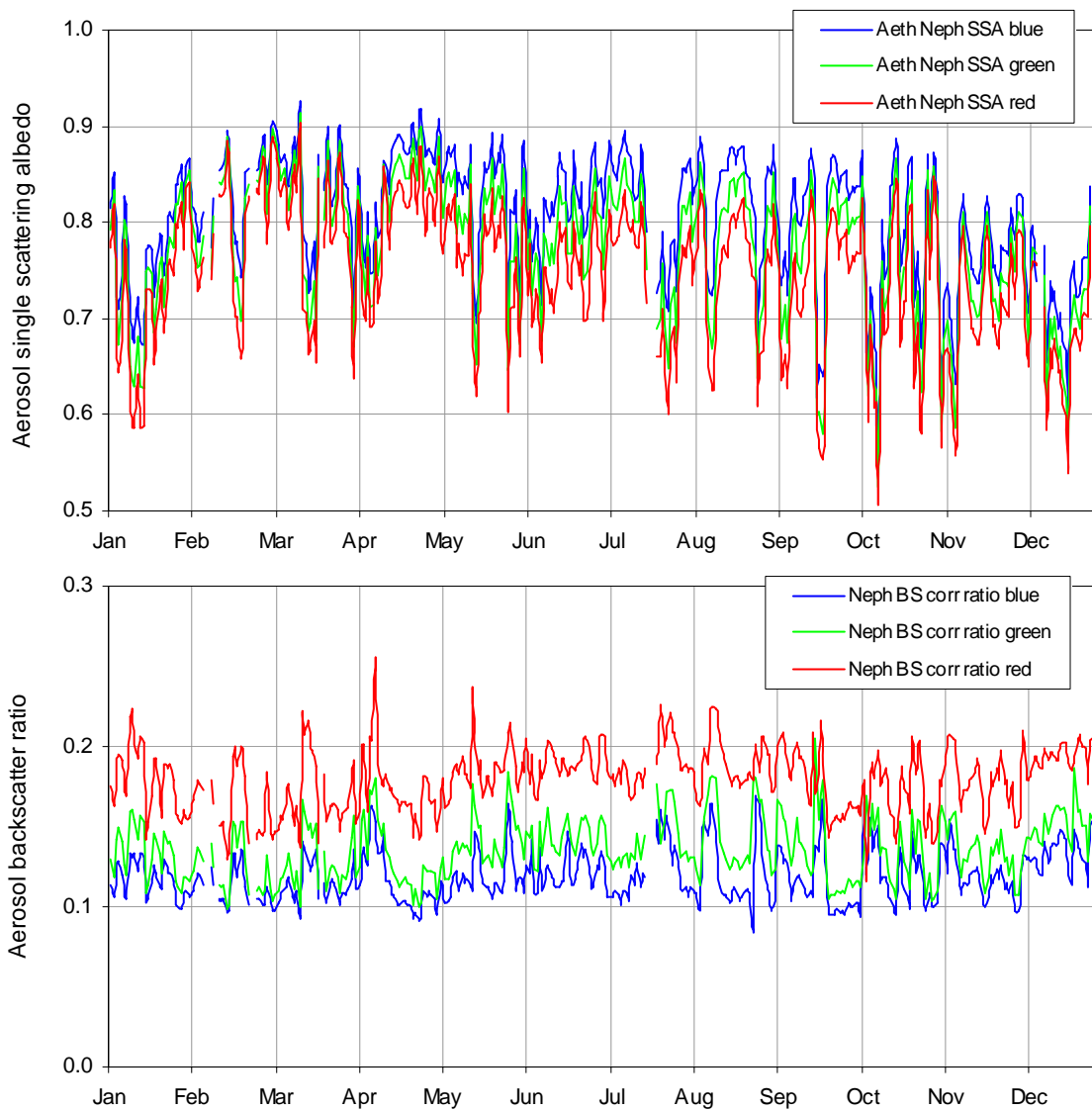
Fig. 36. Aerosol 24-hr average single scattering albedo and backscatter to total scatter ratio at three wavelengths corresponding to blue, green and red (RH generally < 40%).

The 24 hr averaged single scattering albedo at λ = 550 nm (at RH generally < 40 %) ranged from 0.53 to 0.91 (annual average 0.77), with generally higher values in summer compared to winter (Fig. 36a). In 2011, the aerosol single scattering albedo was slightly higher than in 2010 (0.75). The backscatter / total scatter ratio generally ranged from ca. 10 to ca. 20 % (Fig. 36b).

The aerosol extinction coefficient and particle mass or volume concentrations are rather well correlated (Fig. 37). The slope of the regression between extinction and mass shows that the extinction mass efficiency is on average 4.0 m^2g^{-1}, i.e. low compared with 4.5 m^2 g^{-1}, the value calculated based on the aerosol mean chemical composition during 2011, and mass cross section coefficients for the various constituents found in the literature (see Table 4). The agreement between these two estimates of the aerosol extinction cross section deteriorated compared to 2010. The slope of 6.2 observed in the extinction to volume correlation, together with the extinction to mass ratio (6.2/4.0 = 1.53), agrees marginally with the aerosol particle density of 1.32 found in Fig. 33).
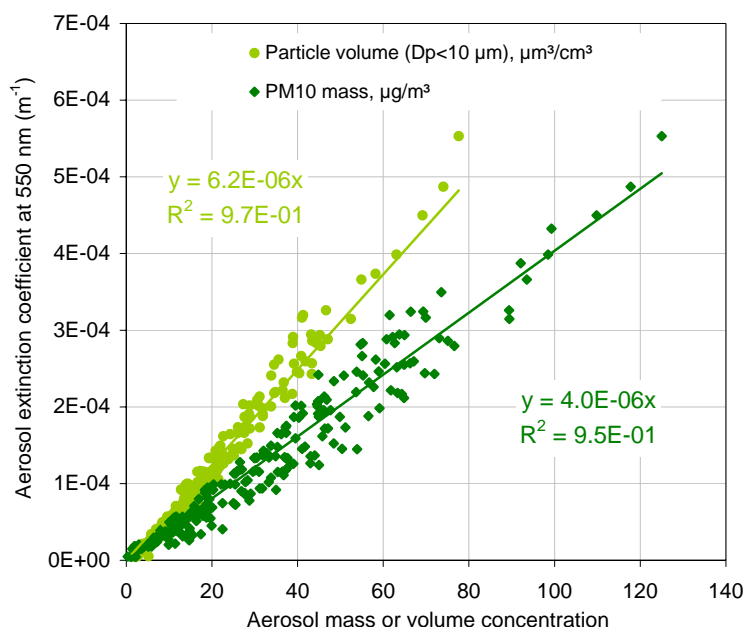

Fig. 37. *Regression between the aerosol extinction coefficient and PM10 mass (FDMS-TEOM) and volume (DMPS + APS) concentrations. PM10 mass data from Jan.-July 2010.*

Table 4. *Mean aerosol chemical composition (PM2.5) in 2011 and extinction efficiency.*

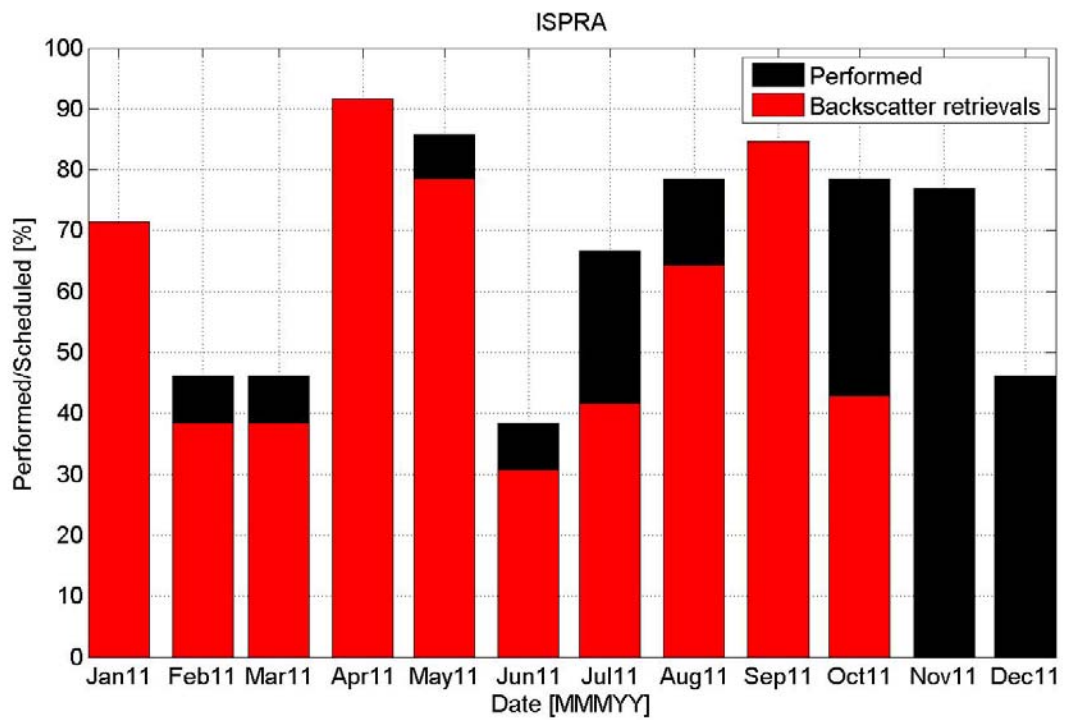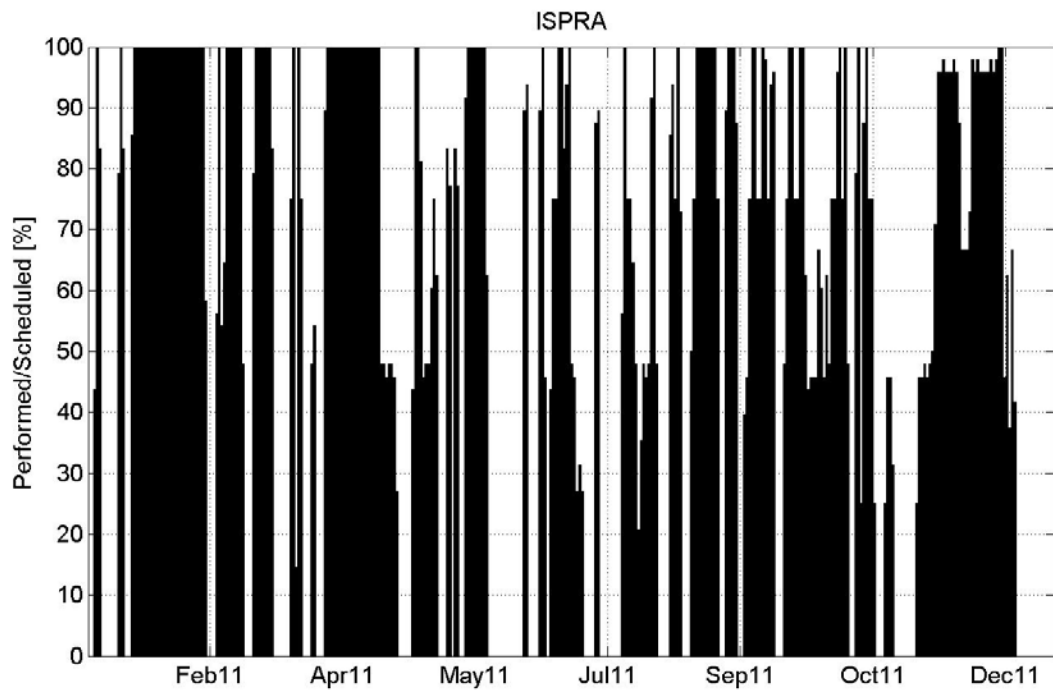|	2011 PM2.5 comp. (%)	σ_{ext} (m²/g)	Reference (for σ_{ext})
"sea salt"	3	1.3	Hess et al., 1998
NH_4^+, NO_3^- and SO_4^{2-}	37	5.0	Kiehl et al., 2000
organic matter	46	3.6	Cooke et al., 1999
elemental carbon	9	11	Cooke et al., 1999
Dust	2	0.6	Hess et al., 1998
Total	**97**	**4.5**	

Fig. 38. *Performed/scheduled measurements for 2011 on daily (upper plot) and monthly bases.*

<u>Aerosol vertical profiles</u>

The backscatter LIDAR was operated almost continuously, mainly based on weather conditions (no rainfall/snow, storm etc.). However, aerosol backscatter and extinction profiles have been retrieved so far mainly for the measurements periods scheduled by <u>Earlinet</u> and for <u>Calipso</u> overpasses.

From 156 scheduled measurements (following the Earlinet schedule), 106 were performed (68%) for the whole year 2011, from which 77 (49%) backscatter coefficients profiles were retrieved (Fig. 38). The data upload to <u>Earlinet</u> database was completed till October 2011. Statistics on daily basis are shown in Fig. 38. Note that the percentage of the backscatter coefficient retrieval is usually smaller than the percentage of the performed to the scheduled measurements and this is due to the fact that not all the measured profiles are suitable for the inversion (in order to obtain the backscatter coefficient).

Out of 80 Calipso overpasses over Ispra, we have 47 days of measurements (52.5 %) and 34 backscatter retrievals (42.5%). However, none of them covers a complete day. Fig. 19 shows an example of simultaneous measurements by the backscatter Lidars in Ispra and and onboard Calipso overpasses (for the 18th of January 2011).

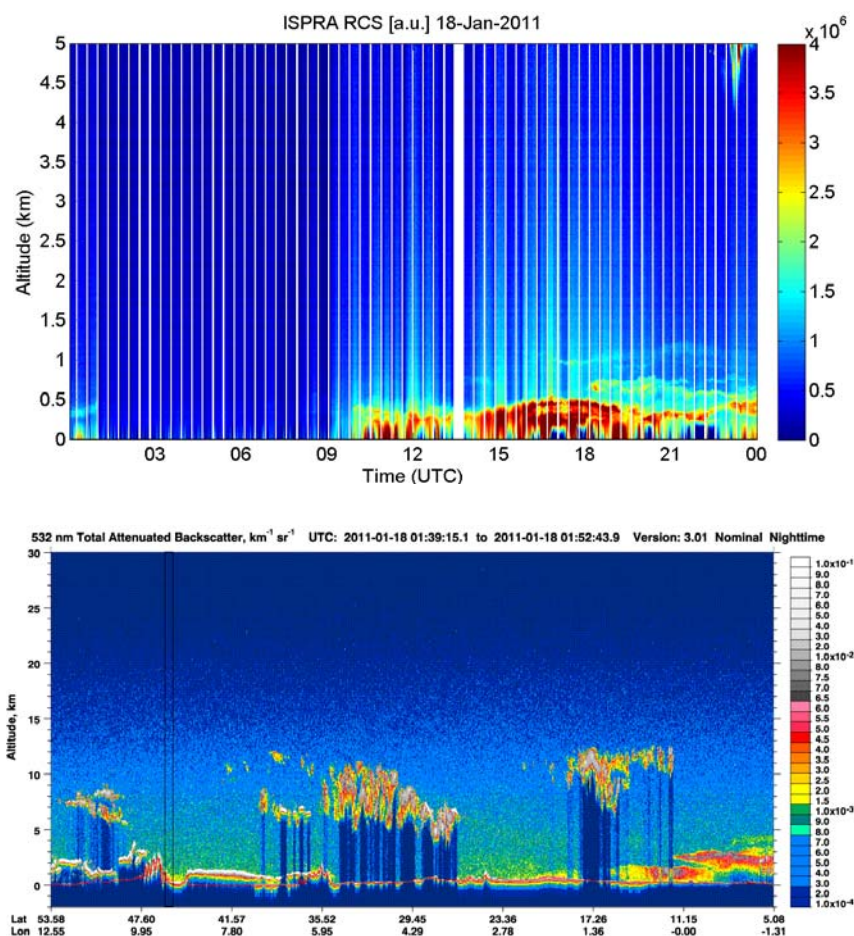Results based on Lidar (CAML) measurements can be found in Barnaba et al., 2010.

Fig 39: Lidar signal obtained at ABC-IS on Jan. 18th, 2011 (upper panel), and simultaneous measurement from Calipso (lower panel, black rectangle).
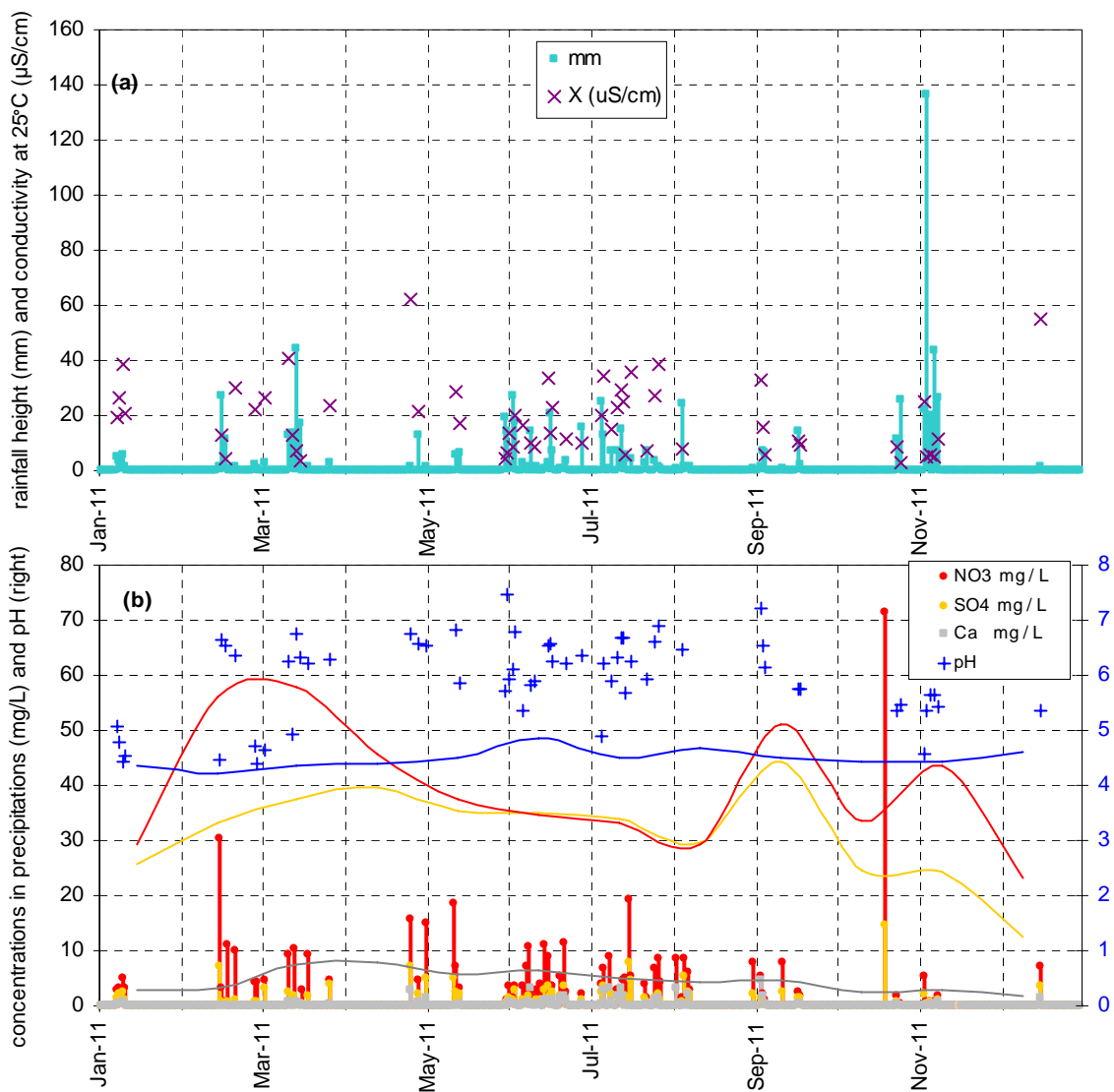
Fig. 40. *(a) Precipitation amount, conductivity and (b) concentrations of 3 major ions in precipitation and pH in 2011 (bars and crosses), and during the 1990-99 period (lines)*
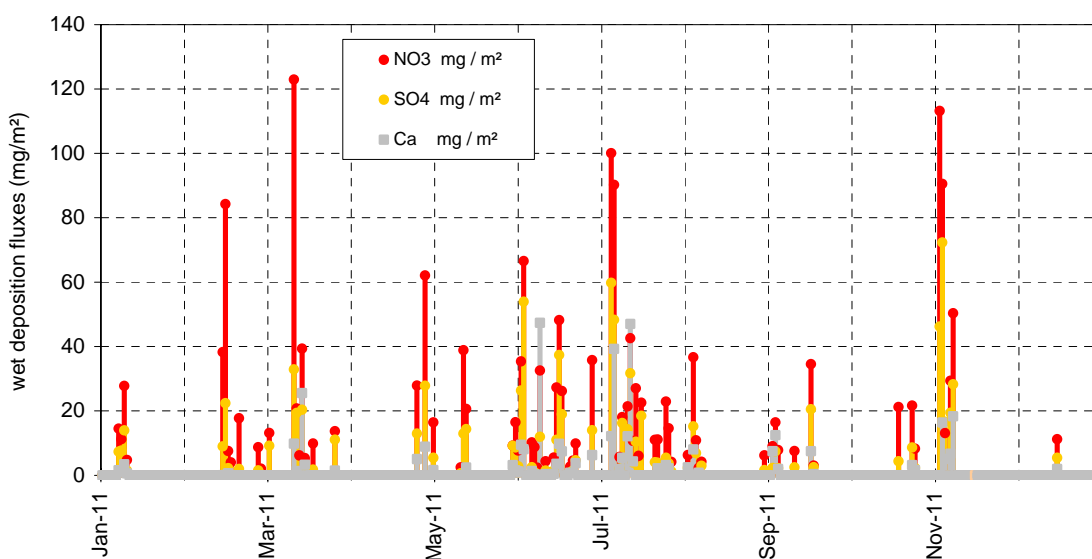

Fig. 40c. *Wet deposition fluxes of 3 main components in rain water in 2011.*

Precipitation chemistry

In 2011, 82 precipitation samples were collected and their ion content determined. Acidity (pH) and conductivity were also measured in 60 and 56 of those samples, respectively (not sufficient water volume was available for the remaining samples). The precipitation height of the collected events ranged from 0.04 to 137 mm (Fig. 40a) for a total of 784 mm *vs.* 1067 mm detected by the rain sensor at the station (including data gap filling based on Bd 51 data). Four major rain events were not sampled.

The ranges of concentrations measured in these samples are indicated in Table 5. Volume weighted mean concentrations of all species but Na^+ and Ca^{2+} were in 2011 smaller than the 1990-1999 averages. All precipitation samples collected in 2011 but 2 were acidic (pH < 7.0). However, pH<5.6 (equilibrium with atmospheric CO_2) was measured in 17 samples only and pH < 4.6 in 5 samples only.

Wet deposition occurred rather evenly from mid February till mid December (Fig. 40c). The annual wet deposition flux of the main acidifying and eutrophying species was 0.9, 1.9, and 0.8 g m^{-2} for SO_4^{2-}, NO_3^-, and NH_4^+, respectively. These fluxes were much smaller than in 2010, where the values were 1.5, 3.1, and 1.3 g m^{-2} for the respective species, at least partly because precipitations were less abundant than average.

Table 5. *Statistics relative to the precipitation samples collected in 2011 (averages are volume weighted)*

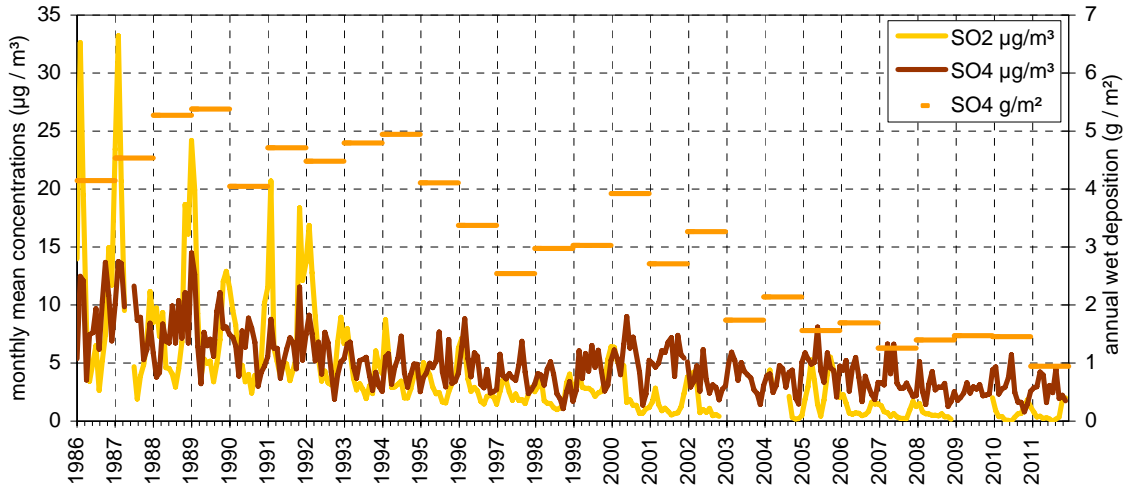|	pH	cond.	Cl^-	NO_3^-	SO_4^{2-}	Na^+	NH_4^+	K^+	Mg^{2+}	Ca^{2+}
		$\mu S\ cm^{-1}$	$mg\ l^{-1}$	$mg\ l^{-1}$	$mg\ l^{-1}$	$mg\ l^{-1}$	$mg\ l^{-1}$	$mg\ l^{-1}$	$mg\ l^{-1}$	$mg\ l^{-1}$
Average	5.44	11.9	0.24	2.4	1.2	0.23	0.99	0.04	0.05	0.51
Min	4.39	2.9	0.02	0.3	0.1	0.01	0.05	<0.01	<0.01	<0.01
Max	7.45	62	11.4	71.4	14.7	7.8	13.5	1.2	0.9	4.6
1990-1999 average	4.40	24.9	0.44	3.9	3.1	0.23	1.3	0.09	0.06	0.45

Fig. 41. Oxidized sulfur species monthly mean concentrations and yearly wet deposition.
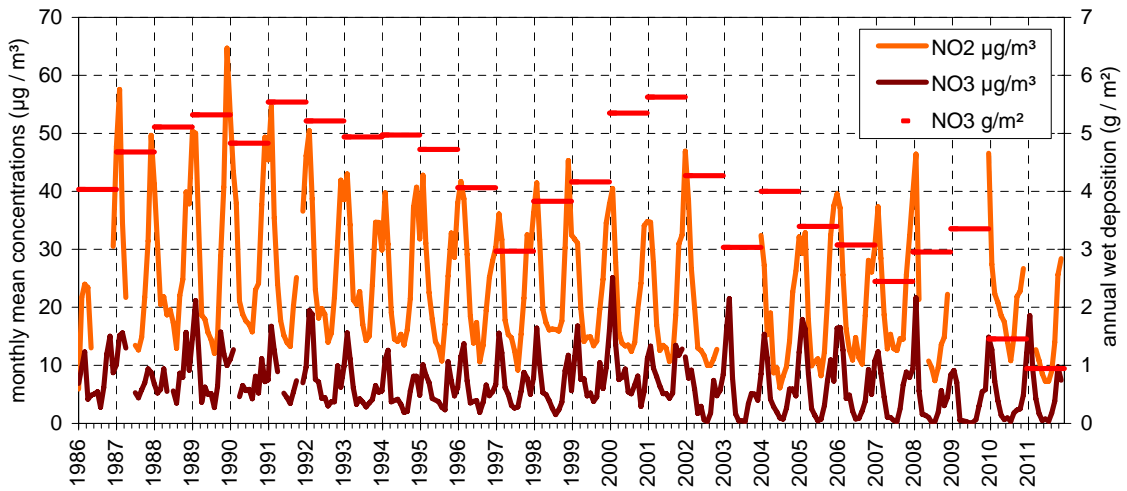

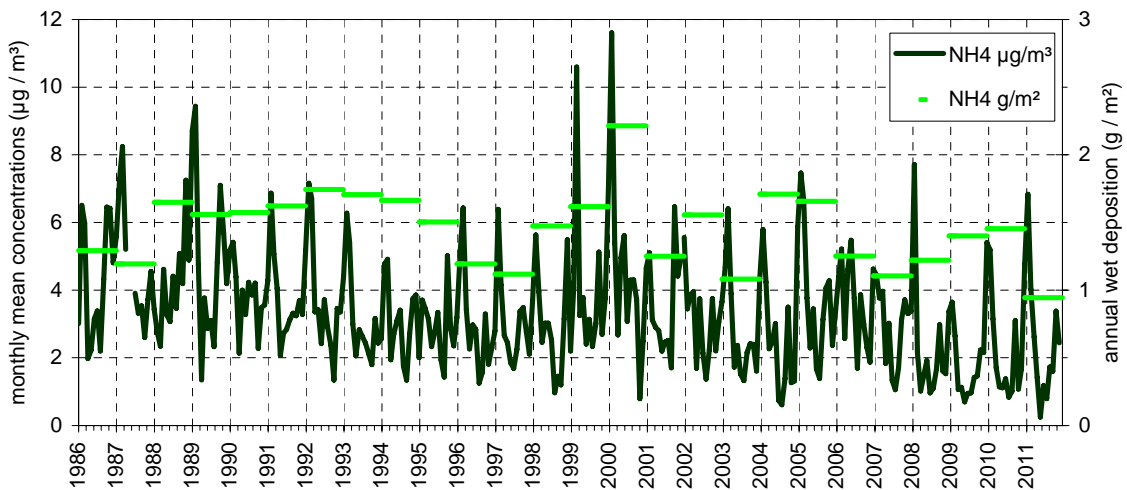Fig. 42. Oxidized nitrogen species monthly mean concentrations and yearly wet deposition.

Fig. 43. Reduced nitrogen species monthly mean concentration and yearly wet deposition.

Results of year 2011 in relation to 25 years of monitoring activities

Sulfur and nitrogen compounds

The 2011 yearly averages for particulate SO4, NO3, and NH4 in PM10 (estimates) were similar or larger than over the past 5 years (2.8, 5.9 and 2.6 μg/m³, respectively).

Indeed, particulate SO_4^{2-} showed a clear decreasing trend from 1986 to 1998 (a factor of about 3), but seems to have been stabilized around the mean value for the 90's since then (see Fig. 41). Both winter maxima and summer minima monthly mean concentrations of sulfur dioxide (SO_2) decreased by a factor of more than 10 over the past 20-25 years (Fig. 41). These data show that locally produced SO_2 decreased much more than possibly long-range transported SO_4^{2-} over the past 20-25 years. It should be kept in mind that SO_4^{2-} concentrations were measured in PM10 or in PM2.5 from 2002 onwards, whereas it was measured in TSP (Total Suspended Particulate) from 1986 to 2001. However, simultaneous sampling of PM10 and TSP over 14 months showed that SO_4^{2-} in PM10 is generally less than 5 % lower than in TSP. It should also be mentioned that SO_4^{2-} is mainly present in the PM2.5 fraction (see Fig. 24). From 2005 onwards the calculations were as following $SO_4^{2-}(PM10) = SO_4^{2-}(PM2.5) \times <SO_4^{2-}(PM10)/ SO_4^{2-}(PM2.5)>$ (the average $<SO_4^{2-}(PM10)/ SO_4^{2-}(PM2.5)>$ is calculated based on the 4-6 simultaneous PM10 and PM2.5 samples collected each month). SO_4^{2-} wet deposition in 2011 was among the lowest values ever recorded at the station.

Monthly mean concentrations of nitrogen dioxide (NO_2) do not show such a pronounced decreasing trend over the last 20-25 years (Fig. 42) as seen for SO_2. Wintertime NO_2 maxima indeed remained quite constant over 1993-2000, and did not reflect the 30 % abatement in NO_x emissions reported for this period (Perrino and Putaud, 2003). Particulate NO_3^- wintertime concentration observed in 2003 - 2011 were comparable to values observed in the mid-90's, mainly due to high wintertime values. It should be noted that since October 2000, NH_4 and NO_3^- have been measured mostly from quartz fibre filters, which are known to lose NH_4NO_3 at temperatures > 20 °C. This might contribute significantly to the fact that NO_3^- summertime minima are particularly low since 2002. Furthermore, NO_3^- was measured from PM10 or in PM 2.5 from 2002, and no more from TSP, as over the 1986 to 2001 period. However, simultaneous sampling of PM10 and TSP over 14 months showed that NO_3^- in PM10 is generally less than 5 % lower than in TSP, like SO_4^{2-}. From 2005 and onwards the calculations were as following $NO_3^-(PM10) = NO_3^-(PM2.5) \times < NO_3^-(PM10)/ NO_3^- (PM2.5)>$ (the average $< NO_3^-(PM10)/ NO_3^-(PM2.5)>$ is calculated based on the 4-6 simultaneous PM10 and PM2.5 samples collected each month. NO_3^- wet deposition annual flux observed in 2011 was the lowest ever recorded during the last 20-25 years recorded in Ispra, and about 4-5 times smaller than in the 90's.

Monthly mean concentrations of NH_4^+ in the particulate phase seem to decrease slightly over 1986 – 2011 (Fig. 43), especially because summertime minima decreased. There is no clear trend regarding NH_4^+ wintertime maxima.
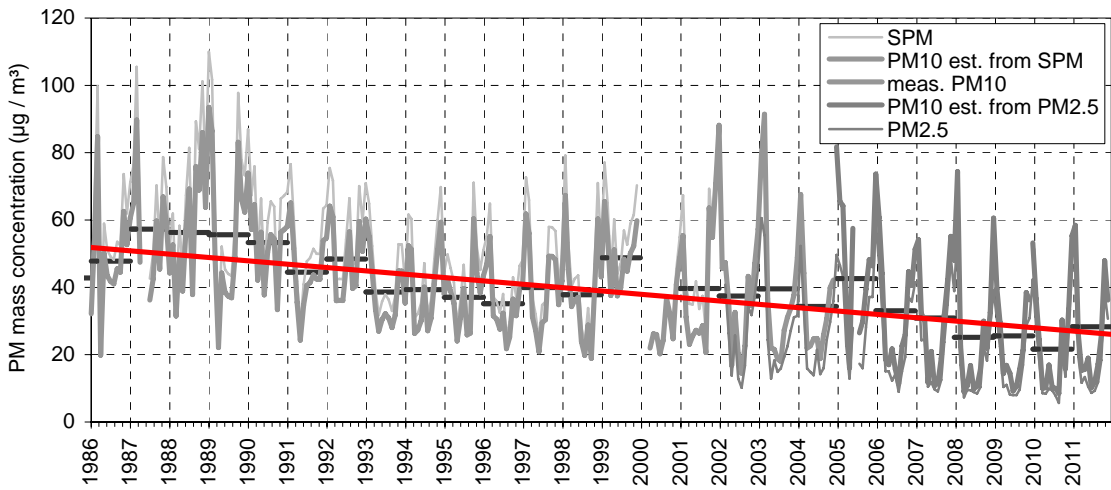
Fig. 44. Particulate matter mass concentration monthly(grey) and annual(black) averages. The red line is the long term trend over annual averages. All values in the figure are from gravimetric measurements or estimated from gravimetric measurements.
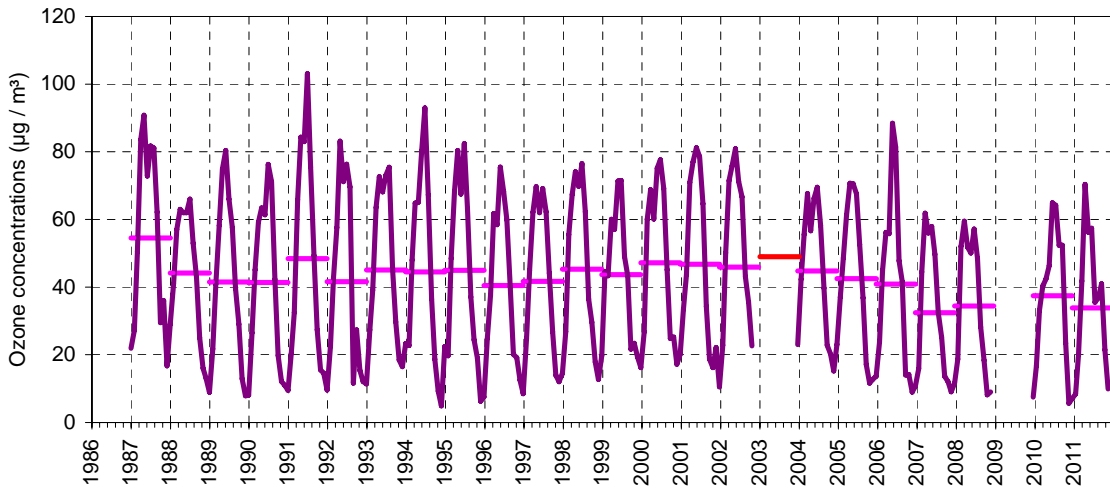

Fig. 45. Ozone yearly and monthly mean concentrations at JRC-Ispra. 2003 (heat wave) yearly average is from Malpensa airport (Source: ARPA Lombardia).
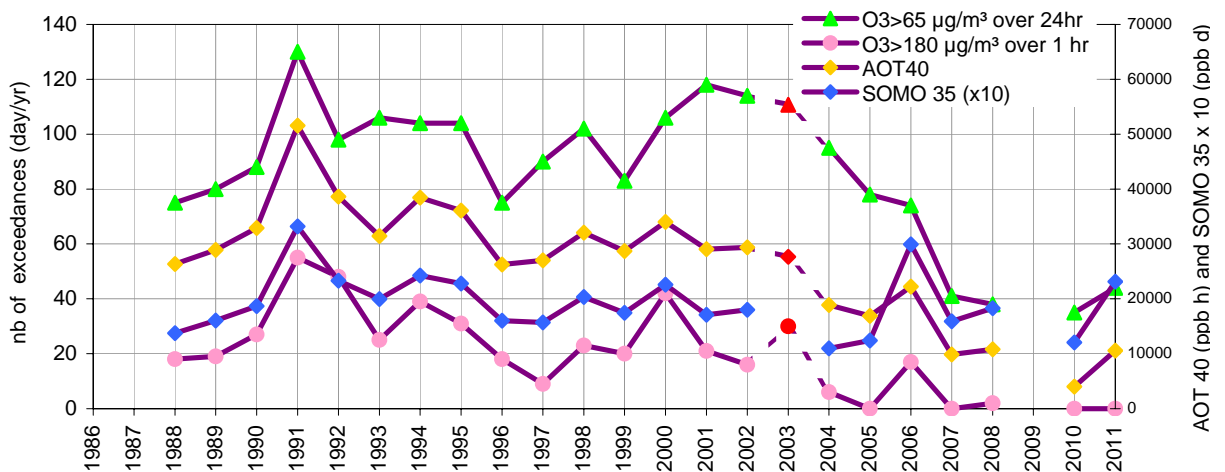

Fig. 46. AOT40, SOMO35 values, and number of days on which O3 limit values were reached. The 3 red spots are data points from Malpensa.

It should be mentioned that from the year 2002 NH_4^+ was measured in the PM10 or in the PM2.5 fraction (from 2005 and onwards the calculations were as following NH_4^+(PM10) = NH_4^+(PM2.5) x < NH_4^+(PM10)/ NH_4^+(PM2.5)> (the average <NH_4^+ (PM10)/ NH_4^+(PM2.5)> is calculated based on the 4-6 simultaneous PM10 and PM2.5 samples collected each month). On average, NH_4^+ can neutralize close to 100% % of the acidity associated with NO_3^- and SO_4^{2-} in the particulate phase (see Fig. 21). NH_4^+ is also quite well correlated with NO_3^- + SO_4^{2-} in rainwater. NH_4^+ annual wet deposition was the lowest recorded in Ispra during the last 20-25 years.

Particulate matter mass

The PM10 values observed in 2011 somewhat breaks the decreasing trend in PM10 observed over the last 2 decades (Fig. 44). Indeed, the annual average PM10 concentration (estimated from PM2.5 measurements) reached 28.3 µg/m³ in 2011, i.e. a larger than the historic minimum of 21.6 µg/m³ observed in 2010, and comparable to the 2007 and 2008 values. This relatively high PM_{10} annual mean value is probably at least partly due to the fact that January and December 2011 were particularly dry. However, a linear fit indicates that PM10 has been decreasing by 1.0 µg m^{-3} yr^{-1} between 1986 and 2011. It should be kept in mind that PM10 concentrations were estimated from TSP mass concentration measurements (carried out by weighing at 60 % RH and 20 °C cellulose acetate filters sampled without any particle size cut-off and "dried" at 60 °C before and after sampling) over 1986-2000, based on a comparison between TSP and PM10 over the Oct. 2000 - Dec. 2001 period (R² = 0.93, slope = 0.85), and based on measured PM2.5 values for years 2005-2011.

Ozone

Figure 45 shows monthly and yearly mean O_3 concentrations observed since 1987. It should be mentioned that ozone was not measured in 2009 and that there were an acquisition breakdown in 2003. No clear trend in O_3 annual mean concentrations can be deduced from the observations over 1987-2006, but the annual averages observed from 2007 are the lowest measured since 1986. Wintertime minimums keep on decreasing since 2003, while summer time maximums are more variable, with greater values observed on particularly warm and sunny summer months.

All ozone indicators (Figure 46) but the number of days on which the limit of 180 µg/m³ over 1hr was exceeded (still equal to 0) increased in 2011 compared to 2010. The number of days with a 24-hour mean O_3 concentration > 65 µg/m³ (vegetation protection limit) increased from 35 (2010) to 44 (2011), but remains among the lowest ever recorded in Ispra. AOT40 (Accumulated Ozone exposure over a Threshold of 40 ppb), the vegetation exposure to above the O_3 threshold of 40 ppb - about 80 µg/m³), increased from 4000 ppb h (2010) to 10500 ppb h (2011), which remains the 2nd lowest value ever measured since 1988. The population exposure indicator SOMO 35 (Sum of Ozone Means Over 35 ppb, where means stands for maximum 8-hour

mean over day) increased significantly from1200 ppb d in 2010 to 2300 ppb d in 2011, and is back to values observed in the late 1990's.

Conclusions

Meteorological data acquired at the EMEP-GAW site of JRC-Ispra indicate that 2011 was a particularly dry, sunny and warm year.

This may at least partly explain that various indicators for O_3 pollution increased compared to 2010 (during which data coverage and data quality were less satisfactory). However, the annual mean concentrations of SO_2, NOx, CO and even O_3 remained among the lowest observed over the past 25 years.

Aerosol sampling on quartz fibre filter, and subsequent gravimetric and chemical analyses were also performed over the whole year. We collected PM2.5 daily and PM10 five times a month using two Partisol samplers, with and without a carbon monolith denuder, respectively. With the assumption used to estimate POM and dust from organic carbon (OC) and Ca^{2+}, respectively, the whole PM2.5 mass concentration could be explained rather well in 2011, except for a few occasions. PM2.5 average chemical composition was dominated by carbonaceous species (POM: 46%, EC: 9%), followed by secondary inorganics (NH_4^+:9%, NO_3^-: 12%, SO_4^{2-}: 16%). The contribution of sea-salt ions and mineral dust were about 2-3 % each. However, there is a clear increase of the NO_3^- contribution when shifting from cleaner (PM2.5 < 15 µg/m³) to more polluted periods (PM2.5 > 25 µg/m³). The PM10 mass annual average of 28 µg/m³ did not exceed the EU annual limit value (40 µg/m³), but 54 exceedances (derived from TEOM measurements) of the 24-hr limit value (50 µg/m³) were observed. The long term time series still suggests a PM10 mass concentration decreasing trend of 1.0 µg m^{-3} yr^{-1} over the last 25 years of records. It should be mentioned that the three lowest PM10 values since 1986 were measured in 2008, 2009 and 2010 (see Figure 44).

The average particle number in 2011 (average: 6870 cm^{-3}, range 1620 – 16400 cm^{-3}) was close to the 2010 value (6800 cm^{-3}). Particle number size distributions were generally broadly bimodal, with a submicron mode at ca. 100 nm (dry) and a less pronounced coarse mode around 2 µm. The particle mean geometric diameter ranged 30 – 130 nm (maximum values observed in winter) and averaged 77 nm. Atmospheric aerosol scattering and absorption coefficients at various wavelengths were derived from Nephelometer and Aethalometer measurements in dried atmosphere (generally lower than 40%). The mean single scattering albedo at λ = 550 nm (not corrected for hygroscopic growth) was 0.77 in 2011.

The aerosol extensive variables measured at JRC-Ispra (at ground level) all follow comparable seasonal variations with minima in summer. These variables are generally well correlated and lead to reasonable degrees of chemical, physical, and optical closures. However, the average aerosol density of 1.32 g/cm³, derived from the gravimetric mass and DMPS + APS volume was still a bit low, compared to 1.38 g/cm³ in 2010, and especially to the 2005 value of 1.50 g/cm³. Also, the extinction-to-mass ratio of 4.0 m^2 g^{-1} observed in 2011 is comparable to 3.9 m^2 g^{-1}

observed in 2010, but also low compared with the value that can be calculated from the mean PM2.5 chemical composition, which sums up to 4.5 m^2 g^{-1} in 2011 (see Table 4).

Aerosol backscatter and extinction profiles were obtained with a LIDAR across the whole during 2011. Due mainly to unsuitable meteorological conditions, 106 out of the 156 profiles scheduled by EARLINET could be measured. Aerosol backscatter profiles were retrieved for 77 of these measurements (from January to October), but results are still being inspected before submission to the EARLINET data base.

The concentrations of all rainwater components (Cl$^-$, NO$_3^-$, SO$_4^{2-}$, NH$_4^+$, K$^+$, Mg^{2+}), but Na$^+$ and Ca^{2+} were lower in 2011 compared to the 1990-1999 average. The annual wet deposition flux of the main acidifying and eutrophying species were 0.9, 1.9, and 0.8 g m^{-2} for SO$_4^{2-}$, NO$_3^-$, and NH$_4^+$, respectively. These annual fluxes are the lowest ever observed at the EMEP-GAW station in Ispra.

The 2011 data listed by EMEP and ACTRIS as core parameters have been reported to EBAS in 2012, as requested by the networks.

Fig.47: Trailer mast in San Rossore that holds the sonic anemometer and Infra Red Gas Analyser
(IRGA) used for flux measurements (on the left picture in retracted configuration for service, on
the right at measurement position).

Atmosphere – Biosphere flux monitoring at San Rossore

Location and site description

The measurement site 'San Rossore' (43°43.68'N, 10°17.04E, 6 m a.s.l.) operated by the Climate Change and Air Quality Unit is located in the Parco San Rossore (www.parcosanrossore.org), approximately 9 km west of Pisa and 500 m east of the seashore in a Mediterranean forest ecosystem (see Fig.). The Climate Change and Air Quality Unit operates the site in the Parco San Rossore site since 1999.

The measurement site is situated in an almost flat area with a morphology characterized by the presence of sandy dunes. The vegetation in the direct vicinity is a pinewood established in 1953 following artificial seeding and it is dominated by the evergreen tree Pinus pinaster with sparse trees of Pinus pinea and Quercus ilex. The average canopy height is approximately 18 m. The understorey vegetation is confined to the forest edges and canopy gaps.

The area has a Mediterranean – type climate within the sub-humid zone, with a mean annual rainfall of 876 mm yr^{-1} and a range of 534 – 1270 mm for the period 1980 – 2005. The long term data were obtained from a meteorological station located at a distance of approximately 10 km and managed by the Regional Hydrologic Service of Tuscany. Rain falls mainly during autumn and winter with about 50% occurring between September and November, while the driest months are July and August. The average annual temperature is approximately 15 °C with the average temperature of the coldest month (January) being 7 °C and that one of the warmest month (August) being 25 °C. The wind regime is characterized by a sea – land breeze circulation, i.e. the air flows quite predictable from the west (sea) during day and from east (land) during night.

Starting in 2009, major clear cuts of the forest in the vicinity of the measurement site were initiated as a response of the park management to the infection of the Pinus pinaster with 'Matsucoccus feytaudi' (see Fig. 48). As it is obvious from the satellite picture, the cuts destroy the homogeneity of the canopy around the measurement site (red circle). This inhomogeneity of the ecosystem in the fetch of the flux tower now renders eddy covariance measurements of ecosystem fluxes almost meaningless. It has therefore been decided to move to a new location within the park that is not threatened by the 'Matsucoccus feytaudi' and has a homogeneous canopy suitable for micrometeorological measurements. The new site has been identified in 2011 (blue circle in Fig. 49), approximately 700m away and within a quite homogenous stand of Pinus pinea. The construction of a new tower for eddy covariance measurements of fluxes and the start of equipping the site is foreseen for autumn 2012.
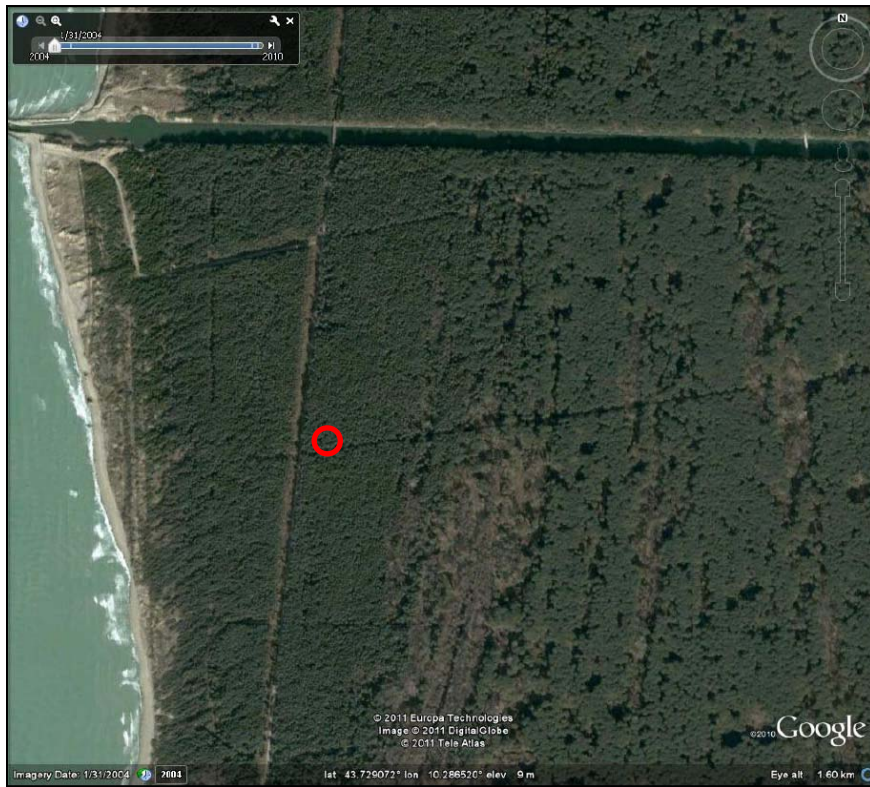
Fig. 48: Location of the measurement site in the Parco San Rossore (red circle). The picture from Google Earth taken on 31.01.2004 shows a homogenous canopy around the flux tower.
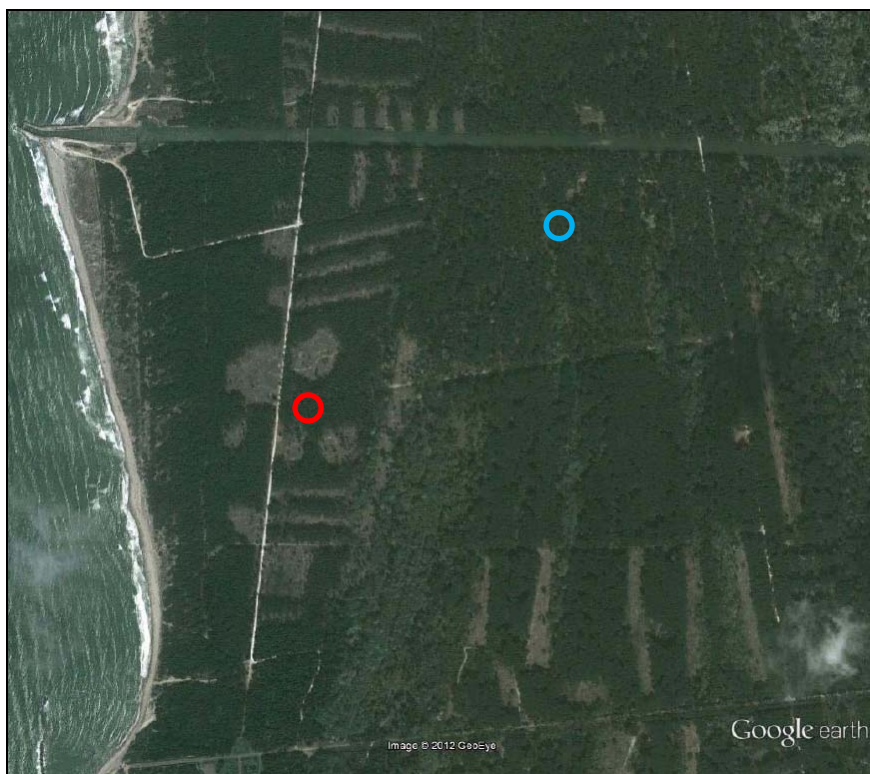

Fig. 49: The picture of the vicinity around the measurement site from Google Earth taken on 04.08.2011 visualizes the severe cutting of tries due to infection with 'Matsucoccus feytaudi'. The blue circle shows the location of the new tower at ~700 m distance.

With regards to data reporting as in the previous years, quality checked data for 2011 have been submitted to the Fluxnet database at the European Fluxes Database Cluster at gaia.agraria.unitus.it/home (ex IMECC Terrestrial Carbon Data Centre).

Monitoring program

The measurement site in the Parco San Rossore will be a level 2 Ecosystem Station within ICOS. The project ICOS (Integrated Carbon Observation System, www.icos-infrastructure.eu) is one of the pan-European research infrastructure projects identified by the European Strategy Forum on Research Infrastructures (ESFRI) for implementation. After its preparatory phase planned for 2008 until 2013, during which monitoring infrastructure and technical procedures are developed, its operational phase will run for 20 years from 2014 until 2033. Once in operational mode, greenhouse gas concentrations and fluxes will be monitored on a routine basis following a very strict quality controlled protocol, both in terms of measurement instrumentations required to be used and procedures to be followed. Level 2 stations provide data for less parameter compared to level 1 stations and thus require less investment for instrumentation and have lower running costs in terms of instruments and staff. The mandatory variables to be monitored at the level 2 Ecosystem Station Parco San Rossore are shown in Table 6.

Table 6: *ICOS level 2 Ecosystem Station core parameters.*

Core variables continuous	Core variables daily to monthly	Core variables yearly
CO_2, H_2O and energy fluxes	leaf area index	biomass (above ground)
wind speed and direction	CH_4, N_2O by manual chambers during sporadic short-term campaigns	soil carbon
CO_2 concentration vertical profile, normal precision	phenology	stem diameter
net radiation: • incoming/reflected global radiation • incoming/outgoing longwave radiation • Albedo		above-ground Net Primary Production (NPP)
diffuse global radiation		litter fall
incoming / reflected under canopy Photosynthetic Active Radiation (PAR)		land-use history
temperature and relative humidity vertical profile		managements and natural disturbances
air pressure		C and N import and export on managed sites
precipitation, through-fall, snow depth		
soil heat flux		
ground water level		
soil temperature profile		
water content profile		

The measurement techniques

Fluxes of CO_2, H_2O and sensible heat were measured with eddy covariance technique and evaluated using the EdiRe software package from the University of Edinburgh (www.geos.ed.ac.uk/abs/research/micromet). The ancillary parameters (meteorology, radiation and soil) were obtained with respective sensors and the data quality checked for instrument malfunctioning, obvious outliers and consistency. Daily averages of the different parameters measured during the course of 2011 are presented in the section "Measurements in 2011" as an overview.

Infrastructural:

Sensor location

The instruments for eddy covariance flux system, i.e. sonic anemometer and fast gas analyser, are mounted on the top of a temporary trailer mast with a height of 22 m. Soil parameters are measured at close vicinity to the trailer on the forest ground. Radiation and meteorological sensors are placed on top of a scaffold tower structure at a distance of approximately 500 m from the main measurement site.

Data acquisition

Eddy covariance flux data are stored with high frequency, i.e. 10 Hz, as chunks of 30 minutes on a local laptop connected to the sonic anemometer. Data from all other sensors are read every 10 s by a DL2e data logger from Delta-T Devices (www.delta-t.co.uk) which saves 30 minute averages of the acquired data.

For eddy covariance flux data, the start time of every 30 minutes measurement period is saved as the reference time, whereas for all other data, the end of the 30 minutes measuring period is used. The time reference used for all San Rossore measurements is local time, not corrected for summer time.

Ecosystem fluxes:

Sonic Anemometer for 3D wind direction Gill R3-50

Sonic anemometers determine the three dimensional wind vectors at high frequency using the speed of sound. The Gill R3-50 (www.gill.co.uk) emits ultrasonic pulses between its pairs of transducers, measures the flight time of the pulses to the paired transducer and calculates the wind speed in the direction of the transducer pair (see Fig 50). Combining the results from the three transducer pairs, the 3 dimensional wind speed is calculated at a frequency of 20 Hertz. After a rotation of the coordinate system during the data processing to align it with the north direction, horizontal and vertical wind speeds and the wind direction are calculated besides their use for flux calculations. As the speed of sound measured with the anemometer depends on the temperature, the so-called sonic temperature is reported by the instrument as well.

Due to the absence of moving parts and the fact that no calibration is required, the instrument is very robust and reliable. Instrument servicing is done at the manufacturer.
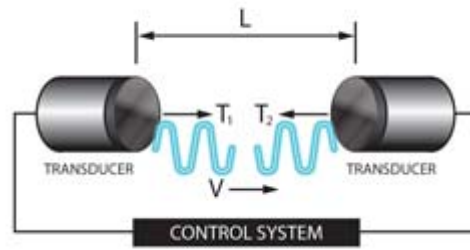
$$T_2 = \frac{L}{C - V} \quad \text{and} \quad T_1 = \frac{L}{C + V}$$

therefore

$$V = \frac{L}{2}\left\{\frac{1}{T_1} - \frac{1}{T_2}\right\} \qquad C = \frac{L}{2}\left\{\frac{1}{T_1} + \frac{1}{T_2}\right\}$$

Fig. 50: Measurement principle of sonic anemometers, T: travelling time of sound pulses, L: distance between transducers, C: speed of sound, V: wind speed in direction of transducers (sketch from www.gill.co.uk)

Fast infrared gas analyser for CO_2 & H_2O concentration (IRGA) LI-7500 A

For the determination of CO_2 and H_2O fluxes with the eddy covariance technique, fast analysers (10 to 20 Hertz) for concentration measurements of the gases of interest are obligatory. At San Rossore, a LI-7500A Open Path CO_2/ H_2O Analyser from LI-COR (www.licor.com) has been installed.

The LI-7500A is a high performance, non-dispersive, open path infrared CO_2/H_2O analyser based on the infrared absorption of CO_2 and H_2O at ambient conditions that provides concentration measurements at a frequency of up to 20 Hertz. In the sampling volume (see figure Fig. 51), light from the infrared source is absorbed at characteristic wavelengths for CO_2 and H_2O. This specific absorption is a function of the gas concentration in the sampling volume. Using the absorption measurements at the CO_2 & H_2O wavelengths, at a non-absorbing wavelength plus calibration factors and measured temperature and pressure, the LI-7500A provides number-, mass densities or mole fraction of the two gases.

Zero and span checks and calibrations are done regularly using zero gas from a cylinder plus a dew point generator (LI-COR 610) and a CO_2 standard from a cylinder.
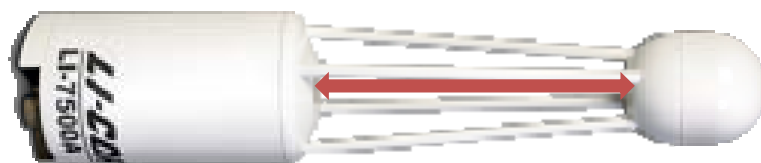

Fig.51: LI-7500A analyser head (from www.licor.com), arrow indicates sampling volume

Radiation instruments

Short wavelength incoming radiation Li-Cor Li-200 Pyranometer

The incoming short wavelength solar radiation is measured with a Li-200 Pyranometer from Li-Cor (www.licor.com). It is a low price device compared to first class thermopile-type pyranometers such as the CM11 used et the EMEP station. The LI-200 features a silicon photovoltaic detector mounted in a fully cosine-corrected miniature head. Current output, which is directly proportional to solar radiation, is calibrated against an Eppley Precision Spectral Pyranometer (PSP) under natural daylight conditions in units of watts per square meter (W m^{-2}). Under most conditions of natural daylight, the deviation of the Li-200 compared to the reference instrument is <5%.

Photosynthetic active radiation Delta-T BF3

With the Sunshine Sensor BF3 from Delta-T (www.delta-t.co.uk), total (in the sense of direct plus diffuse) solar radiation, diffuse radiation and the sunshine state is measured as photosynthetic active radiation (PAR) of the solar spectrum, i.e. from 400-700 nm. To distinguish between direct and diffuse radiation, a set of seven photodiodes (PD) is arranged under a patterned hemispherical dome with 50% black bands such that at any position of the sun in the sky at least one photodiode is completely in the shade and at least one is fully exposed to direct sunlight. This design eliminates the necessity of frequent alignment of the shading parts to the position of the sun. The diffuse radiation is then given by:

$$PAR_{diffuse} = 2 \cdot PD_{\min} \quad \text{and the direct by} \quad PAR_{direct} = PD_{\max} - PD_{\min}$$

The instrument reports $PAR_{diffuse}$, $PAR_{total} = PAR_{diffuse} + PAR_{direct}$ and sunshine state. The latter one indicates sunshine if $PAR_{total}/PAR_{diffuse} > 1.25$ and $PAR_{total} > 50 \, \mu mol \cdot m^{-2} \cdot s^{-1}$.

Soil instruments

Soil heat flux sensors Hukseflux HFP01

A set of 5 thermal sensors HFP01SC from Hukseflux (www.hukseflux.com) have been buried a few centimetres underground in the undisturbed soil around the tower to obtain a good spatial averaging of the soil heat flux. The determination of the heat flux is based on measuring the temperature difference of two sides of a plate that is exposed to a heat flow using a number of thermocouples connected in series (see Fig. 52). Ignoring possible errors, the temperature difference between the hot and cold side of the sensor is proportional to the heat flow. As the thermocouples provide a voltage proportional to the temperature, the voltage output of the sensor is proportional to the heat flow across the sensor.
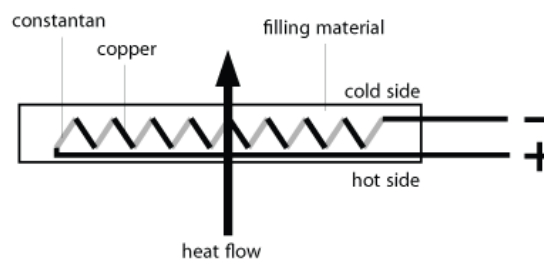

Fig. 52: *Sketch of a soil heat flux sensor (drawing from www.wikipedia.org)*

Soil water content vertical profile with TRIME-TDR from IMKO

Profile measurements of soil water content are performed using the TRIME-TDR (Time domain Reflectometry with Intelligent MicroElements with) from IMKO (www.imko.de). Based on Time-Domain-Reflectometry, the sensor generates high frequency electromagnetic pulses that propagate along a wave guide and reflected back into the sensor. Depending on the dielectric constant of the material surrounding the waveguide, the round trip time of the hf-pulses varies between some tens and thousand picoseconds. As the dielectric constant of soil and thus the round trip time strongly depends on the soil moisture content, measuring this time gives the water content of the soil surrounding the sensor. Burying several sensors at depths of xx, yy, zz cm below ground provides the soil humidity profile.

Soil temperature profile with PT-1000

For the measurement of the soil temperature profile, three PT-1000 temperature sensors with 3 cable wiring setup are buried at 3 cm, 15 cm and 50 cm below ground.

Ground water level Micro-Diver DI6xxx from SWS

The ground water level is monitored with Micro-Divers from Schlumberger Water Services (www.swstechnology.com). The device is placed in a water filled hole, 1 m below ground, and logs autonomously the pressure. Combining the measurement with the barometric pressure at the site gives the height of the water column above the sensor. Together with the known sensor depth below ground, the water table height can be easily calculated (see also Fig. 53):

$$WL = TOC - CL - WC \text{ with } WC = 9806.65 \cdot \frac{\left(p_{Diver} - p_{baro}\right)}{\rho \cdot g} ; \, g = 9.81 \text{ m/s}^2, \quad = 1.00 \text{ kg/m}^3$$
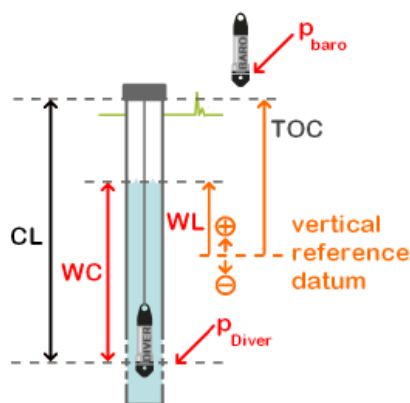
Fig. 53: Principle of water level calculation using the Diver (sketch from www.swstechnology.com). CL: cable length, TOC: top of container, WC: water column, WL: water level relative to a reference, p: pressure.

Flux data processing

Data evaluation (Table 7) for flux data is done using the free EdiRe software package developed at the micrometeorology group from the University of Edinburgh. (www.geos.ed.ac.uk/abs/research/micromet/EdiRe/). As input data, EdiRe uses the 30 min raw flux data files in the binary *.slt format plus 30 minute averaged pressure, temperature and relative humidity data in ASCII format. As time convention, the start of the measurement period has to be assigned to the input data, the middle of the measurement period is assigned to the output data.

The main processing steps used within EdiRe to arrive at final, 30 minute averaged flux data that are corrected for various effects are the following:

Measurements performed in 2011

Despite the unfortunate circumstances of tree cutting activities described in the preceding chapter, the measurement program at the San Rossore site continued also in 2011. The main parameters measured are summarized in Table 8. In addition, sensors already installed for sap flow and stem temperature measurements continued to record data.

Table 8*: parameters measured during 2011*

FLUXES	CO_2, latent heat, sensible heat
METEOROLOGY	3D wind speed, temperature, relative humidity, pressure, precipitation
RADIATION	short wave incoming, direct & diffuse photosynthetic active radiation
SOIL	temperature profile, water content profile, heat flux, water table height
BIOLOGICAL	litter fall

Table 7: *Processing steps for flux calculations using the EdiRe Software package.*

| EdiRe Process	brief description
Preprocessed Files	data from input file, gas concentrations as molar densities
Extract	all high speed data
Despike	all high speed data
Linear	conversion of raw data from voltages into physical variables
1 chn statistics	averages of 3D wind, sonic temperature and gas concentration
Gas conversion	conversion of molar densities to molar fraction
Filter – detrend	linear detrending of gas concentrations
Wind direction	align with geographic direction
Rotation coefficients	perform 3D coordinate rotation
Cross Correlate	gas concentrations with vertical wind speed
Remove Lag	remove time lag between anemometer and gas analyser
Friction Velocity	calculate u*
Sensible heat flux coefficient	
Latent heat of evaporation	
2 chn statistics	calculate covariances, i.e. uncorrected fluxes
Sonic T - heat flux correction	
Stability - Monin Obhukov	calculate z/L stability parameter
Frequency response	calculate high frequency correction for all fluxes
Webb correction	calculate water density fluctuation correction for all fluxes
Stationarity	perform stationarity test
Integral Turbulence	calculate integral turbulence
Cospectra	calculate co-spectra for all fluxes
Storage	calculate storage term
User defined	determine quality flag (0,1,2) for all flux data according to Carboeurope methodology
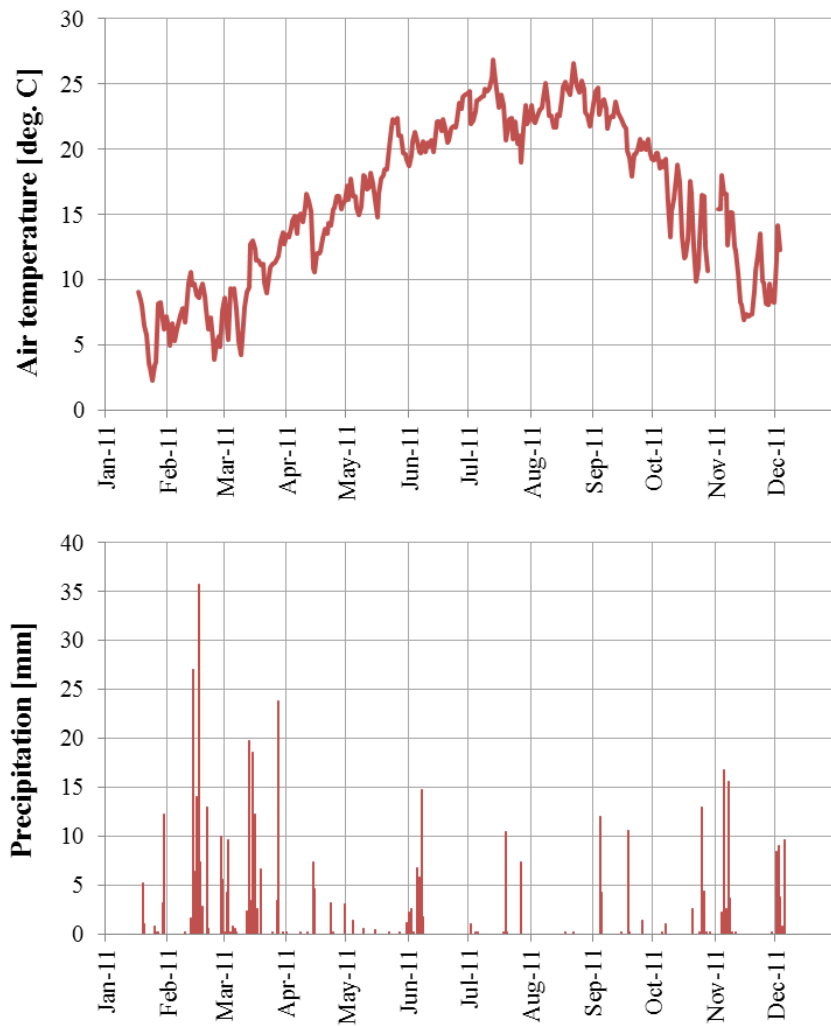
Fig. 54: Daily averages of air temperature (top) and daily sum of precipitation (bottom) as measure in the Parco San Rossore. Gaps in the temperature curve show periods with missing data.
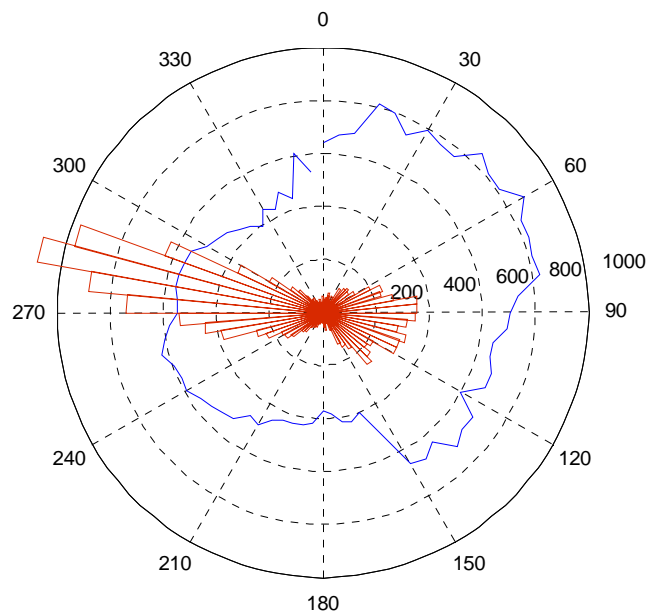

Fig. 55: Wind rose for 30 min. averages of wind measurements with wind speed >0.5 m/s. Red: wind directions, blue: average wind speeds per direction interval in a.

Results of the year 2011

Meteorology

Daily averages for the annual cycle of air temperature, pressure and precipitation are shown in Fig. . Taking the data gaps in January and December into consideration, the annual mean temperature for 2011 is an upper limit and results in 16.1° C. The total measured rainfall was 456.8 mm and due to the same data gaps as for temperature measurements a lower limit. Despite the gaps, 2011 was an extremely dry year in San Rossore compared to the mean annual rainfall of 876 mm yr^{-1}.

The predominant sea – land breeze wind circulation can be seen from the statistical evaluation of the 3D wind direction measurements and is shown in Fig. . The red plot shows the frequency distribution the wind directions for wind speed > 0.5 m/s; the blue line indicates the average wind speeds per directional bin.

Radiation

In Figure 56, the annual cycle of short wave incoming radiation is shown on the top graph, the photosynthetic active radiation (PAR) in terms of total and diffuse contribution on the bottom.
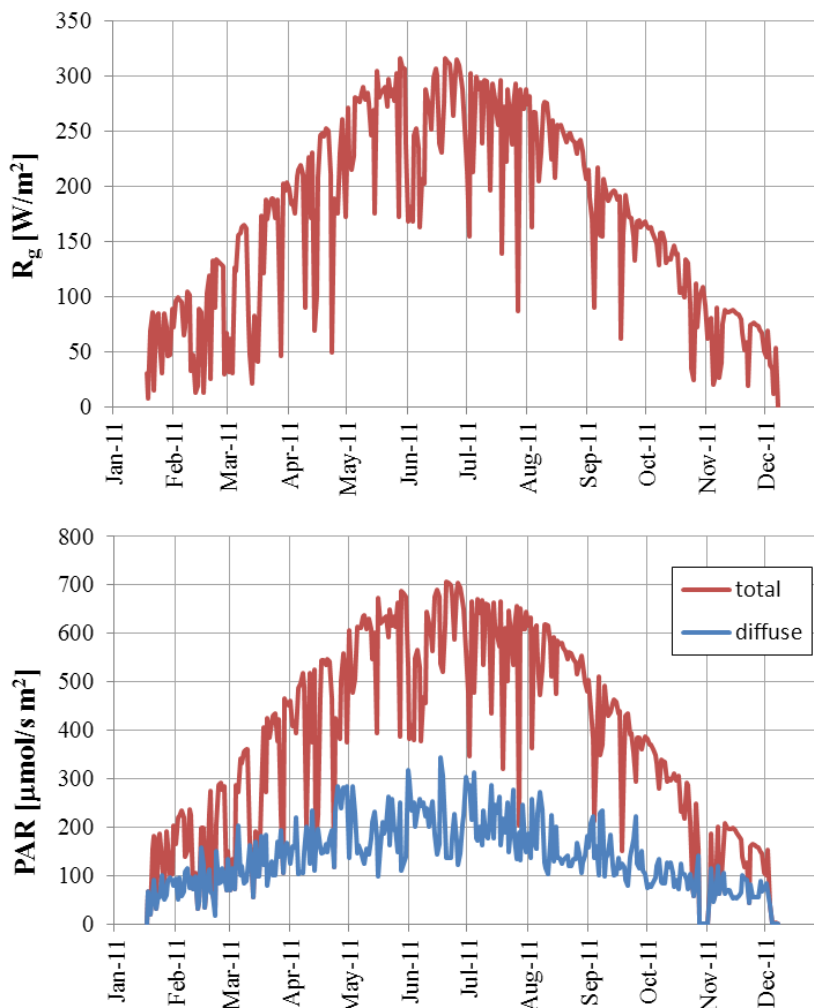
Fig.56: Daily averages of short wave incoming radiation (top) and incoming photosynthetic active radiation (bottom). Gaps in January& December show periods with missing data.
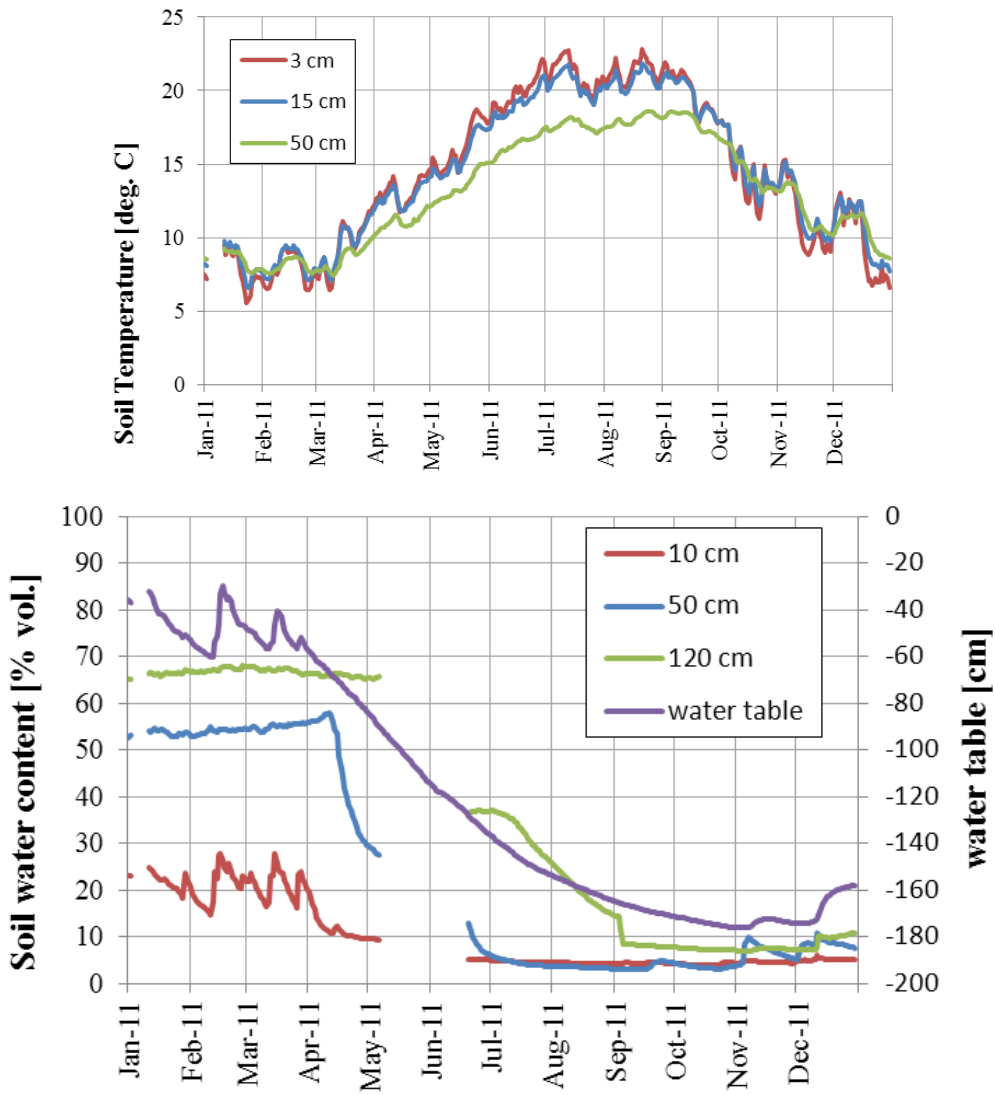
Fig. 57: Profiles of soil temperature (top) and soil water content plus water table (bottom) measured as daily averages.
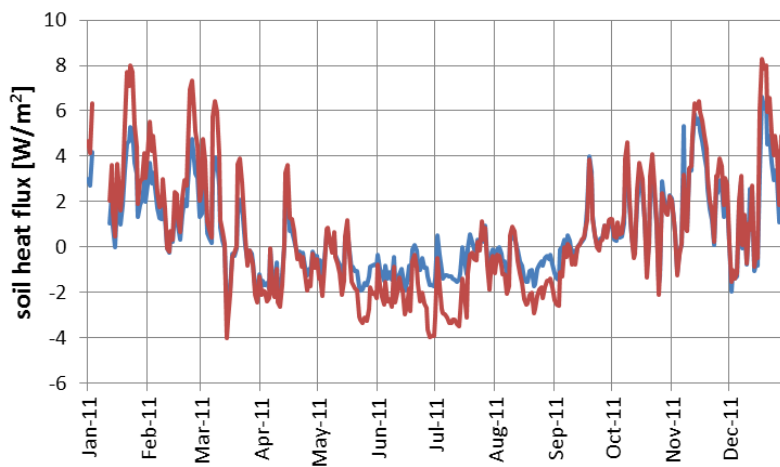

Fig.58: Soil heat fluxes measured with two identical sensors located some meters apart.

Soil parameters

Soil parameters monitored in 2011 were the temperature at three different depths (3, 15 and 50 cm), soil water content profile (10, 50 and 120 cm) plus water table depths. Daily averages of these values are illustrated in Fig. 577. The consequence of 2011 being a very dry year is an extremely low water table going down to almost -180 cm as shown in Fig. 57 as well. The soil heat flux measured with two identical sensors located a few meters apart in the forest soil is shown in Fig. 58. The differences between the two sensors originate from the different light intercept by the canopy at the two locations and the soil inhomogeneity.

Flux measurements

The daily averages of CO_2 and heat fluxes measured during 2011 are shown in Fig. 59a and 59b, respectively.

To obtain the eddy covariance flux data for the 30 minute measurement periods, the high frequency data from the LiCor 7500A open path CO_2 and H_2O analyser have been evaluated together with the anemometer data using the EdiRe software package from the University of Edinburgh (Table 7). Using the CarboEurope quality classification for the 17520 flux data points for 2011, 64% of the CO_2 fluxes are of good quality (class 0), 16% middle quality (class 1), 7% low quality (class 2) and 13% are missing due to instrument malfunctioning or rain conditions. Gap filling of the dataset has been performed without u* filtering using the 'Eddy covariance gap-filling & flux-partitioning tool' online available at: www.bgc-jena.mpg.de/~MDIwork/eddyproc/ for missing and quality class 2 data.

Fig. 59b shows the latent (red) and sensible (blue) heat fluxes for 2011 as daily averages. The dry situation especially in summer can be seen here as well, the latent heat flux is much smaller than the sensible heat flux.

The cumulated sum of the gap filled 30 min. CO_2 fluxes is shown in Fig. 60a. Using the flux partitioning module of the above mentioned online tool, the Net Ecosystem Exchange (NEE), i.e. the CO_2 flux measured, has been partitioned into Gross Primary Production (GPP) and Ecosystem Respiration (Reco) and plotted as daily averages in Fig. 60b. Calculating the carbon budget for 2011, NEE sums up to -322 g C m^{-2} year^{-1}, GPP to -1734 g C m^{-2} year^{-1}, and Reco to 1412 g C m^{-2} year^{-1}.
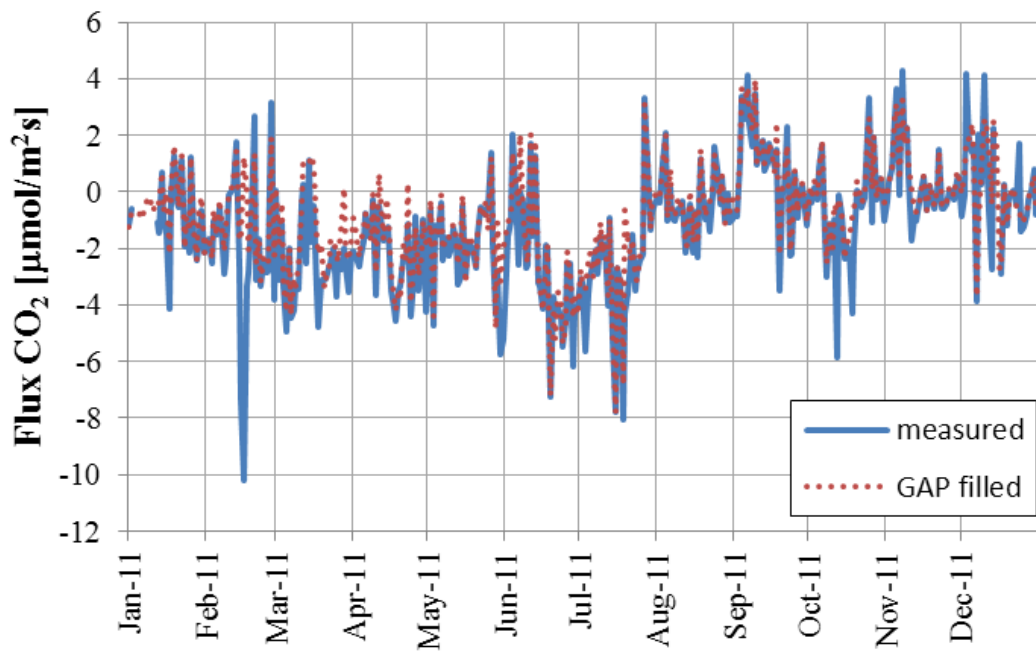
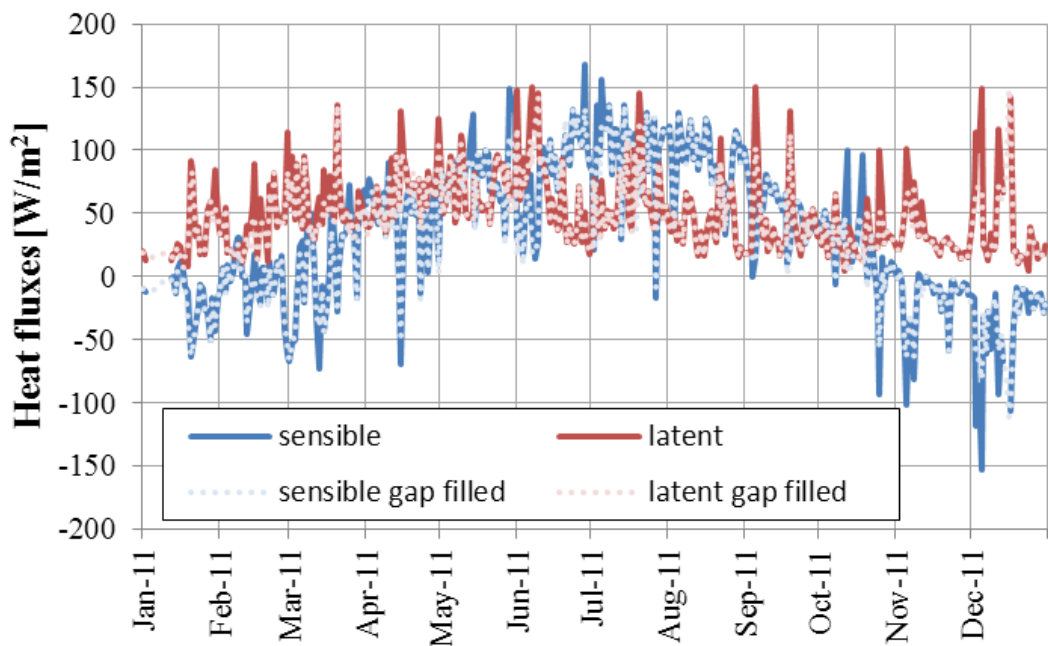*Fig. 59a: Daily averages of measured (blue) and gap filled (red) CO₂ fluxes.*

Fig. 59b: Daily averages of latent (red) and sensible (blue) heat fluxes.
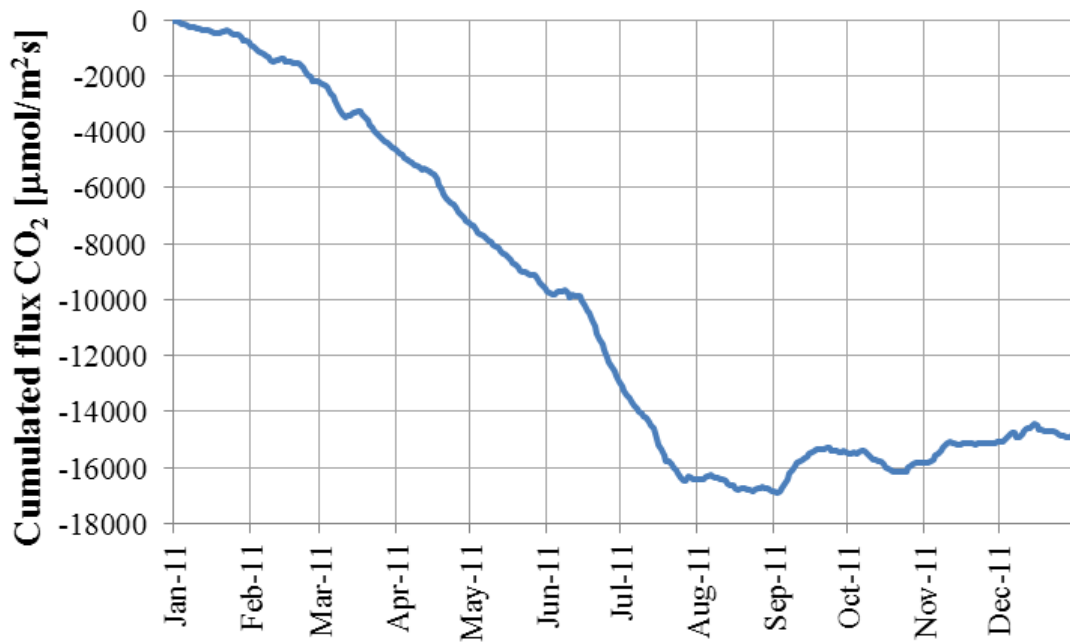
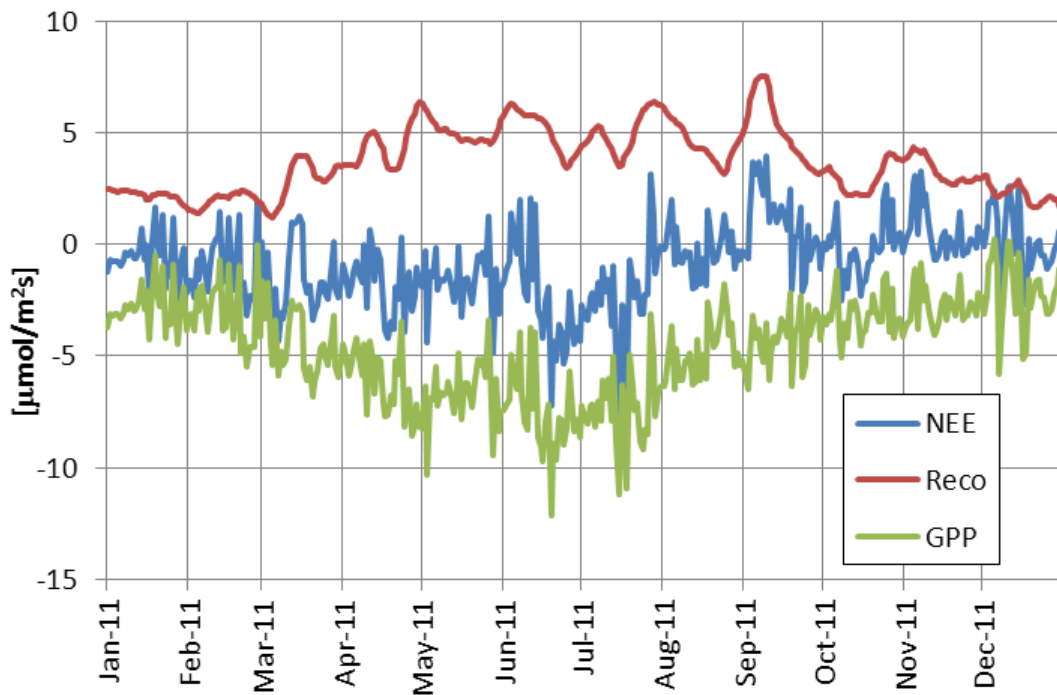*Fig. 60a: Cumulated sum of 30 min averages of gap filled CO_2 fluxes.*

Fig. 60b: daily averages of Net Ecosystem Exchange (NEE), Gross Primary Production (GPP) and Ecosystem Respiration (Reco) for 2011.

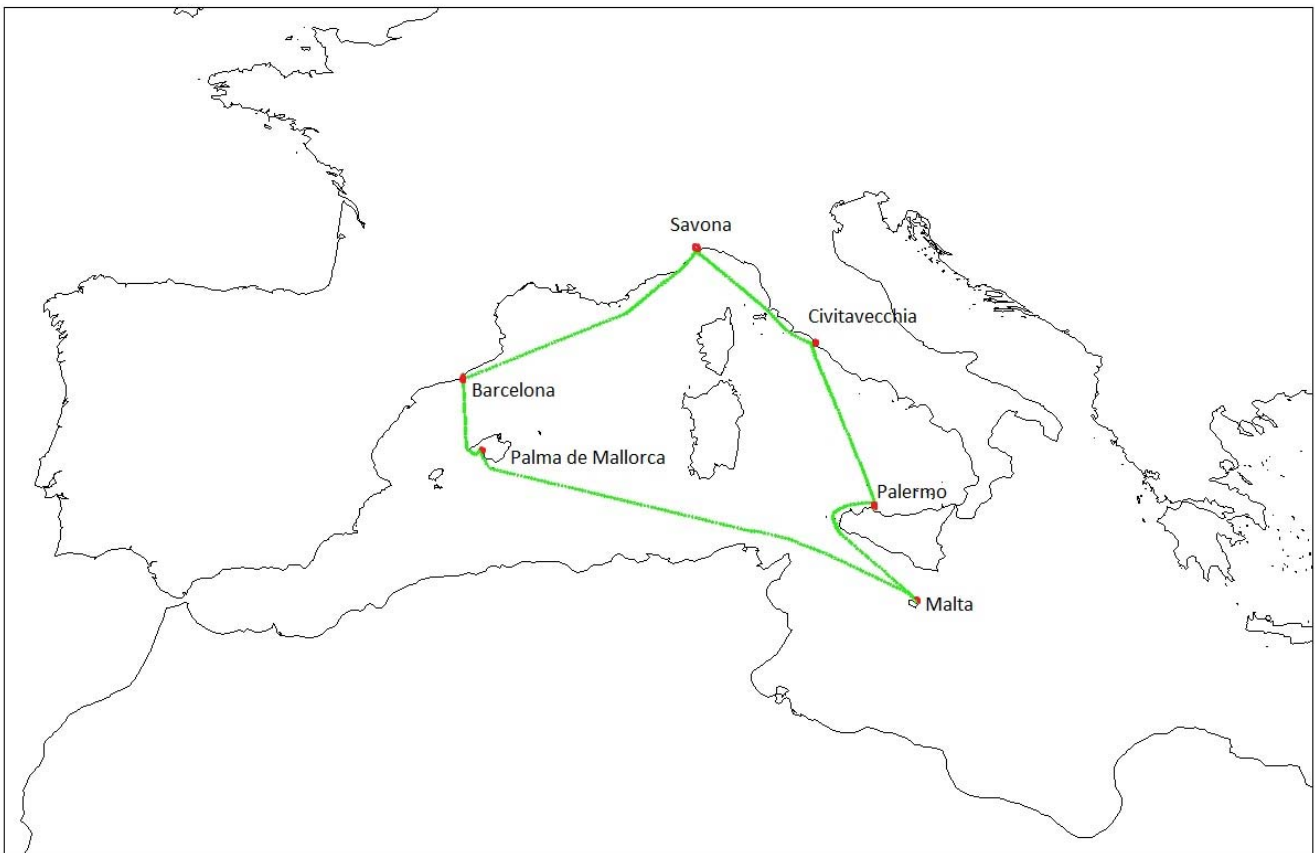*Fig.61: Costa Concordia and the cabin on Deck 14 with the JRC air monitoring station.*

Fig 62: Costa Concordia's route in 2011.

Air pollution monitoring from the cruise ship

Introduction

Measurements of air pollutants over the Western Mediterranean have been carried out regularly since the autumn of 2005 during spring, summer and autumn from a monitoring station placed in a cabin on cruise ships belonging to the fleet of the Italian cruise line Costa Crociere. The basis for this monitoring activity is a collaboration agreement between the Costa Crociere and the JRC. The scope of this activity is to obtain information about the concentration levels of air pollutants in this area, to improve the understanding of their sources and to test the performance of air pollution chemical transport models. Further, as this is intended as a long term monitoring activity, it is also potentially useful for analysis of trends and changes related to introduction of new legislation. So far three scientific papers have been published based on the data obtained from this monitoring activity (Marmer et al. 2009, Velchev et al. 2011 and Schembari et al. 2012).

In order to obtain a dataset that allows to observe year-to-year variations, the measurements have, as far as possible, been performed on ships that follow the same weekly route in the Western Mediterranean. This implies that the monitoring station occasionally must be moved from one Costa Crociere ship to another.

Measurement platform location

The measurements of air pollutants in 2011 were performed on the cruise ship Costa Concordia (Fig. 61). In 2011 this ship (now famous because of the accident in January 2012) was following a fixed weekly route in the Western Mediterranean (see Figure 62 and Tables 10).

Table 10. *Time schedule for Costa Concordia in 2011during the period of the measurements (May 30 – October 17)*

Day of week	Place	Country	Start	End
Monday	SAVONA	ITALY	8:00	17:00
Tuesday	BARCELONA	SPAIN	13:30	20:00
Wednesday	PALMA DE MALLORCA	SPAIN	8:00	
Thursday	PALMA DE MALLORCA	SPAIN		1:00
Thursday	At sea			
Friday	LA VALLETTA	MALTA	9:30	18:00
Saturday	PALERMO	ITALY	8:00	17:00
Sunday	CIVITAVECCHIA	ITALY	8:00	19:00

Instrumentation

On-line measurements

The automatic monitoring station on Costa Concordia contains the following measurement equipment

- Ozone Analyser (Model C49, Thermo Electron Instruments Inc., USA, S/N 0503110497),

- Trace level SO_2 Analyser (Model 43i-TLE, Thermo Electron Instruments Inc., S/N 0724324323)

- Trace level NOx-analyser (Model 42i-TL, Thermo Electron Instruments Inc., S/N 0710820808).

- Carbon monoxide IR analyser (Model 48, Thermo Electron Instruments Inc., S/N 68275-360).

- Aethalometer (AE 21, 2 wavelengths, Magee Scientific, USA, S/N 552:0503)

- Delta Ohm HD2003 ultrasonic anemometer (S/N 10007572); the built-in compass in this instrument allowed also to obtain the course of the ship.

- GPS Evermore SA320 instrument.

The measurement principle of these instruments is described in the chapter "Measurement techniques" (p. 21-22). The inlets to the gas and Aethalometer have a cut-off respectively at 1 µm and 10 µm particle diameter by a homemade inertial impactor. Before entering the gas analysers the air passes through 5 µm pore size PTFE Millipore membrane filters in order to remove particles. The measurement procedure complies with the recommendations in the EMEP manual (EMEP, 1996). The anemometer as well as the GPS were placed at the top of the cabin housing the other instruments.

Off-line measurements

- Sampling
During specific campaigns, Teflon (Whatman, 2 µm pore size 47 mm diameter) and Pallflex 47mm diameter quartz fibre filters were sampled using two Leckel (Sven Leckel Ingenieurburo) sequential samplers with a PM10 inlet head, flow rate 2.3 m^3 h^{-1}. The two samplers were placed at the deck above the cabin where the JRC monitoring station is placed.

- Gravimetric analyses
Before and after the sampling, quartz filters were pre-conditioned for 2 days in an air-controlled room with temperature = 20 $\pm$ 1 °C, relative humidity = 20 $\pm$ 5 % and weighed using a microbalance Sartorius MC5 (sensitivity = 1 µg), preventing electrostatic effects by the use of an ionizing gun.

- Elemental analyses
Teflon filter samples were analyzed by ED-XRF (Energy Dispersive – X Ray Fluorescence) at the Department of Physics of Genoa (Ariola et al., 2006) to determine the aerosol elemental composition. Light elements were determined by Dr. Massimo Chiari at Labec, INFN in Florence (IT), using EBS-PESA (Elastic Backscattering Spectroscopy - Particle Elastic Scattering Analysis).

- Organic and Elemental Carbon (OC & EC)
OC & EC concentrations were determined at the ABC-IS Laboratory (JRC). For the OC & EC thermo-optical analysis a Dual Optical Carbonaceous analyzer from Sunset Laboratory was used adopting the EUSAAR-2 protocol, optimized for analyzing carbonaceous aerosols at European regional background (Cavalli et al., 2010).

- Ion analyses
Ions were analysed at the University of Milan by Prof. Andrea Piazzalunga. An ICS-1000 Ion Chromatograph (Dionex) was set up for the water-soluble inorganic determination. Major ion analyses were carried out by means of a Ion Pac AS14A (Dionex) column using a mixture 8 mM Na_2CO_3 / 1 mM $NaHCO_3$ as eluent at 1 mL min^{-1} flow rate and a conductivity detector with a ASRS-ULTRA suppressor (Dionex). Cations' determination was performed by means of a CS12A (Dionex) column using 20 mM MSA as eluent at 1 mL min^{-1} flow rate and a conductivity detector with a CSRS-ULTRA suppressor (Dionex). Methanesulphonate (MSA) was analysed using an AS11HC column, gradient elution with 2-17 mM KOH solution with a flow of 1.5mL min^{-1}.

Data quality control and data processing

Calibrations are performed by use of certified standards of NO, CO SO_2 from Air Liquide and zero air generated by a Breitfuss zero air generator. Before being brought on the ship the Air liquid standards were certified by comparison to VSL primary standards in the ERLAP laboratory in Ispra. Calibrations were performed automatically during the week while the measurements were running unattended. NOx and SO2 were calibrated once per week while CO zero calibrations were performed daily because of rapid baseline drift. CO span calibration was performed once per week. Ozone was calibrated by comparison to a portable primary standard (Thermo Electron 49C PS).

The ozone analyser (Model C49) showed very good stability over the period of the measurements: All span and zero calibrations gave results within +/- 2 ppbV of the initial values. This stability is related to the fact that the instrument is using a two-channel system: one channel measures ambient air while the other channel measures ambient air, filtered by an ozone scrubber, and thus it provides a continuously updated zero point for the measurements.

The NOx calibrations showed weekly variations of the zero values of maximum 0.1ppbV for NO and 0.2 ppbV for NO_2; the measured span gas values were between 100% and 108% of the certified value. For SO2, the maximum zero value measured was 0.06 ppbV; the span gas calibration gave values between 98% and 102% of the certified value. CO showed by far the largest drift of the zero point (see Fig. 63). In addition the CO measurements were influenced by variations in the internal temperature; a correction for this temperature related variations was performed (Fig. 63).

The Aethalometer collects particles in spots on a periodically moving filter-ribbon and measures optical attenuation of light at 880 nm and 370 nm transmitted through the filter. The attenuation is mainly caused by the presence of Elemental Carbon. With the aethalometer, an equivalent BC concentration (EBC) is estimated adopting the proportionality factor set by the manufacturer; however the factor depends on how the aerosol is coated by organic and inorganic material (Bond and Bergstroem, 2006). Furthermore, the measurements are influenced by multiple scattering of light on the particles at the filter, which increases the attenuation and thus reduces the proportionality factor, and by 'shadowing', which has the opposite influence. The Aethalometer was used with the standard settings, where EBC is calculated from the attenuation at 880 nm; the data were corrected for multiple scattering and shadowing using a Matlab software (author: Carsten Gruening) based on the papers by Schmid et al. (2006) and Arnott et al. (2005).

Raw data are averaged over a 10 minute interval and stored in a computer in an ACCESS database, using a LABVIEW software developed by NOS S.r.l. (Fabrizio Grassi).
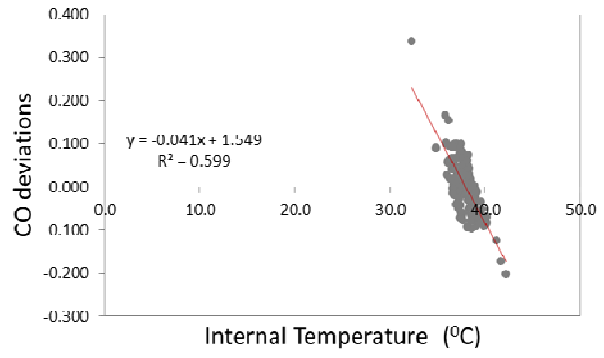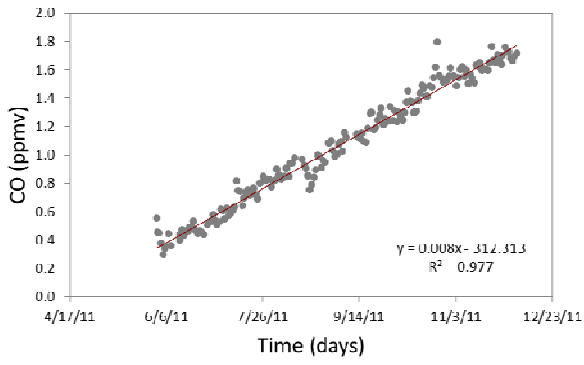
Figure 63: Linear fit for the zero air, and the deviations of measurement from the linear fit, plotted against temperature.

Measurement program in 2011

Measurements were carried out continuously from May 30 apart from interruptions of, altogether, approximately 15 measurement days due to various technical problems, mainly related to the data acquisition system. The measurements were stopped when the ship started following a different route by the end of November 2011.

In addition to the continuous measurements on board, three week-long measurement campaigns were carried out in collaboration with Prof. Paolo Prati, University of Genova and I.N.F.N., on weeks 18-25 July, 15-22 August and 12-19 September, during which aerosol was sampled in parallel on Tefon and Quartz fiber filters with normally 5 hours sampling time. Filters were collected at the sea as well as in harbours.

Information about meteorological parameters (wind speed and direction, temperature, humidity) was available with 10 min intervals for the months June and July from the meteorological station of the ship together with information about the ships position, speed and sailing direction. This information was used to identify situations where the measurements might be influenced by emissions from Costa Concordia: in all cases where the inlets to the measurement station were downwind of the stack of the ship within an angle of ± 40 degrees the data were discarded because of the risk of contamination from the stack.

In August and the following months meteorological information and GPS data were not anymore received from the ship, but measurements were now available from the HD2003 ultrasonic anemometer and from JRC's GPS. This allowed us to perform the same 'filtering' of the data that previously was done based on the information received from Costa Crociere.
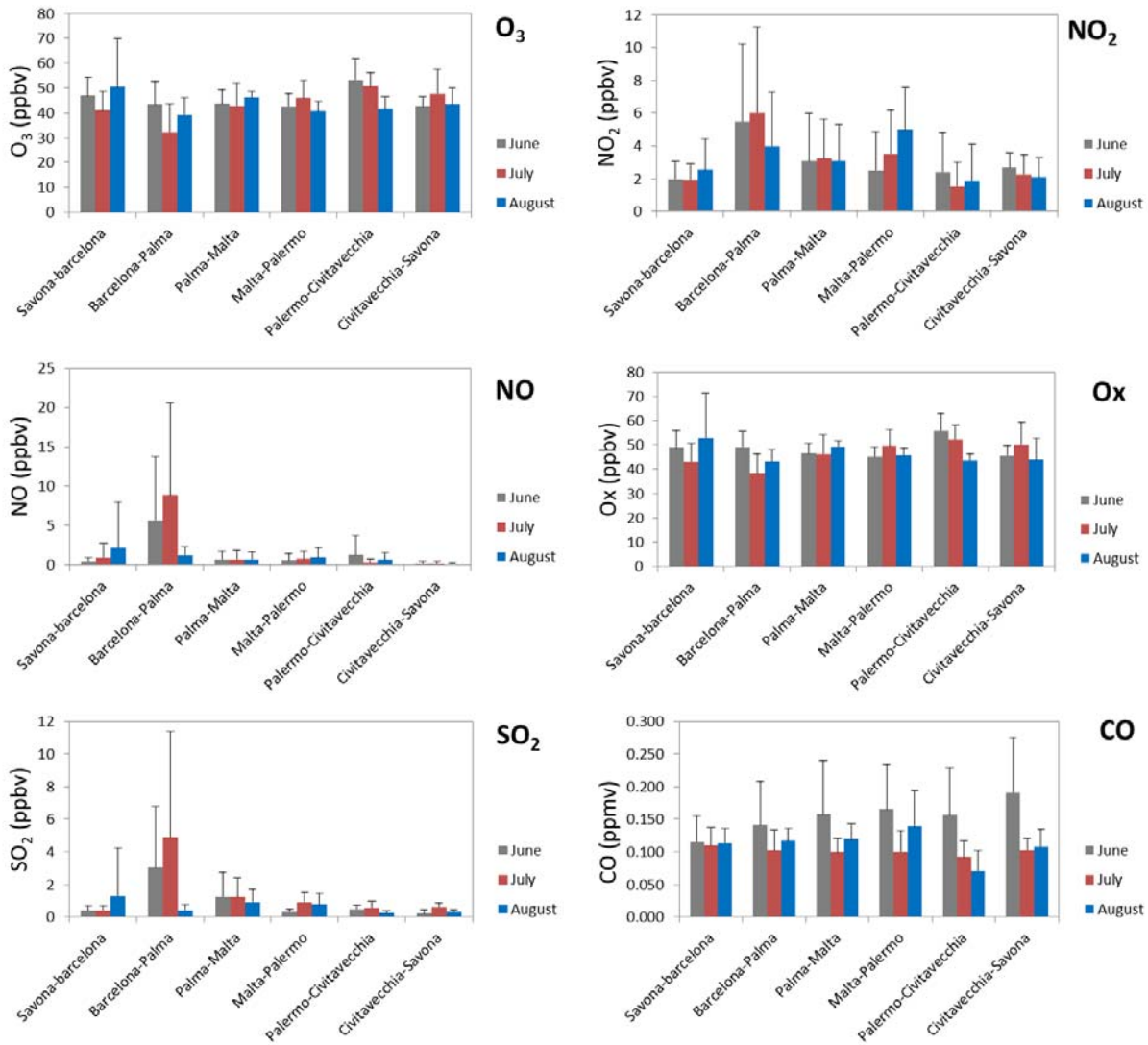
Fig. 64: Average concentrations of gaseous air pollutants measured over the route of Costa Crociere in the summer months of 2011. Data measured in harbours and one hour before and after the harbours are not included.

Results

Gas phase pollutants

Figure 64 shows the average concentrations of O_3 and $O_3 + NO_2$ (called 'Ox') measured over the different parts of the weekly route of Costa Concordia. 'Ox' is a useful parameter to look at because it is insensitive to the impact of nearby, local NO-sources (normally combustion sources) that can have a strong influence of ozone because of the fast reaction

$$NO + O_3 \rightarrow NO_2 + O_2$$
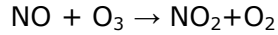
The smallest variations are shown by Ox, which lie within the range from 43 to 55 ppbV. NO and SO_2 show much larger variations. They are both likely to be occasionally strongly influenced by local sources.

The average diurnal variation of ozone and Ox is shown in Fig 65. The diurnal variation of Ox is clearly less pronounced than the diurnal variation of O_3 showing the importance of titration of ozone by NO in the harbours and in the vicinity of harbours. Local time (LT) in this area is UTC +2 so the minimum Ox concentration is found around 7 LT while minimum O_3 is found about one hour later. These diurnal variations mainly depend on the combination of photochemical production from precursor gases (particularly VOCs in combination with NOx, destruction of O_3 by titration with NO or surface deposition, combined with the influence of transport, particularly vertical transport in the atmosphere.
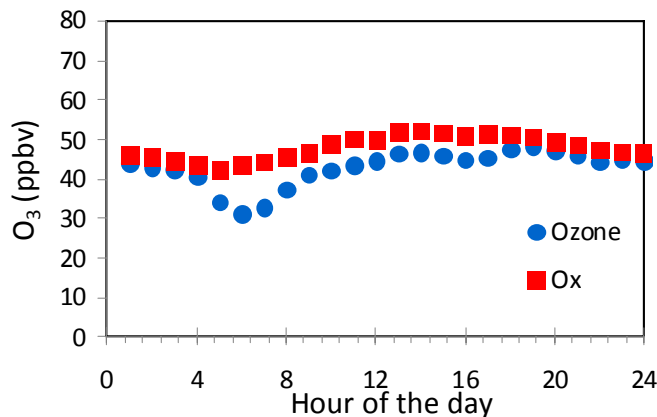

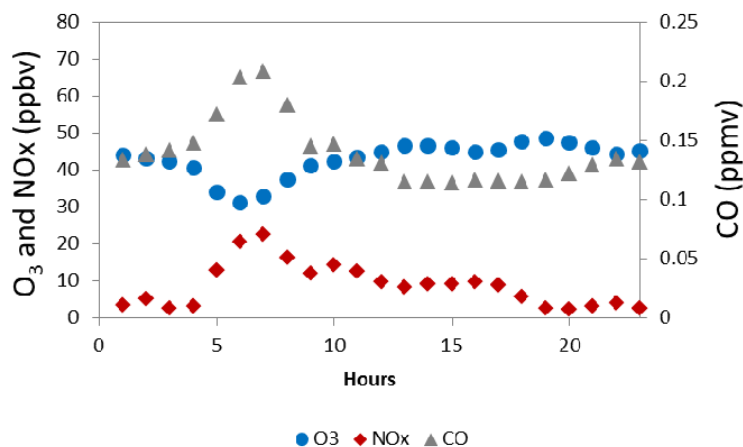Fig. 65. Diurnal variation of O_3 and Ox ($O_3 + NO_2$), June-August 2011. Hours in UTC

Fig. 66 – Diurnal variation of O_3, NOx and CO. Hours are in UTC.
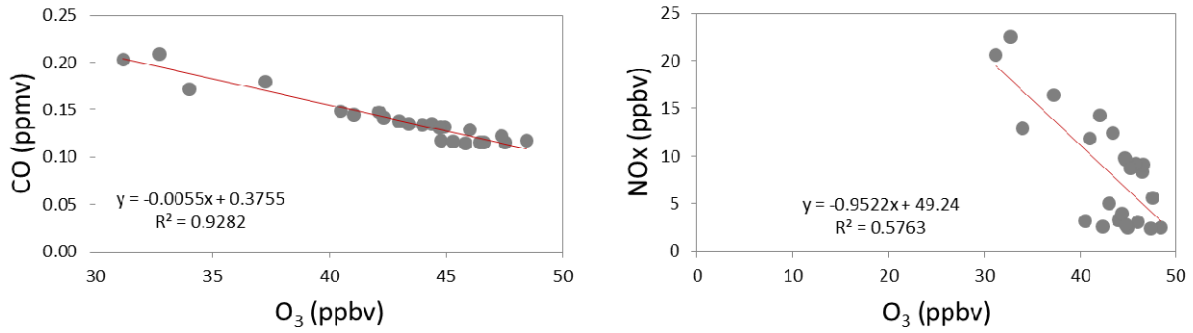
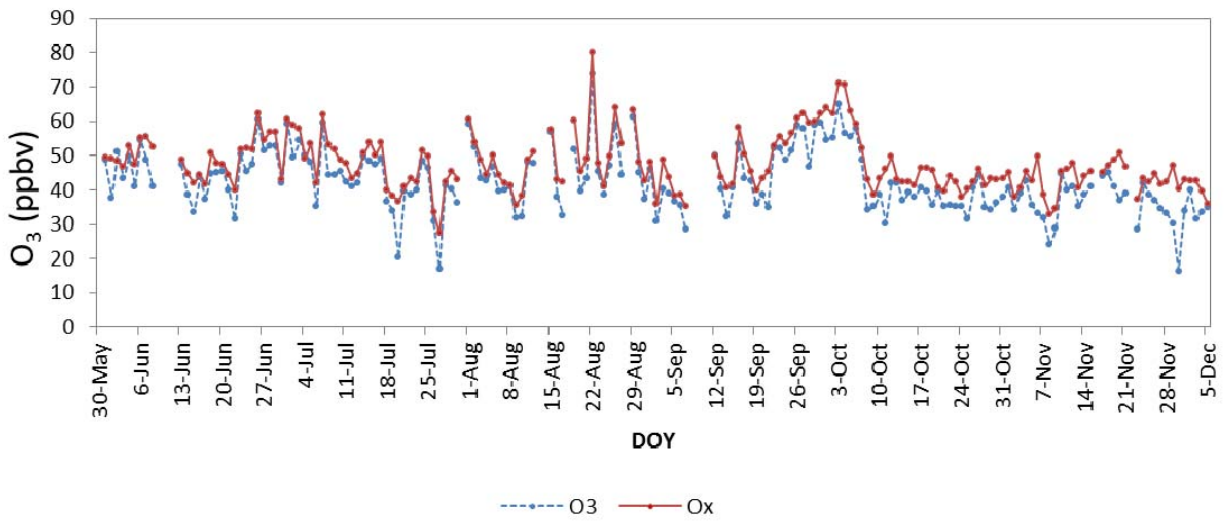*Figure. 67: Regressions between CO and NOx vs. O₃*

Figure. 68: Daily averages for O₃ and Ox over the measurement period (30 May-5 December). Harbours are not included.
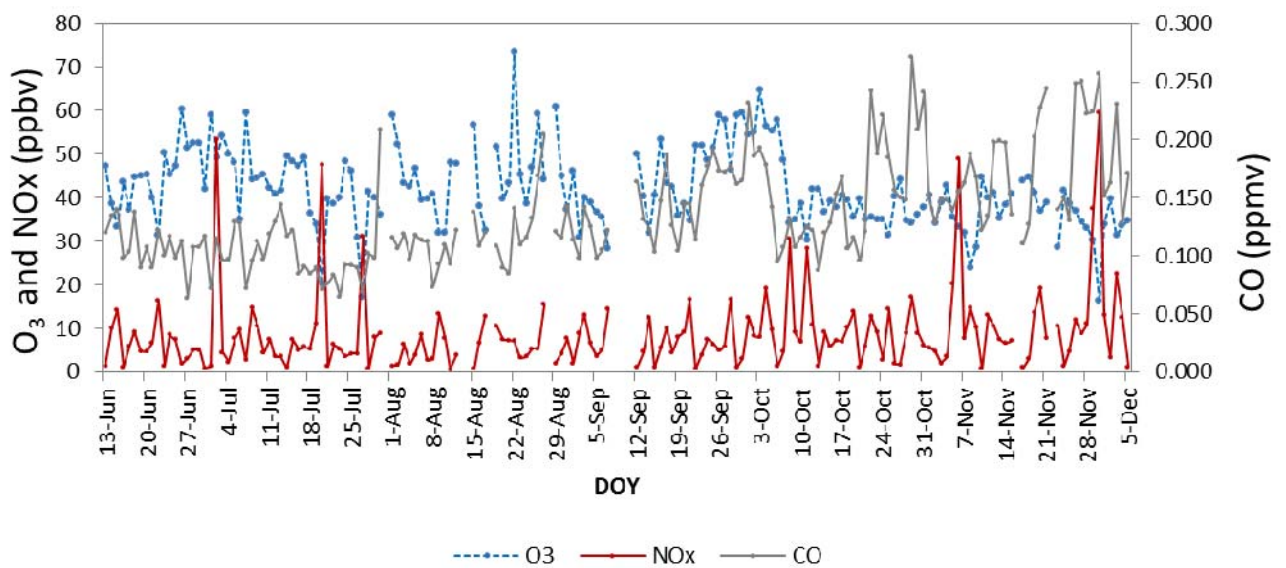

Figure 69: Daily averages for O₃, CO and NOx over the period 13 June-5 December 2011. Harbours are not included.

92

Figure 66 shows the average diurnal variation of CO together with those of O_3 and NOx while Figure 67 shows the relationship between ozone and CO and O_3 and NOx, that both are emitted by combustion sources. Contrary to NOx, which has a lifetime at the order of one day in the sunlit atmosphere, CO has a relatively long atmospheric lifetime (a few months). Thus the diurnal variation of CO will mainly depend on physical factors (emission, transport, dilution). As the diurnal variation of CO and NOx show a clearly similar behaviour there is evidence that these are much influenced by the combination of local emissions, transport and dilution during the day and, of course, by the fact that the ship is typically in a harbour during the day and at the sea during the evening and night..

The day to day variations of O_3 and Ox over the route of Costa Concordia (excluding harbours and one hour before and after being at berth in the harbours) are illustrated in Figure 68. Both concentrations are typically between 35 and 55 ppbV. The highest values were observed for the 22nd of August (80 ppbv) and 3rd October (71 ppbv). The Ox values follow the same pattern as O_3, but with a smaller daily variation because the variations caused by the titration of ozone with NO are eliminated.

The comparison between O_3, CO and NOx daily averages (Fig. 69) could be made only for the measurements made after the 13th of June, because of technical problems with the CO measurements in the first period. Harbours are not included in this plot and it can be seen that ozone and NOx do not show the same degree of covariation as in the diurnal plots that include the harbours where local sources are particularly important. It is also observed that high levels of ozone in some cases are associated with high levels of CO.
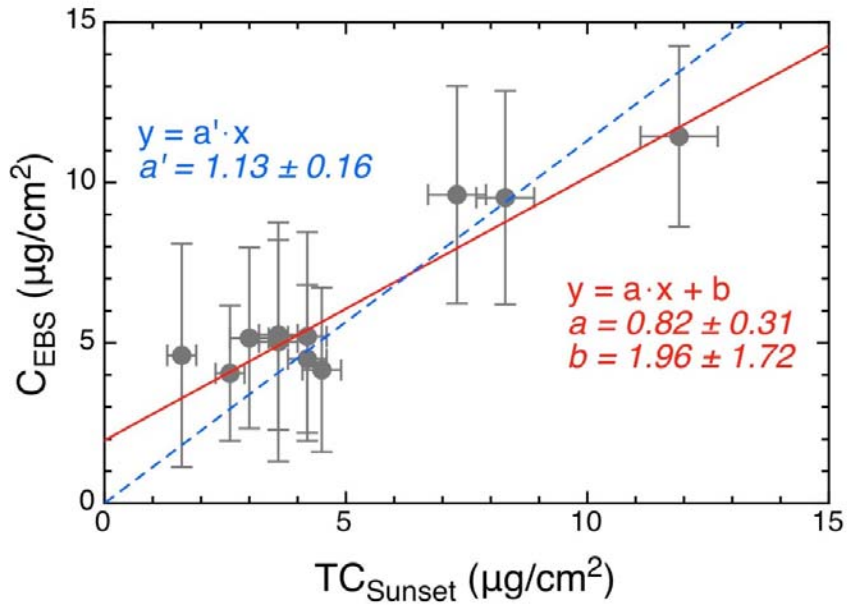
Fig.70. Total carbon as determined by the thermo-optical Sunset instrument and by EBS-PESA (courtesy Dr. Massimo Chiari).
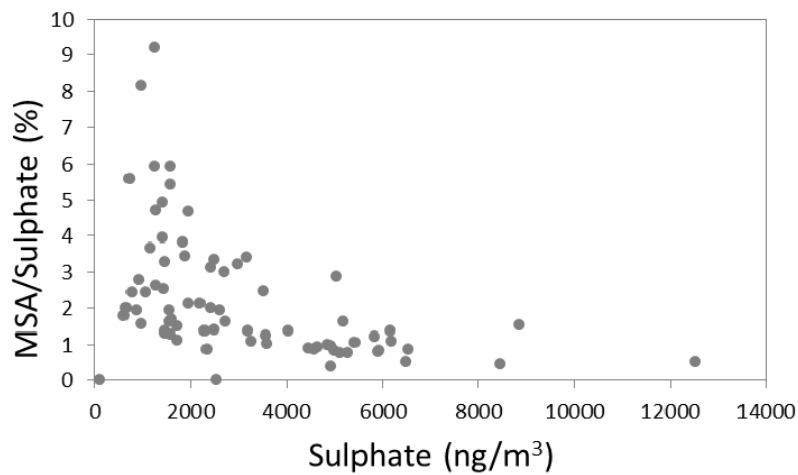

Fig. 71. The observed ratios of MSA to sulphate vs. sulphate concentrations in aerosols during the three campaigns in 2011.
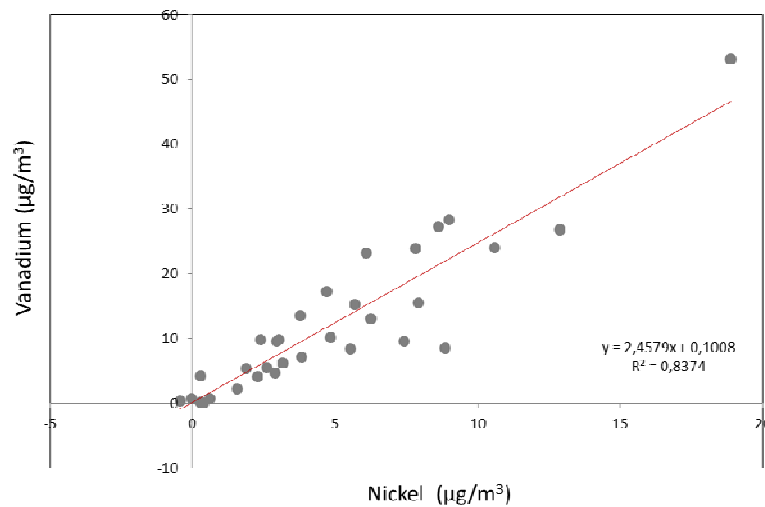

Fig. 72: Vanadium vs. Nickel in filter samples, as measured by XRF.

94

Aerosols

While all necessary checks and corrections have been performed to the gas phase measurements, the aerosol measurements are still to be considered as being preliminary and only some first observations can be reported.

The measurements performed during the three campaigns with filter sampling have provided a comprehensive dataset on ambient concentrations of main ions, elementary and organic carbon, as well as on the elemental composition of the aerosol. The XRF measurements did not allow us to determine elements lighter than sodium. However hydrogen, carbon, nitrogen and oxygen were measured by EBS-PESA for the campaign in September. The fact that carbon was measured by EBS-PESA as well as by the thermo-optical method allowed us to compare these two independent determinations of the C aerosol content (Fig. 70).

Some of the aerosol components are typical of specific sources and may thus be used for evaluating the contribution of these sources to the aerosol burden. This is for instance the case for MSA which is a product of the atmospheric oxidation of dimethylsulfide (DMS). DMS is emitted by algae in seawater; in the atmosphere it forms MSA and SO_2, which eventually is oxidized to sulfate. The ratio between the yields of MSA and sulfate appears to be temperature dependent, and should be equal to 0.12 at 20°C according to the empirical relationship found by Bates et al. (1992). The observations made from Costa Concordia are shown in Fig 71. It is seen from the graph that the highest values of the ratio are found at the lowest sulphate concentrations, suggesting that the influence of DMS emissions is most important in areas with a relatively low pollution level.

Other important tracers are nickel (Ni) and vanadium (V), which are emitted from combustion of heavy fuel oil, most often used by ships. However, Ni and V do have several other sources and are thus not as specific tracers as MSA. More information about the origin of Ni and V can be obtained by looking at the ratio between their concentrations. For ship emissions this ratio lies typically in the range between 2 and 3 (Viana et al, 2009; Pey et al., 2010), which is found to be the range typical of the observations made on Costa Concordia (Fig.72).

Conclusion

Measurements of gaseous pollutants and Equivalent Black Carbon were carried out continuously from May 30 until the end of November 2011. In addition, particle chemical and elemental composition was studied in three week long campaigns in July, August and September. The measurements are found to provide a dataset useful for studies of air pollution over the Western Mediterranean and its sources.

A first glance at the data shows a characteristic diurnal variation of O_3, Ox (= O_3 + NOx), NOx and CO which suggests that titration of O_3 by NO in the harbours, as well as transport phenomena (e.g. breeze circulation and vertical transport), which have a strong influence on the O_3 concentrations at sea level.

The aerosol measurements, performed in collaboration with Italian partners from Genova, Florence and Milan, have not yet been fully evaluated. First observations suggest that these data will be useful for the evaluation of the impact of ship traffic and biogenic sources on particulate sulfate concentrations.

References

Adam, M. Atmos. Chem. Phys. Discuss., 12, 5293–5340, 2012

Anderson, T.L., and Ogren, J.A., Determining aerosol radiative properties using the TSI3563 integrating nephelometer, *Aerosol Sci. Technol.*, **29**, 57-69, 1998.

Arnott, W.P., Hamasha, K., Moosmüller, H., Sheridan, P.J., and Ogren, J.A., Towards aerosol light-absorption measurements with a 7-wavelength Aethalometer: Evaluation with a photoacoustic instrument and a 3 wavelength nephelometer., *Aerosol Sci. Technol.*, **39**, 17-29, 2005.

Barnaba, F., Putaud, J.P., Gruening, C., Dell'Acqua, A., Dos Santos, S., Co-located in-situ, total-column and height-resolved aerosol observations: Implications for ground-level PM estimation from remote sensing. *J. Geophys. Res.*, **115**, D10204, doi:10.1029/2009JD012451, 2010.

Bates T., Calhoun J., Wang Y., Quinn P., variations in the methanesulphonate to sulphate molar ratio in submicrometer marine aerosol particles over the South Pacific Ocean, Journal of Geophysical research 1992, 97, 9859-9865.

Burch, D. E.; Gates, F. J.; Pembrook, J. D., Ambient carbon monoxide monitor. Research Triangle Park, NC: U.S. Environmental Protection Agency, Environmental Sciences Research Laboratory; report no. EPA-600/2-76-210, 1976.

Cavalli, F., Putaud, J.P., Toward a standardised thermal-optical protocol for measuring atmospheric organic and elemental carbon: the EUSAAR protocol, *Atmos. Meas. Tech.*, **3**, 79-89, 2010.

Cooke, W.F., Liousse, C., Cachier, H., and Feichter, J., Construction of a 1x1°fossil fuel emission data set for carbonaceous aerosol and implementation and radiative impact in the ECHAM4 model, *J Geophys. Res.*, **104**; 22,137-22, 1999.

Dell'Acqua, A., Putaud J.P., Gruening, C., Study of the JRC-Ispra EMEP site representativeness for short-lived atmospheric species measurements, *JRC report* EUR 24312 EN, 2010.

EMEP manual for sampling and chemical analysis (1995). *EMEP/CCC-Report 1/95. (Revised 1996; 2001; 2002).* 1995*.

European Directive 1999/30/EC. Relating to limit values for sulphur dioxide, nitrogen dioxide and oxides of nitrogen, particulate matter and lead in the ambient air. 1999.

European Directive 2008/50/EC. On ambient air quality and cleaner air for Europe. 2008.

Gruening, C., Adam, M., Cavalli, F., Dell'Acqua, A., Martins Dos Santos, S., Pagliari, V., Roux, D., Putaud J.P., Gruening, C., JRC Ispra EMEP – GAW regional station for atmospheric research. 2008 report. *JRC report* EUR 24088 EN, 2009.

Hess, M., Koepke, P. Schult, I., Optical Properties of Aerosols and Clouds: The Software Package OPAC, *Bull. of Am. Meteorol. Soc.*, **79**; 831-844, 1998.

Jensen, N. R., Gruening, C., Adams, M., Cavalli, F., Cavalli, P., Grassi, F., Dell'Acqua, A., Martins Dos Santos, S., Roux, D., Putaud, J.-P. JRC Ispra EMEP – GAW regional station for atmospheric research, 2009 report, *EUR 24678 EN*, (2010), *JRC62602*.

Jensen, N. R., Gruening, C., Adams, M., Cavalli, F., Grassi, F., Dell'Acqua, A., Martins Dos Santos, S., Scheeren, H. A., Douglas, K., Roux, D., Putaud, J.-P. JRC Ispra EMEP – GAW regional station for atmospheric research, 2010 report, *EUR 25219 EN*, (2012), *JRC68181*.

Kiehl, J. T., Schneider, T. L., Rasch, P. J., Barth, M. C., Wong, J., Radiative forcing due to sulfate aerosols from simulations with the National Center for Atmospheric Research Community Climate Model, Version 3 (Paper 1999JD900495), *J. Geophys. Res.,* **105**; 1441-1458, 2000.

Marmer, E., Dentener, F., Aardenne, J, Cavalli, F., Vignati, E., Velchev, K., Hjorth, J., Boersma, F. and Raes, F.: What can we learn about ship emission inventories from measurements of air pollutants over the Mediterranean Sea, Atmos. Chem. Phys., 9, 6815-6831, 2009

McMurry, P., Wang, X., Park, K., and Ehara, K. The relationship between mass and mobility for atmospheric particles: A new technique for measuring particle density, *Aerosol Sci. Tech.*, **36**, 227–238, 2002.

Mira-Salama, D., Van Dingenen, R., Gruening, C., Putaud, J.-P, Cavalli, F., Cavalli, P., Erdmann, N., Dell'Acqua, A., Dos Santos, S., Hjorth, J., Raes, F., Jensen, N.R. Using Föhn conditions to characterize urban and regional sources of particles, *Atmospheric Research* **90**, 159–16, 2008.

Nessler, R., Weingartner, E., and Baltensperger, U., Adaptation of dry nephelometer measurements to ambient conditions at the Jungfraujoch, *Environ. Sci. Technol.*, **39** (7), 2219-2228, 2005.

Pépin, L., M. Schmidt, M. Ramonet, D.E.J. Worhty and P. Ciais, Notes des Activités Instrumentales, A new gas chromatographic experiment to analyze greenhouse gases in flask samples and in ambient air in the region of Saclay, Institut Pierre-Simon Laplace (2001), http://www.ipsl.jussieu.fr.

Perrino, C., and Putaud, J.P., Assessment of the EMEP measurement and modelling work in Europe from 1977 until Today: national contribution of Italy, *EUR* 20979 EN, 2003.

Petzold, A., H., Schönlinner, M., Multi-angle absorption photometry - A new method for the measurement of aerosol light absorption and atmospheric black carbon, *Journal of Aerosol Science*, **35** (4), 421-441, 2004.

Pey, J., Xavier Querol, Andrés Alastuey, Discriminating the regional and urban contributions in the North-Western Mediterranean: PM levels and composition, Atmospheric Environment 44 (2010) 1587-1596

Putaud, J.-P., et al. (21 authors), 2004, A European aerosol phenomenology—2: chemical characteristics of particulate matter at kerbside, urban, rural and background sites in Europe. *Atmospheric Environment*, **38**, 2579-2595.

Putaud, J.-P., et al. (39 authors), 2010, A European aerosol phenomenology—3: Physical and chemical characteristics of particulate matter from 60 rural, urban, and kerbside sites across Europe. *Atmospheric Environment*, **44**, 1308-1320.

Rembges, D., Brun, C., Duane, M., Fantechi, G., Geiss, O., Larsen, B., Putaud, J.-P. JRC – Ispra air monitoring station 2000-2001 report. *JRC report* EUR 20998 EN, 2003.

Russell, L.M.: Aerosol organic-mass-to-organic carbon ratio measurements, *Environ. Sci. Technol.*, **37**, 2982-2987, 2003.

Schmid, O., et al., Spectral light absorption by ambient aerosols influenced by biomass burning in the Amazon Basin I: comparison and field calibration of absorption measurements techniques, *Atmos. Chem. Phys.*, **6**, 3443-3462, 2006.

Scheeren, H. A., P. Bergamaschi, N. R. Jensen, C. Gruening, I. Goded, and J. van Aardenne, First results from the new JRC greenhouse gas monitoring site at Ispra, Italy. In Willi A. Brand (ed.) Report of the 15th WMO/IAEA Meeting of Experts on Carbon Dioxide, Other Greenhouse Gases and Related Tracers Measurement Techniques, Jena, Germany, 7-10 September 2009, WMO GAW report N. 194, 2010.

Scheeren, H. A., P. Bergamaschi et al., An analysis of four years of CO_2, CH_4, N_2O and SF_6 observations and [222]Radon-based emission estimates from the monitoring station at Ispra (Italy), for submission to Atmos. Chem. Phys. Discuss., 2013.

Schembari, C., F. Cavalli, E. Cuccia, J. Hjorth, G. Calzolai., N. Pérez, J. Pey, P. Prati, F. Raes: Impact of a European directive on ship emissions on air quality in Mediterranean harbours, Atmospheric Environment (2012), doi: 10.1016/j.atmosenv.2012.06.047

Stratmann, F., Wiedensohler, A. A new data inversion algorithm for DMPS-measurements. *J. Aerosol Sci.*, **27** (Suppl 1), 339-340, 1996.

Van Dingenen, R., et al. (28 authors), 2004, A European aerosol phenomenology −1: Physical characterization of particulate matter at kerbside, urban, rural and background sites in Europe, *Atmospheric Environment*, **38**, 2561-2577.

Velchev, K. ., Cavalli F., Hjorth J., Vignati E., Dentener F., Raes F., Ozone over Western Mediterranean Sea-results from two years of shipborne measurements., Atmospheric Chemistry and Physics, 11, 675-688, 2011.

Viana M., Amato F., Alastuey A., Querol X., Chemical Tracers of particulate emissions from commercial shipping., Environmental science and technology, 43, 7472-7477, 2009.

Weingartner, E., Saathoff, H., Schnaiter, M., Streit, N., Bitnar, B., and Baltensperger, U., Absorption of light by soot particles: determination of the absorption coefficient by means of aethalometers, *J. Aerosol Sci.*, **34**, 1445-1463, 2003.

Weitkamp, C. (editor), LIDAR Range-Resolved Optical Remote Sensing of the Atmosphere, *Springer*, New York, 2005.

WHO, Health risks of ozone from long-range transboundary air pollution, 2008.

Worthy, D. E. F., I. Levin, N. B. A. Trivett, A. J. Kuhlmann, J. F. Hopper, and M. K. Ernst, Seven years of continuos methane observations at a remote boreal site in Ontario, Canada, J. Geophys. Res., 103 (D13), 15995-16007, 1998.

Zahorowski, W., S. D. Chambers, A. Henderson-Sellers, Ground based radon-222 observations and their application to atmospheric studies, J. Environm. Radioact., 76, 3-33, 2004.

Links

ACTRIS, *http://www.actris.net/*

ARPA Lombardia, *http://ita.arpalombardia.it/ITA/qaria/doc_RichiestaDati.asp*

Calipso, *http://www.nasa.gov/mission_pages/calipso/main/*

Chemical Co-ordinating Centre of EMEP, *http://www.nilu.no/projects/ccc/*

CLRTAP, *http://www.unece.org/env/lrtap/welcome.html*

EARLINET, *http://www.earlinet.org/*

EMEP, *http://www.emep.int/*

European Pollutant Release & Transfer Register*,* EPRTR*,* http://prtr.ec.europa.eu/MapSearch.aspx

European Committee for Standardisation (CEN), *http://www.cen.eu/cen/pages/default.aspx*

EUSAAR, *http://www.eusaar.net/*

Global Atmosphere Watch (GAW), *http://www.wmo.int/pages/prog/arep/gaw/gaw_home_en.html*

ICOS, *http://www.icos-infrastructure.eu/*

WDCA, *http://www.gaw-wdca.org/*

World Meteorological Organization (WMO), *http://www.wmo.int/pages/index_en.html.*

Abstract

The Institute for Environment and Sustainability provide long-term observations of the atmosphere within international programs and research projects. These observations are performed from the research infrastructure named ABC-IS: Atmosphere – Biosphere – Climate Integrated monitoring station. Most measurements are performed at the JRC-Ispra site. Observations are also carried out from two other platforms: the forest station in San Rossore, and a ship cruising in the Western Mediterranean sea. This document reports about measurement programs, the equipment which is deployed, and the data quality assessment for each site. Our observations are presented, compared to each other, as well as to historical data obtained over the past 25 years at the Ispra site.

As the Commission's in-house science service, the Joint Research Centre's mission is to provide EU policies with independent, evidence-based scientific and technical support throughout the whole policy cycle.

Working in close cooperation with policy Directorates-General, the JRC addresses key societal challenges while stimulating innovation through developing new standards, methods and tools, and sharing and transferring its know-how to the Member States and international community.

Key policy areas include: environment and climate change; energy and transport; agriculture and food security; health and consumer protection; information society and digital agenda; safety and security including nuclear; all supported through a cross-cutting and multi-disciplinary approach.